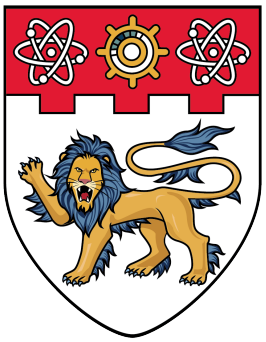

NANYANG TECHNOLOGICAL UNIVERSITY
SINGAPORE

RESILIENCE ASSESSMENT OF INTEGRATED ENERGY SYSTEMS UNDER HURRICANES

HUAJUN ZHANG

Interdisciplinary Graduate School
Institute of Catastrophe Risk Management (ICRM)

2019

RESILIENCE ASSESSMENT OF INTEGRATED ENERGY SYSTEMS UNDER HURRICANES

HUAJUN ZHANG

Interdisciplinary Graduate School
Institute of Catastrophe Risk Management (ICRM)

A thesis submitted to Nanyang Technological University
in partial fulfillment of the requirements for the degree of
Doctor of Philosophy

2019

Statement of Originality

I hereby certify that the work embodied in this thesis is the result of original research, is free of plagiarised materials, and has not been submitted for a higher degree to any other University or Institution.

30 December, 2019

. . . . . .

Date

. . . . . .

Zhang Huajun

Supervisor Declaration Statement

I have reviewed the content and presentation style of this thesis and declare it is free of plagiarism and of sufficient grammatical clarity to be examined. To the best of my knowledge, the research and writing are those of the candidate except as acknowledged in the Author Attribution Statement. I confirm that the investigations were conducted in accord with the ethics policies and integrity standards of Nanyang Technological University and that the research data are presented honestly and without prejudice.

31 December, 2019

. . . . . .

Date

. . . . . .

WANG Peng

Authorship Attribution Statement

This thesis contains material from 2 papers published and 1 paper submitted in the following peer-reviewed conference proceedings and journals where I was the first author.

Chapter 3 is published as H. Zhang, T. Zhao, P. Wang, and S. Yao, "Power System Resilience Assessment Considering of Integrated Natural Gas System," *IET Int. Conf. Resil. Transm. Distrib. Networks (RTDN)*. DOI: 10.1049/cp.2017.0334.

The contributions of the co-authors are as follows:

I prepared the manuscript drafts, designed the case studies and analyzed the results.

Dr. T. Zhao, Prof. P. Wang and Mr. S. Yao revised and proofread the manuscript.

Chapter 4 is published as H. Zhang, L. Cheng, S. Yao, T. Zhao, and P. Wang, "Spatial-temporal Reliability and Damage Assessment of Transmission Networks under Hurricanes," *IEEE Trans. Smart Grid*. DOI: 10.1109/TSG.2019.2930013.

The contributions of the co-authors are as follows:

I prepared the manuscript drafts, designed the case studies and analyzed the results.

Prof. L. Cheng, Mr. S. Yao, Dr. T. Zhao, and Prof. P. Wang revised and proofread the manuscript.

Chapter 5 is submitted as H. Zhang, P. Wang, S. Yao, X. Liu, and T. Zhao, "Resilience Assessment of Interdependent Energy Systems under Hurricanes,"

IEEE Trans. Power Syst.. (Under Review)

The contributions of the co-authors are as follows:

I prepared the manuscript drafts, designed the case studies and analyzed the results.

Prof. P. Wang, Mr. S. Yao, Mr. X. Liu, and Dr. T. Zhao revised and proofread the manuscript.

Zhang Huajun

30 December, 2019 .....

Date

..... Zhang Huajun

Abstract

Our modern society depends deeply on critical infrastructure (CI) systems, such as the energy, transportation and water system, etc., for normal function and development. Among these CIs, energy systems are of fundamental importance as they provide energy for all other systems as well as themselves to maintain normal operation. Power systems and natural gas (NG) systems are two vitally important energy supply systems that are very vulnerable to some relatively rare but extreme weather events (EWEs), such as ice storms and hurricanes. EWEs could cause extensive damage to exposed energy facilities, which may lead to disruptions of energy service, and could further result in enormous impacts on the whole society and economics. Considerable public concern has been raised on the threat of EWEs on energy systems. On the other hand, complex interdependence among CIs is increasing due to the expanded connections among them. Specifically in the energy systems, the power system increasingly relies on the NG system for the primary fuel of gas due to the building of considerably gas-fired generation plants for its promising potentials. At the same time, the NG system is gradually dependent more on the power system to operate, for example, using electricity to drive gas compressors instead of gas as before. With the ever-growing interdependence, it is clear that the conventional stand-alone system analysis viewpoint becomes insufficient and inadvisable. The CI internal complexity, rising interdependence as well as environmental risks from EWEs could work together to amplify undesirable disruptive effects and threat the reliable and continuous supply of energy.

To manage this increased exposure to threats induced by EWEs and risks associated with interdependence, this thesis seeks to integrate the existing knowledge and develop methods to evaluate the impact of gas fuel supply on the reliability

of transmission power systems, to assess the power system performance under the spatial-temporal impact of hurricanes, to quantify the resilience of integrated transmission power systems and NG systems under hurricanes, and to measure the frequency resilience of transmission power systems under hurricanes. It includes investigating the impact of gas fuel supply on the power system reliability from a long-term time scale, exploring the hurricane wind and rainfall impact on the power system reliability during the hurricane event, establishing integrated power and NG system resilience analysis models and framework, studying the effect of frequency control process on power system performance under hurricanes, and proposing corresponding assessment methods. Besides, this thesis also develops a multi-attribute construct of indices to quantify the power system and the NG system performance from both the operation and the infrastructure perspective, e.g., load shedding related indices, frequency related indices, and component damage related indices. Based on the assessment indices, integrated proactive suggestions can be provided to guide the preparation of the power system or the integrated energy systems for the approaching hurricane.

The methods generated could also be used in the co-planning of power systems and fuel supply systems or serve as a decision-making tool for the selection of resilience enhancement strategies in the future.

Acknowledgements

First of all, I would like to express sincere gratitude to my supervisor, Prof. Wang Peng for his patience, encouragement and invaluable guidance. He creates a free research environment and indicates the direction when I was lost. Besides, I would like to acknowledge my co-supervisor, Asst Prof. Cheung Sai Hung, and my mentor, Assoc Prof. Dr. Lo Yat-Man, Edmond for their insightful comments and encouragement.

I am particularly grateful for the assistance of Dr. Zhao Tianyang. He gave me selfless assistance in coding, provided guidance in academic writing and inspired my spirit when I was in frustration. I would also like to thank Mr. Yao Shuhan, Mr. Lin Pnegfeng, Mr. Liu Xiaochuan, etc., for their helpful discussions and cooperation we had.

I also want to thank the research team of the Institute of Catastrophe Risk Management(ICRM) for their constructive suggestions. I would also like to thank the researchers of "Future Resilient Systems" (FRS) in Singapore-ETH Center for their great advice and cooperative support. In particular, I would like to express my earnest thanks to Prof. Hans Heinimann for his listening, support and advice when I was stuck in the unending pressures of life.

My sincere thanks are then given to the technicians in Water and Energy Research Lab (WERL), Mr. Tan Peng Chye and Mr. Lee Chew Siong, for their helpful technical supports.

Finally, I have to thank my husband and parents for their understanding, care, and support. My family refueled me when I was exhausted and pushed me forward. I cannot complete this hard journey without them. I am thankful for my two kids and what they bring to my life.

Table of Contents

List of Tables

List of Figures

List of Abbreviations

CI	Critical Infrastructure
NG	Natural Gas
EWE	Extreme Weather Event
GFG	Gas-Fired Generator
MILP	Mixed-Integer Linear Programing
OPF	Optimal Power Flow
GF	Gas Flow
PF	Power Flow
SCIP	Solving Constraint Integer Programs
UC	Unit Commitment
OGF	Optimal Gas Flow
MIP	Mixed-Integer Programing
GB	Great Britain
U.S.	United States
U.K.	United States
RESNET	Resilient Electricity Networks for Great Britain
CIGRE	Conseil International des Grands Réseaux Électriques
Bcm	Billion cubic meters
IEA	International Energy Agency
EDNS	Expected Demand Not Supplied
PLC	Probability of Load Curtailments
RO	Robust Optimization
AGC	Automatic Generation Control

Chapter 1

Introduction

This chapter gives an introduction of the research background, motivations, major contributions, and the organization of this thesis. It starts with a brief introduction of CIs with a focus on the power system and the NG system, then investigates the rising interdependence among them, especially due to the increasing share of NG as the primary fuel in power generation and the electrification of gas compression stations. Secondly, it introduces extreme weather events (EWEs), their characteristics, and their impacts on the energy systems, especially on power systems. After that, motivations and major contributions of the thesis are presented. Finally, the thesis organization is described.

1.1 Background

CIs are large-scale complex networks constituting of interconnected components, such as the energy, water and transportation system, which are cornerstones of our modern developed society. Among these CIs, the energy systems are of vital importance, such as power systems and NG systems, as they are designed and expected to provide a reliable and continuous supply of energy to all other sectors as well as themselves. However, the risk they are facing are not fixed but continually changing in response to various factors from the economy, regulation, technology, market dynamics and so on.

EWEs such as hurricanes and ice storms usually lead to wide-spread even devastating disruptions of energy service by causing extensive damages to energy infrastructures. Under the harsh conditions of EWEs, the deep interdependence between energy systems brings additional challenges. At the same time, the requirement for a high level of reliability of energy supply, especially of power, has never changed. The conventional individual system reliability analysis method for the long-time application purpose can neither well reflect the short-term characteristics of the EWEs' impact on the energy systems nor identify potential interdependence risks and thus is not sufficient or advisable under this background.

1.1.1 Energy Systems and Rising Interdependence

Our modern society depends deeply on CIs for proper function and development, such as the water, energy, health care, transportation, communication and finance system, among which the energy systems, such as power systems and NG systems, deserve particular attention as they supply primary and second energy to all other sectors as well as themselves to maintain their regular operation. For example,

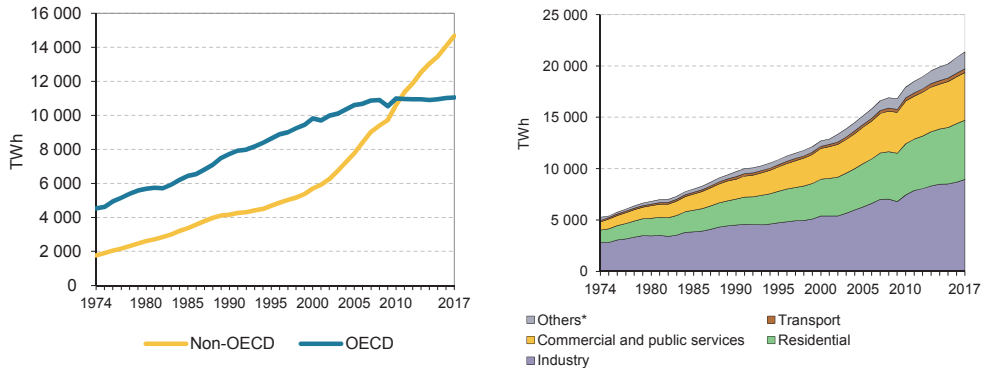

(a) Total gross electricity production (b) World electricity final consumption by sector

Figure 1.1: World electricity production and consumption [1].

electricity is essential for almost all other systems.

The power system is particularly important in energy systems because it is the backbone of several other key sectors. Along with society's development, the demand for power supply has also increased. According to statistics from International Energy Agency (IEA) [1], the global production and consumption of electricity have sustained growth for eight years from 2009 after a slight decline from 2008 to 2009 caused by the global financial crisis, as shown in Fig.1.1. In 2017, world gross electricity production and consumption reached 25721 TWh and 21 372 TWh, with a growth of 2.5% and 2.6% compared to 2016, as shown in Fig.1.1a and Fig.1.1b (* includes agriculture, fishing and non-specified other), respectively. As presented in Fig.1.2 [2], electricity has increased from 9.4% of the total world consumption of energy in 1973 to 18.9% in 2017, which indicates that our society depends more and more on electricity. Blackouts in a power system could lead to disastrous consequences, such as traffic gridlock, communication interruption and industrial production interruption, resident panic and chaos, as well as a breakdown of government and health sectors. Thus, high reliability is the primary criteria of power supply to enable normal society function. However,

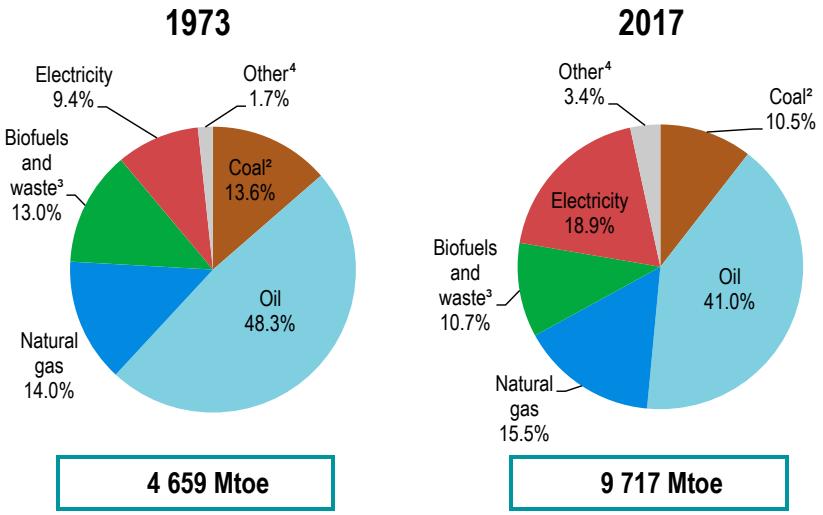

Figure 1.2: 1973 and 2017 world total final consumption by source [2].

there are both internal and external threats to the reliability of power systems, such as threats from fuel supply shortage and EWEs.

The NG system is also a lifeline utility system playing a vital role in achieving social wellbeing. It is an essential energy source for activities of business, industry, agriculture and residents, especially as an increasing fuel supply for power generation.

The global gas production and demand are increasing dramatically according to statistics of IEA [3]. The NG production in Fig.1.3a and consumption in Fig.1.3b (includes agriculture, fishing and non-specified other) have been keeping a consecutive increase from 2009 to 2018. In 2018, global NG production reached a new high of 3937 Billion cubic meters (Bcm), increased by 4.0% in comparison with 2017, while global demand for NG rose to 3922 Billion cubic meters, a 4.9% increase compared to 2017. Besides, between 1971 and 2017, the share of NG in the total world primary energy supply grew from 16% to 22% [2] as shown in

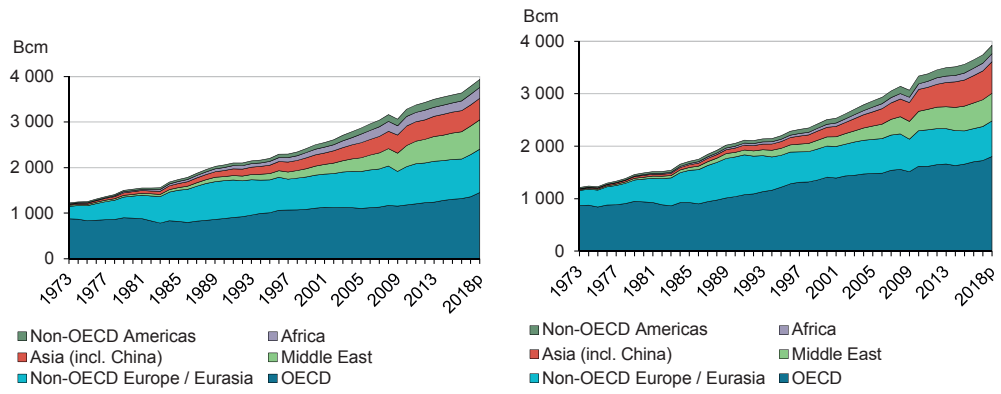

(a) World NG production by region (b) World NG demand by region

Figure 1.3: World NG production and demand [3].

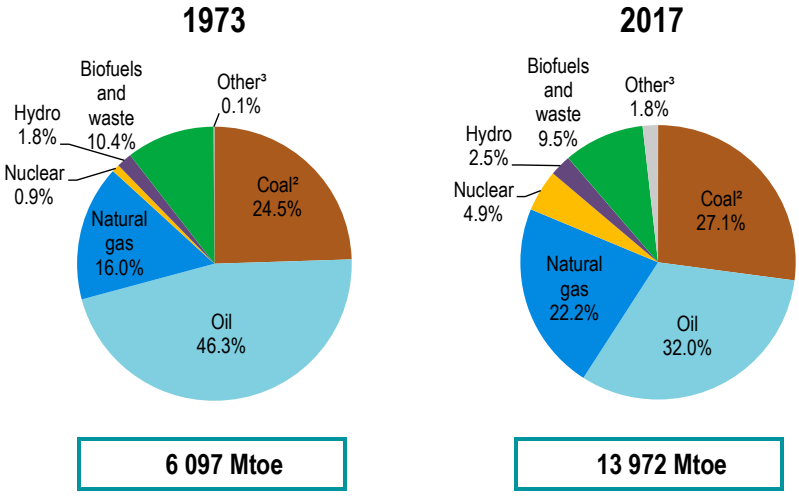

1. World includes international aviation and international marine bunkers.
2. In these graphs, peat and oil shale are aggregated with coal.
3. Includes geothermal, solar, wind, tide/wave/ocean, heat and other sources.

Figure 1.4: World total primary energy supply by source [2].

Fig.1.4. This trend indicates that NG takes a more and more critical role in the world energy structure.

Traditionally, power systems and NG systems are designed and operated in their own right or loosely coupled, and the stand-alone perspective is effective in

such cases. However, scenarios are changing with significant uncertainties arising from complex interdependence between the power system and NG system [9], which results from the accelerating transition from coal to gas and renewable resources for electricity generation, as well as the electrification of NG systems.

Electricity is historically generated from coal, which remains the predominant fuel currently. Coal is an nonrenewable fossil fuel with high carbon-intensive and not compatible with low carbon emission expectations. In order to find a sustainable and environmental solution to reduce fossil fuel dependency and carbon emission, the exploration of alternative fuels has never stopped. Renewable generation such as solar and wind is developed broadly, which contributes greatly to the sustainable energy transformation as they are environment friendly. However, the intermittent and fluctuant characteristics of renewable resources limit the penetration level, because a high penetration level could cause system stability issues. Besides, fast and flexible power generation is required to compensate for the variation and uncertainties induced by renewable resource generation.

Gas-fired generators (GFGs) provide an almost ideal solution to the problems associated with renewable resources as they can respond faster than traditional units depending on coal or nuclear energy. In addition to the flexibility feature, the lower carbon nature of NG also meets expectations for clean energy and is compatible with environmental objectives under tight standards. Besides, technological advancements promoted the utilization of GFGs. Additionally, increased availability and relatively low capital expenditure make NG more competitive. As a result, more and more NG is used for power generation, as shown in Fig.1.5 [3] and NG gradually took an increasing proportion of fuel in power generation throughout the past decades all over the world. According to detailed data from IEA [2], in 2017, 23.0% of world electricity production was from NG as the second largest preliminary single fuel, compared to about 12.1%

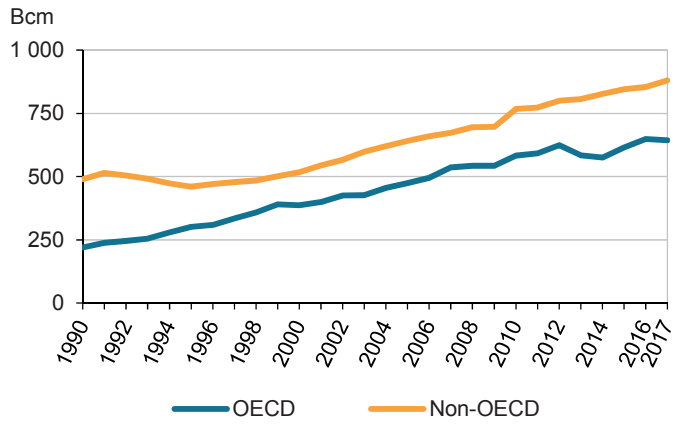

Figure 1.5: NG used for power generation [3].

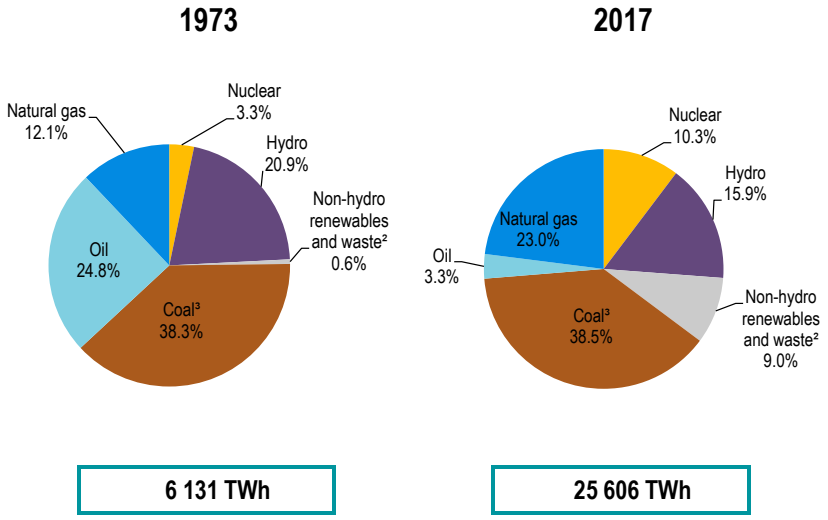

Figure 1.6: 1973 and 2017 source shares of electricity generation [2].

in 1973, as illustrated in Fig.1.6.

Power generation consumers build the dominant end users of NG and this substantial increase of NG in power generation would inexorably continue. The employment of NG for power generation provides the power system a resource

diversity, environmental and efficiency benefits but also raises complex challenges. The NG availability is constrained by several factors, such as source capacity, pipeline capacity, terminal pressure and load priority level. Accidents in the NG system that influence production and delivery facilities may directly cause gas deficiencies or disruptions of gas deliveries to GFGs. Citing some examples, on 29 June 2004, the unplanned interruption of the piped gas supplied from Indonesia made Singapore suffer a partial electricity blackout [10]; in Colorado 2006, low temperature caused demand surge of NG. As a result, node pressures decreased, and therefore NG supplied to GFGs was reduced [11]. Besides, the power system can also impact the NG system adversely through sudden demand or generation changing.

More recently, the NG system incorporates more compressor stations driven by electricity within its transportation [12]–[16], which are used to be driven by gas turbines. For example, the number of compressors driven by power accounts for about half of the total compressors in Texas Eastern [17]. There is also quite an amount of penetration of electric motor-driven compressors in California. The increasing prevalence of compressors powered by electric motors [13], [18], due to lower installation and maintenance cost, wide availability of power, as well as emissions concerns, leads to the increased reliance of the NG system on the power system and brings extra challenges. Interruptions in the power system may also cause the cut off of electricity to gas compressor stations driven by electric motors, and they will not operate without electricity.

Obviously, the increasingly tighter bi-directional physical dependence among energy systems leads to a higher risk of the EWEs' negative impacts to be amplified through the coupling link.

In this light, the bi-directional physical dependence between energy systems is

increasingly deep, which could amplify negative impacts of external disruptions, and present challenges to both systems. When a disruptive event occurs in one system, the effects can permeate to the connected ones, and maybe further loop back. Under the new situation, the conventional viewpoint of treating the NG and the power system as a stand-alone energy supply system is inadvisable. However, there is still a lack of scrutiny of the effects of infrastructure interdependence. It highlights the necessity to recognize, understand, model and analyze the interdependence between the NG and power systems for risk mitigation and fast system restoration.

1.1.2 EWEs and Impacts on Energy Systems

CIs are all subject to diverse operating conditions as both the internal and external environments are changing continuously. In comparison with normal and foreseeable weather conditions, EWEs are extensive and significantly uncertain in scale, space and time, and could place much higher stress on CI components even exceeding the design criteria, due to which CIs may suffer devastating damage with a higher probability when under EWEs. Thus, in addition to risks placed by complex interdependence, another challenge posed to the operation of CIs comes from EWEs, such as ice storms and hurricanes. For example, the 2008 China ice storm [19] and Hurricane Michael in 2018 [20] both led to widespread power outages.

In recent years, EWEs occurred more frequently. Taking the U.S. as an example, it has experienced ten severe weather events in 2019, which is the fifth consecutive year with ten or more billion-dollar weather and climate disaster events that have caused significant economic loss and casualties for the country. It also took an extended period to burn off the impacts that resulted in these events.

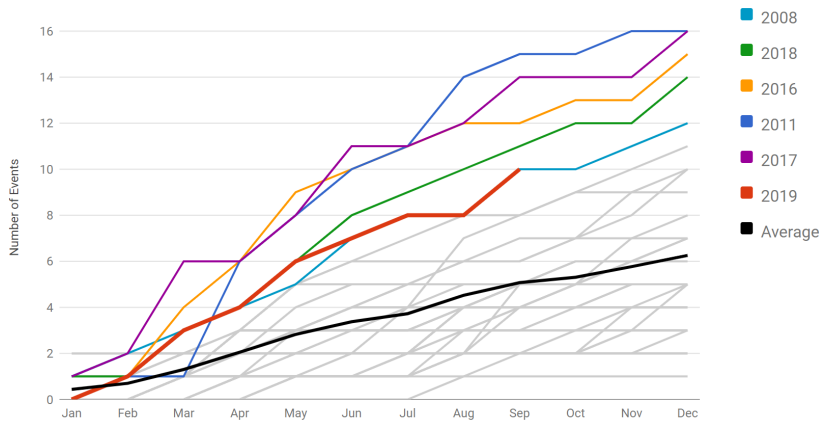

Figure 1.7: 1980-2019 year-to-date U.S. billion-dollar disaster event count (CPI-Adjusted) [4].

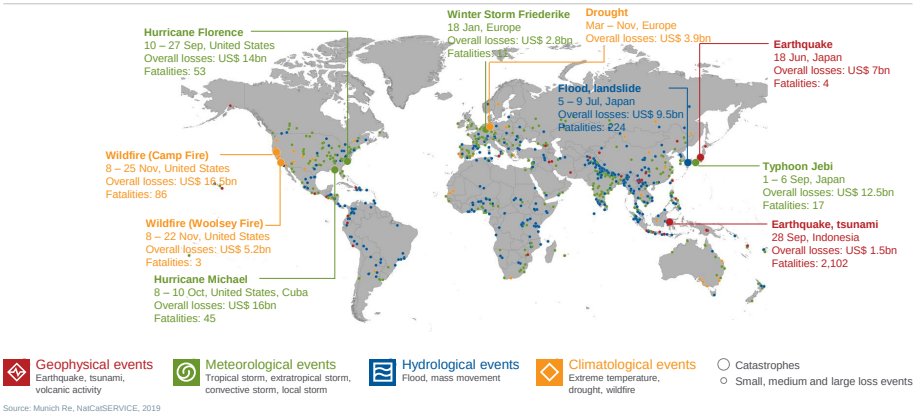

Figure 1.8: Natural loss events worldwide 2018 geographical overview [5].

The average events occurring annually is 6.3 for 1980–2018, then increased by one time to 12.6 for 2014–2018 (CPI-adjusted) as shown in Fig.1.7 [4].

Fig.1.8 [5] shows the geographical overview of natural loss events worldwide in 2018. It can be seen clearly that a large number of natural loss events distributed at every continent. What's more, the frequency and intensity of EWEs are expected to change in the future [21]. A complex mix of efforts is needed to withstand such harsh conditions that challenge the reliability of energy systems.

Unfortunately, CIs are easy to suffer extensive damage under EWEs, exposed to which energy system components do not fail randomly as in normal conditions but could sustain severe damages and result in disruption of service with a larger area and longer duration. Taking the power transmission network as an example, it consists of interconnected transmission lines, delivering electricity from power generation plants to substations over a large area. Its design and operation are under the key principles of reliability, such as adequacy and security [22], [23], to ensure a degree of reliability under normal conditions and foreseeable contingencies, where considerable research has been carried out and is already relatively mature. Nevertheless, it is impossible for the power system to withstand all kinds of unpredictable events, for example, hurricanes. The strong wind, together with torrential rain induced by a hurricane, could cause the failure of transmission lines in ways of damaging, collapsing transmission towers or blowing down conductors. Take the U.S. for instance, 800 to 1,000 tornadoes occur each year, leading to extensive damage and failure of transmission structures [24]. The majority of weather-related failures of transmission lines in the U.S. have been attributed to hurricanes. For example, Hurricane Rita in 2005 caused several power transmission towers damaged and collapsed [25], and left more than 1.3 million customers out of power at its peak [26]. In 2008, an unprecedented ice storm hit southern China, especially Hunan Province, where the power system suffered considerable damage of transmission lines, steel towers and transformers according to the State Grid Corporation of China [19]. New York City and the surrounding east coast were the hardest hit place of hurricane Sandy in 2012. It broke NG lines, and left approximately 8.5 million people dark, caused liquid fuel shortages and shutdown of the region's transportation system [27]. The state of Florida especially the South area was heavily affected by hurricane Irma in September 2017. Hurricane Irma caused significant damage to electrical facilities.

For example, it affected 120 transmission lines and 12 substations [28].

Besides, the interactions among power system elements, increasing demand, deregulation of the power market, hidden failures of delay protection devices (malfunction), lack of operators' experience all make the system operated closer to its designed margin when the criteria of security become more stringent. As a result, it is more challenging to provide a reliable power supply and restore the power system fast under EWEs.

Even worse, the threat from the EWEs and the risk introduced by interdependence working together can exacerbate the disastrous consequences. For instance, several gas facilities were closed due to electricity outages caused by hurricanes in 2005 and 2008 [26] in the U.S. In February 2011, the extreme cold and windy weather relentlessly assaulted Texas. The production decline of NG propagated downstream was among the issues plaguing the generation loss of GFGs. On the other hand, the electricity blackout in the gas production area aggravated the reduction of gas production [29].

1.2 Motivations

As introduced in the background, energy systems are facing challenges not only from increasing complex interdependence but also from frequently occurring EWEs, and these two kinds of risks could work together to make things worse. However, there is still a lack of consideration of this joint impact in a compatible way because of the complexity and interdisciplinary characteristics of the issue. In face of these challenges, we are motivated to investigate fully, understand deeply, model effectively, quantify properly, and manage actively of the combined effect of the EWEs and interdependence on the performance of integrated energy systems

to provide information for effective, coordinative and proactive preparedness to maintain reliable energy supply of interconnected energy systems under EWEs.

1.3 Major Contributions of the Thesis

This thesis explores the effect of NG fuel on power system reliability from a long-term time scale using the multi-state model of GFGs, investigates the spatial-temporal impacts of hurricanes on the short-term power system reliability, establishes the combined NG and power system analysis model considering inherent properties of each system and characteristics of interdependence coordinately, studies power system reliability considering the frequency control process under hurricanes, and develops a multi-attribute construct of metrics to evaluate energy system performance under hurricanes. Based on the assessment results, corresponding suggestions are provided, which can serve as a decision-making guide.

A: Reliability Evaluation of Power Systems Considering the Fuel Supply System

The utilization of NG as a primary fuel for electricity generation has been increasing in the past decades and is still a preferable choice for new generation capacity to overtake and replace the units relying on coal, leading to the rising dependence of the power system on the NG system. The reliance on NG for generating capacity imposes risks to power systems, such as failure propagation trigged by NG network contingencies. Taken together with the power system's intrinsic complexity, these factors could operate to amplify the power system's exposure to disruptive events. In this context, an effective method is developed to assess the impact of the associated NG fuel supply system on the long-term reliability of the transmission power system. The contribution can be summarized

as follows: 1) It integrated steady-state NG system model, optimal power flow model and the dependence model of power system on NG system for quantitative measurement purpose. 2) It proposed an integral simulation frame using non-sequential Monte Carlo simulation. The validity of the proposed method has been verified by simulations.

B: Spatial-temporal Reliability and Damage Assessment of Transmission Networks under Hurricanes

Hurricanes can damage power transmission network structure components, e.g., towers and conductors, and threat the power system reliability. To quantify the consequence severity of hurricanes on transmission networks, a spatial-temporal reliability and damage assessment method is proposed to evaluate the effect of a hurricane. The contribution can be summarized as follows: 1) The time-space varying impact of the hurricane with uncertainty on transmission network is considered through the component outage models. 2) Reliability indices, i.e., energy not supplied and asset damage indices, are integrated to quantify the performance of transmission networks under extreme weather events. The effectiveness of the proposed method has been verified by simulations. Simulation results show the method can quantify the hurricane impacts, identify the weak network parts, and provide information for pre-event preparedness and forecasting event applications.

C: Resilience Assessment of Integrated Energy Systems under Hurricanes

Energy systems, e.g., power systems and NG systems, are increasingly interdependent, which brings benefits under normal conditions and introduces risks under extreme weather events, e.g., hurricanes. A comprehensive method is proposed to reflect the spatial-temporal hurricane impacts on interdependent power and NG systems. The contribution can be summarized as follows: 1) it developed

a method that evaluates hurricane impacts on the performance of interdependent power and NG systems. 2) it proposed the integrated energy flow taking into account individual system properties and interface characteristics to minimize the joint load shedding. 3) It integrate operational and infrastructure indices to quantify the performance of interdependent systems. The effectiveness of the proposed method has been verified by simulations. Simulation results show the method can identify weak parts and quantify the performance of interdependent power and NG systems under hurricanes to provide information for effective and coordinative preparedness.

D: Resilience Assessment of Power Systems Under Hurricanes Considering Frequency Control Process

Under EWEs, e.g., hurricanes, failures of transmission lines due to strong wind and intense rainfall can cause significant generation and load imbalance and further result in unexpected frequency deviation from the required nominal value. An assessment method is proposed to reflect the negative hurricane impacts on the frequency performance of transmission networks. To mitigate these impacts on the day-ahead market from a probabilistic perspective, a resilient UC problem is formulated as a two-stage robust optimization (RO) problem solved using a column-and-constraint generation scheme. The contribution can be summarized as follows: 1) Develop a method that evaluates hurricane impacts on the frequency performance of power systems. 2) Propose the two-stage robust UC to mitigate the hurricane impacts on the day-ahead market from a probabilistic perspective. 3) employment of frequency indices to quantify the system performance. The modified IEEE 24-reliability test system under a simulated hurricane is used to validate the effectiveness of the proposed method. Simulation results show the hurricanes could cause frequency nadir or peak out of the required range and neglect of the frequency regulation process would lead to underestimation of the

hurricane adverse impacts. The method developed could be used as guidance of UC and regulation reserve capacity under EWEs.

1.4 Thesis Organization

This thesis explores the effect of NG fuel on power system reliability from a long-term time scale using multi-state models of GFGs, investigates the spatial-temporal impacts of hurricanes on the power system short-term reliability, establishes the combined NG and power system analysis model considering inherent properties of each system and characteristics of interdependence coordinately, studies power system reliability considering the frequency control process under hurricanes, and develops a multi-attribute construct of metrics to evaluate energy performance under hurricanes. Based on the assessment results, corresponding suggestions are provided which can serve as a decision-making guide.

Chapter 1 briefly introduces the research background, including energy systems and their interdependence, EWEs and their impacts on energy systems, research motivations, and contributions of this thesis.

Chapter 2 reviews the related literature on weather effects on power system reliability, focusing on the weather-related power component outage models, interdependence between the power system and NG system, and the development of resilience and its application in energy systems. It introduces the work that has been done on related topics and summarizes the limitations of current research work.

Chapter 3 explores the effect of NG fuel on power system reliability from a long-term time scale. The steady-state NG system model is used to calculate the probability and amount of NG fuel shortage of GFGs. The GFGs are represented

by multi-state reliability models to represent the output limit and probability considering the NG fuel shortage. Case studies are conducted on the modified Belgian gas transmission system and the IEEE-24 reliability test system to justify the validity of the proposed method.

Chapter 4 investigates the hurricane impacts on the power system's short-term reliability. Using both statistical component failure models and mechanism analysis based component failure models, a spatial-temporal reliability and damage assessment method of transmission networks under hurricanes is proposed. Considering the market processes in ERCOT [30] and PJM [31], etc., the load curtailment model is formulated as a RAC problem. The modified IEEE 24-reliability test system and the two-area IEEE reliability test system-1996 affected by a simulated hurricane, respectively, are used in the case study to validate the proposed method.

Chapter 5 proposes a comprehensive method to account for the spatial-temporal hurricane impacts on interdependent power and NG systems. It establishes the combined NG and power system analysis model considering the inherent properties of each system and characteristics of interdependence coordinately, and formulates the integrated energy flow as an optimization problem with the objective of minimum joint load shedding. The modified IEEE 24-reliability test system and the 12-node NG system under a simulated hurricane are used to validate the effectiveness of the proposed method.

Chapter 6 studies the power system performance under hurricanes considering the frequency control process. The primary, secondary and tertiary control considering the constraints of ramp rate and capacity of generators is modeled. The load not satisfied during the primary and secondary frequency process is included in the operational indices. Besides, frequency resilience indices are

proposed to describe system performance from the perspective of frequency and resilience. The modified IEEE 24-reliability test system under a simulated hurricane is used to validate the effectiveness of the proposed method.

Finally, Chapter 7 concludes and gives future works.

Chapter 2

Literature Review

A comprehensive review of the related literature is presented in this chapter. Initially, it investigates the works of weather effects on power system reliability, focusing on the weather-related power component outage models. Subsequently, it reviews papers in the area of interdependence between the power system and the NG system. At last, it introduces the development of resilience and its application in energy systems. The limitations of current work are summarized as well.

2.1 Effect of Weather Conditions on Power System Reliability

Quantitative reliability evaluation has been highly developed and widely applied in the power system planning, design and operation phase to provide electrical energy to customers as reliably and economically as possible. Deterministic criteria, such as N-1 contingency or predefined contingency list, were used to be dominant because it is relatively simple and easy to understand. The main drawback of the deterministic criteria is that it cannot reflect the stochastic behavior characteristics of electrical components, customers or systems, and may lead to underestimation or overestimation of the problem. Then the probabilistic method is used extensively in power system reliability assessment to capture the probabilistic nature of system behavior and reflect both the probability and the consequence severity of undesirable events.

Analytical and simulation methods are two widely used techniques in power system reliability evaluation, both of which have advantages and disadvantages. For large-scale complex systems consisting of a big number of components, the simulation method is a preferable choice. However, the application foundation of these two categories of evaluation techniques is component reliability models. Traditionally, two-state or multi-state component models were established [32], [33] to assess the system behavior for planning purposes, where the component reliability parameters, such as failure rate and repair rate are assumed to be constant in the long- time duration, such as one year. It is not the case when the system is exposed to severe weather conditions, which usually place much higher stress on the electrical components than normal weather conditions and can increase the probability of component failure and significantly affect the system reliability. As a result, reliability evaluation without considering the weather effects may lead to optimistic and misleading results. The impact of weather conditions on

component failure behaviors and further on the reliability evaluation results should be recognized and appropriately modeled.

Considerable works have been done to incorporate weather effects in analyzing power system component behaviors. Two-state weather model was proposed by [34] to divide the broad range of weather conditions into normal and adverse, in each of which the component failure and repair rate is still a constant average value related to outage numbers caused by adverse weather and the duration of adverse weather. The extensive employment of the two-state weather model is an important step to recognize the weather effect, although it is simple and maybe lead to optimistic results [35]. Then, the three-state weather model is proposed [36] to incorporate the massive effects of major adverse weather conditions into a reliability analysis. Besides, the multi-state weather model [36] can be introduced to incorporate the variability stress levels caused by the broad range of weather conditions to increase the weather modeling accuracy. Although the classification of weather states shows the importance of consideration of weather effects, they are developed for long-term power system reliability assessment and inadequate to represent the impacts of continuous time-varying weather conditions. On the other hand, the weather conditions to which electrical components exposed vary from one region to another. The regional weather model [22] is developed to include the regional weather effects on a transmission line traversing a large area by discretizing the large area into a set of subareas, in each of which the weather condition is assumed to be the same. Actually, weather conditions also change continuously over space, which has not been well reflected in regional models.

Under EWEs, the weather conditions, such as the wind and rainfall of a hurricane change with time, and at the same time, the hurricane moves across the networks. The failure probability of exposed components, e.g., power transmission towers, is closely related to the evolving weather conditions. Traditional

models, e.g., the two or multi-state weather models [33] and the regional weather model [37] are not adequate to capture the impact of time-space-changing weather conditions on component failure probabilities. Under the expectation of evaluation accuracy, considerable works have been done to include different factors that affect the component behaviors, such as factors representing weather severity and factors characterizing the terrain of component locations, and formulate the component failure model as functions of these factors. Some effort has been made to the field of operational reliability considering external factors, for example, [38] explores the impact of real-time operating conditions, such as power generation dispatch, load level, and network configuration, on the component's reliability models and fault consequences. [39] focuses on the impact of component overloading operation on component failure rate and system reliability. However, the effects of environmental factors, for example, strong wind or rainfall, are not centered on in these work efforts.

Data based statistical models [40], [41] including parametric [42]–[44] and non-parametric [45], [46] regression models, and mechanism analysis based models [47]–[49] take continuously changing weather severity factors as an input variable to component failure functions, thus can better reflect the spatial-temporal weather impact on component failure probabilities. The effectiveness of statistical models relies on the amount and quality of historical data [40], [41], [50]. In the situation of unavailability or insufficiency of relevant data, mechanism analysis based models are an alternative, such as fragility curves used in [51], [52]. These models can better describe the spatial-temporal impact of the hurricane by taking the continuous time-changing weather condition as an input variable of the component failure model.

Besides, to maintain reliable and stable service, the power system frequency must be regulated to be within the allowed range through frequency control. Many

studies have recognized the changing operation conditions and propose frequency control schemes, methods and strategies to solve problems arising. For example, energy storage is used for quick response [53], [54]; active load management is proposed to deviate the imbalance of generation and load to improve the system frequency performance [55]; load shedding strategies are developed to prevent system frequency out of range [56]. The majority of the studies particularly consider the effects of high penetration of renewable resources on frequency regulation, such as wind turbines and solar panels due to their intermittency and uncertainty features [57]–[60]. Sequential failures of transmission lines under EWEs could isolate loads or generator units and results in an imbalance between load and generation. Some work can be found to evaluate power system resilience under EWEs with indices from the perspective of infrastructure and load shedding [61]–[64], which cannot describe the degradation of system performance caused by the isolation of generators or loads. However, much less work has been done to include the frequency regulation process and its impact on the system performance under EWEs. [65] proposes islanding strategies considering the frequency constraints when splitting the system into islands.

2.2 Interdependent Power System and NG system

Historically, the power system and NG system are operated and managed in a decoupled approach, since there is no sufficient energy exchange between them. However, the increasing coupling makes it necessary to carry out the operation and management in a coordinated manner. It also becomes an active research field, which has drawn much attention. Papers published in this field fall into two broad categories: technical and market fields [14], where the latter one is out of the research scope in this thesis.

The technical analysis mainly for the purpose of operational planning. [66] reviews interdependence factors of power and NG from the perspective of markets and operations, and present potential solutions to address the issues. [67] models linkages among electricity, heat and NG distribution networks, and conduct the integrated analysis.

Under normal weather conditions, the coordination of interdependent power and NG systems has been well studied to utilize interdependence to achieve benefits in, e.g., co-optimal planning [68], [69], energy flow and optimal energy flow [70]–[73], and operation scheduling [74]–[78].

[68] uses the energy hub to represent coupling among multi-energy infrastructure and proposes an optimal planning model at long term timescale for the least-cost combined network of the power system and NG system. [69] proposes a robust co-optimization planning model for interdependent electricity and natural gas systems, intending to minimize total investment and operation costs.

[70] proposes a method for combined NG and electric OPF by solving PF firstly and then solving the GF problem. [71] develops a unified steady-state GF and PF, in which the effect of temperature is included. [72] formulates the optimal power and NG flow with a combination of contingency analysis, and provides preventive adjustments. Dynamic optimal energy flow is proposed in [73] with the integration of transit gas flow and steady state power flow and solved by transformation to linear programming. [79] proposes a data-driven distributionally robust optimization model for the optimal gas-power flow considering the uncertainties of wind generation and develops a convex optimization-based solution procedure.

[74]–[76] solve optimal security-constrained unit commitment (UC) problem with the impact of NG infrastructure. [11] develops a MIP UC that integrates impacts of the NG network. [80] also deals with the security-constrained UC

with uncertainties in the NG system but using fuzzy optimization. [77] proposes an effective multi-objective optimization approach for the coordinated operation of NG and electricity networks, considering the dynamic security of both systems. The [78] presents a two-stage robust generation scheduling model with consideration of dynamic characteristics of gas flow and wind uncertainty.

[81] presents an optimal model to calculate the maximum power that can be generated by GFGs for power system reliability analysis. [82] evaluates the reliability of the NG transmission system and its impact on the operation performance of the power system. [83] develops a sequential Monte Carlo model to minimize the cost of combined GB gas system and power system, calculates reliability metrics for power system and assesses the impact of gas storage capacity on GB gas network reliability.

Under EWEs, interdependence could introduce risks as disruptions in one system can permeate to the connected ones and may loop back through coupling links. For example, quit of gas compressors due to electricity cut off caused by EWEs may lead to gas load shedding, which could result in reduction even cut off of NG supplied to GFGs. A shortage of fuel could further contribute to the outage in the power system. However, little work is done to explore the performance of interdependent power and NG systems under EWEs, considering individual system properties and interdependence characteristics coordinately. [84] examines the extent of resource adequacy and the North American Bulk Power System's resilience to extreme weather events, and highlights the need for system planners to consider generator performance and potential fuel limitations during extreme weather events, the resource in natural-gas fired units for particularly adequacy assessment. [85] proposes an integrated transportation planning algorithm to improve the power system performance under EWEs by using NG transportation as a choice to mitigate the impacts of EWEs on exposed power systems. [86] proposes

a resilience-constrained unit commitment model to enhance the resilience of the integrated power distribution and NG system without modeling the hurricane impact on component failures directly. [87] proposes a proactive method to strengthen the preparedness of multiple energy carrier microgrids by energy storage, using the steady-state gas flow model without modeling compressors.

The background highlights the necessity to investigate, understand, model, and quantify the performance of interdependent power and NG systems under EWEs for coordinative and proactive preparedness.

2.3 Resilience of Energy Systems

The word resilience comes from the Latin word, which originally refers to the ability of an object to recover from or adjust easily to stress [88]. The concept of resilience was first utilized in ecology by the Canadian ecologist, C.S. Holling [89], and then developed broadly. Some literature proposes general concepts that can cover multi-disciplines [90]. Different interpretations of resilience are also offered in specific disciplines, such as organization, society, economy and engineering. "Future Resilient Systems" at Singapore-ETH Centre proposes a resilience framework that is based on eight generic functions: attentiveness, robustness, resistance, re-stabilization, rebuilding, reconfiguration, remembering, and adaptiveness, which are characterized with AR^6A acronym [91] as shown in Fig.2.1.

The more considerable effort has been made in the non-engineering domain, which implies larger space in impacting resilience in engineering [92]. In the context of the power system, although various attempts have been made to define the power system resilience [91], [93]–[96], no universal definition is accepted by

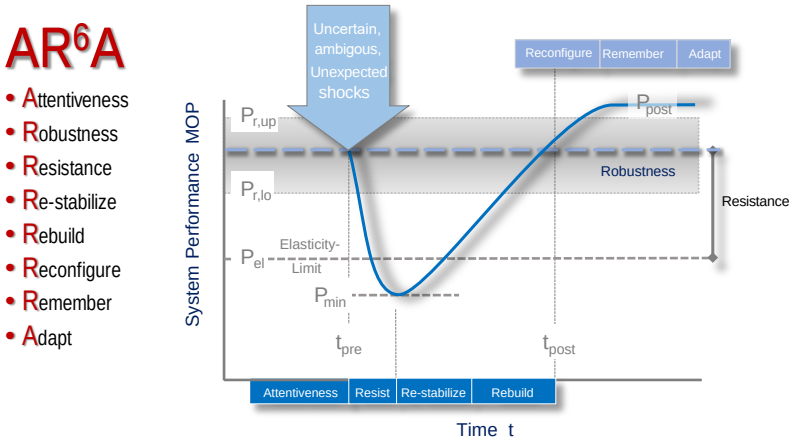

Figure 2.1: AR^{6}A conceptual resilience curve

all. The work of power system resilience tends to be grouped into three kinds: conceptual and qualitative studies, modeling and simulation approaches as well as strategies to improve system resilience.

The first includes related government reports and some framework literature. In 2010, a smart grid system report [97] released by the U.S. Department of Energy first clearly confirmed that resilience should be one main feature of the smart grid. In 2010, the U.S. Department of Homeland Security put forward requirements for power system resilience. The U.S. mainly focuses on investment improvement, resilience theory and metrics, performance promotion of smart grid technology, distributed energy, demand-side response, microgrid under disasters, and interdependence among CIs. In 2009, the U.K. launched a project called "Resilient Electricity Networks for Great Britain (RESNET)." It aims to demonstrate a comprehensive approach, analyze at a national scale of climate-related changes in the reliability of the grid, and develop tools for quantifying resilience enhancement strategies. [98] introduces main research activities and findings of RESNET, and provides useful insights into modeling the impact of weather events and resilience assessment. However, it still relies on the traditional

reliability metrics to evaluate system resilience. From the resilience perspective, multi-dimensional metrics should be introduced. In 2014, CIGRE released the report "Disaster recovery within a CIGRE Strategic framework: network, resilience, trends and areas of future work". It reflects the fact that resilience has become a major topic in the area. H. H. Willis [99] provides a comprehensive literature review on resilience metrics developed for energy systems, including the power system and NG system. M. Panteli and P. Mancarella [88] provide outlines of power system resilience and potential boosting adaptions for general understanding.

The modeling and simulation approach usually aims at quantitative assessment. The resilience of a system is a time-dependent function affected by several factors [100], such as disruptive events, resource constraints, and control strategies. Generic resilience metrics and formulae are proposed in [101], [102] to quantify system resilience. These general resilience metrics cannot be applied directly to power system resilience assessment before refinement to include specific power system characteristics. Great previous efforts have been made to model natural disasters impacts on the power system, such as damage caused, outage duration, and restoration [103]. [104] uses the system performance response process following the occurrence of a hazard to quantify resilience. A time-dependent resilience metric is introduced based on the performance curve. DC-based OPF is used, while hidden failure, as well as operator and communication errors, are also taken into consideration. It can provide decision-making help for operation and enhancement measures. However, the resilience metric cannot describe the system features from multi-dimension. A multi-stage infrastructure resilience analysis framework is proposed in [105]. Resilience-based improvement strategies are also highlighted. The approach proposed can be adequate for both single hazards and concurrent multiple hazard types. [106]

provides two measures to evaluate component importance based on resilience. It can be used to provide information for cascading failure control and restoration strategies. An analysis framework focused on adaptive capacity, absorptive capacity, and recoverability provides different perspectives [107]. [61], [108], [109] assess the power system resilience under EWEs, based on component fragility curve. Furthermore, [110] takes the impacts of load into account. [63] develops a resilience metric to quantify the effects of control strategies for resilient operation purposes or short term planning. [111] creates resilience metrics considering threats, likelihood, consequence, and resilience analysis process for energy systems in the U.S. The process is then applied to different energy systems, such as power systems and NG systems. However, these systems are treated separately instead of an integrated energy system. The smart grid resilience assessment model is outlined in [112]–[114]. [115] explores how winter storm in the UK affects the well-being of household and provides strategies to alleviate this kind of risk to improve resilience from everyday household-level life.

Promoting solutions should be combinations of related factors, such as human, technology, processes, as well as policies and regulations. It also requires coordination and collaboration at different levels to address the issue. There has been extensive work providing the power system resilience enhancement measures [116], [117]. Generally, improvement measurements can be classified into the following catalogs.

1) Grid Modernization ("smart grid") Technologies [118]–[120]

It can be applied to achieve fault location and isolation, and reduce the restoration time through automated feeder switching. Besides, integrated advanced metering infrastructure has helped to limit power outages, as well as the number

of homes and businesses affected.

2) Hardening of Critical Physical Infrastructure

Different from improvement in management and policies, "Hardening" mainly means reinforcement or upgrade of physical components. For example, circuit undergrounding, pole and tower upgrade, flood protection [121] can all increase the system's ability to resist EWEs. Grid modernization ("smart grid") technologies and "Hardening" investments should be integrated to reinforce each other to prevent and decrease the impacts.

3) Microgrids, Energy Storage, Distributed Generation Technologies [63], [121], [122]

Microgrids, energy storage and distributed generation technologies can help to provide power to critical loads in an emergency. Microgrids can be used as a backup power source and operated separately during emergencies, or can serve as start source after power system failures to reduce the restoration time. Mobile generators can provide temporary power to critical loads to ensure basic social functions such as the health system and the transportation signal system.

4) Enhanced Damage Prediction Models [123]

Improved modeling capabilities can promote system resilience by better predicting facility susceptibility and reducing damage to the system. Response planning and personnel safety can also be improved with reduced costs. The effectiveness of potential reinforcements can also be analyzed by predictive models.

The resilience promotion is a complex issue involving cost-benefit analysis, management, personnel even policy and legislation. The published literature cannot provide such tools for quantitative analysis of a specific strategy or

comparison of competitive strategies. General advice cannot be used as decision-making tools to acquire trade-off between investment and benefit; that's why quantitative models and tools should be developed.

2.4 Research Limitations in Literature

Although the impacts of EWEs and interdependence among CIs have been explored respectively in existing research, their combined effects have less been explored due to the complexity and interdisciplinary characteristics of the problem.

Besides, in addition to renewable energy resources, EWEs, as well as interdependence among energy systems could also cause serious system frequency deviation, which has attracted less attention in the literature. EWEs caused power component failures could result in a reduction of transmission capacity or loss of loads and generation units; at the same time reduction or cut off of NG fuel may cause inadequacy of generation capacity. Thus, the system frequency control process should be included in the system performance assessment under EWEs and corresponding indices related to frequency should br proposed to describe and quantify the system frequency behavior in order to provide guidance for regulation reserve setting and resilience improvement.

2.5 Summary

This chapter summarizes the literature in related research areas of this thesis. The models of weather effects on power system reliability are introduced, including the two-state, multi-state weather models, regional weather model, statistic-based models and mechanism-based models. Interdependence between the power system and NG system is investigated, including research works in integrate

energy flow and optimal energy flow, optimal planning and scheduling, reliability analysis. The concept and development of resilience as well as research activities in energy system resilience.

Chapter 3

Reliability Evaluation of Power Systems Considering the Fuel Supply System

The utilization of NG as a primary fuel for electricity generation has been increasing in the past decades and is still a preferable choice for new generation capacity to overtake and replace the units relying on coal, leading to the rising dependence of the power system on the NG system. The reliance on NG for generating capacity imposes risks to power systems, such as failure propagation trigged by NG network contingencies, and affects the power system reliability. In this context, this chapter develops an effective method to assess the impact of the associated NG fuel supply system on the long-term reliability of the transmission power system. It integrates the steady-state NG system model, optimal power flow model and the multi-state GFG model for quantitative measurement purposes, and proposes an integral simulation frame using non-sequential Monte Carlo simulation. The performance of power system is evaluated based on two metrics: Expected Demand Not Supplied (EDNS) and Probability of Load Curtailments (PLC). Case studies are conducted on the modified Belgian gas transmission system and the IEEE-24 reliability test system to justify the validity of the proposed method. The simulation results show the validity of the method.

3.1 Introduction

The power system is the backbone of our modern society, and blackouts in the power system could lead to disastrous consequences. Thus high reliability is the primary criterion of power supply to enable normal social function. However, this is not always the case due to the stochastic behavior of components, customers and the system. In addition to the random component failure, the shift of fuel from coal to NG in power generation also introduces new threats to power system reliability.

The NG has been increasingly used as the primary fuel in power generation and still a preferable choice for a variety of reasons, such as technological advancements, environmental friendliness and economic profit. The power system is linked more closely physically and economically to the NG system. The relying on NG exposes the power system to new challenges from the contingencies in the fuel supply system. For example, outages of pipelines in the NG system could lead to a shortage or cut off of NG providing to some GFGs and result in a decrease of output or quit of these GFGs, even further cause power load shedding due to generation capacity insufficiency. Compared with coal-fired plants that usually maintain fuel to sustain at least several days, the GFGs are more vulnerable to fuel-supply interruptions, which has negative impacts on the power system reliability. Traditionally, the planning and scheduling of power systems and NG systems are incompatible, and the conventional view is treating power system as a stand-alone energy supply system, which is inadvisable any more as the power system is exposed to interruptive events in the NG supply and delivery. The changing scenario highlights the necessity to understand, model and analyze the fuel adequacy impacts on the power system reliability for better planning, operation and risk mitigation.

To address the issue, this chapter aims to generate a preliminary integral analysis frame for power system reliability assessment considering the impact of NG fuel supply by using a multi-state reliability model for GFGs whose reliability parameters are directly related to the point reliability indices of GFGs's locations in the NG system.

The remainder of this chapter is structured as follows. Section 3.2 develops system models, including the steady-state NG and power system model. Section 3.3 presents the reliability model and assessment method. Section 3.4 covers case studies and simulation results. Section 3.5 summarizes.

3.2 System Model

3.2.1 Steady-state NG System Model

Similar to the power system, an NG system can be divided into supplies, transmission system, distribution system and customers. For this thesis, only the NG transmission system with high pressure is considered.

An NG transmission system can be modeled as a directional graph made of nodes and components. Nodes are the terminals of one or more components or the points where the gas is injected in or extracted from. Node connecting components are the elements that connect two nodes, such as pipelines and compressors.

Like PF in a power transmission line, the GF in a pipeline is from the higher-pressure node to the lower-pressure node. The constraint of pipeline operating pressure depends on the pipeline material and age. The general steady-state gas flow rate through a pipeline is governed by the energy balance equation. For a horizontal pipeline k from node i to node j, the NG flow rate is determined by

pressure drop along the pipeline [70], [124] as follows:

$$Q_{\mathrm{gp},k} = S_{\mathrm{gp},k} \times 3.2387 \frac{T_{\mathrm{sc}}}{\mathcal{P}_{\mathrm{sc}}} \sqrt{S_{\mathrm{gp},k} \frac{\left(\mathcal{P}_i^2 - \mathcal{P}_j^2\right) D_{\mathrm{gp},k}^5}{f_k G L_{\mathrm{gp},k} T_{ka} Z_a}}, \ \forall k \in \mathcal{E}_{\mathrm{gp}} \tag{3.1}$$

where $\mathcal{E}_{\mathrm{gp}}$ is the set of gas pipelines. $Q_{\mathrm{gp},k}$ (SCF·h^{-1}) is the flow rate through pipeline k. T_{sc} (R) is the standard temperature. $\mathcal{P}_{\mathrm{sc}}$ (psia) is the standard pressure. $\mathcal{P}_i$ (psia) and $\mathcal{P}_j$ (psia) are the pressure of node i, j respectively. $D_{\mathrm{gp},k}$ (in) is the diameter of pipeline k. f_k is the friction factor. G is the gas specific gravity. $L_{\mathrm{gp},k}$ (km) is the length of pipeline k. T_{ka} (R) is the average gas temperature. Z_a is the gas compressibility factor. $S_{\mathrm{gp},k}^{ij}$ represents the direction of the gas flow. $S_{\mathrm{gp},k}$=1 if $\mathcal{P}_i$>$\mathcal{P}_j$, otherwise $S_{\mathrm{gp},k}^{ij}$= -1.

For a high-pressure NG transmission network, (3.1) can be rewritten as follows [125]:

$$Q_{\mathrm{gp},k} = S_{\mathrm{gp},k} C_{\mathrm{gp},k} \sqrt{S_{\mathrm{gp},k} \left(\mathcal{P}_i^2 - \mathcal{P}_j^2\right)}, \ \forall k \in \mathcal{E}_{\mathrm{gp}} \tag{3.2}$$

where $C_{\mathrm{gp},k} = \eta_{\mathrm{gp},k} 18.062 T_{\mathrm{sc}} D_{\mathrm{gp},k}^{\frac{8}{3}} / \mathcal{P}_{\mathrm{sc}} \sqrt{G L_{\mathrm{gp},k} T_{ka} Z_a}$. $\eta_{\mathrm{gp},k}$ is the pipeline efficiency.

During long distance transportation in pipelines, the NG suffers part of energy loss. Compressors driven by gas or electricity become essential to reduce NG volume and force it to flow. The turbine and engine compress NG by consuming a small amount of gas from the pipeline, while the motor accomplishes compression using reliable electricity. Here only the centrifugal compressor is modeled. The gas flow rate through a compressor is determined by its horsepower consumption that can be expressed as follows [124]:

$$HP_{\mathrm{gc},c} = \frac{\mathcal{P}_i Q_{\mathrm{gc},c} c_{\mathrm{k}}}{\eta_{\mathrm{gc},c} (c_{\mathrm{k}} - 1)} \left[\left(\frac{\mathcal{P}_j}{\mathcal{P}_i} \right)^{\frac{c_{\mathrm{k}}-1}{c_{\mathrm{k}}}} - 1 \right], \ \forall c \in \mathcal{E}_{\mathrm{gc}} \tag{3.3}$$

where $\mathcal{E}_{\mathrm{gc}}$ is the set of gas compressors. $HP_{\mathrm{gc},c}$ (hp) is the horsepower of compressor c with inlet node i and outlet node j. $\mathcal{P}_i$ and $\mathcal{P}_j$ (psia) are the

compressor suction and discharge pressure at node i and j, respectively. $Q_{\mathrm{gc},c}$ ($\mathrm{SCF{\cdot}h^{-1}}$) is the flow rate through compressor c. NG in a compressor always flows from the inlet node to the outlet node. $\eta_{\mathrm{gc},c}$ is the compressor efficiency. c_{k} is the specific heat ratio ($c_{\mathrm{p}}/c_{\mathrm{v}}$, where c_{p} is the heat capacity at constant pressure, c_{v} is the heat capacity at constant volume).

The gas required by a gas-driven compressor c, $Q_{\mathrm{g2c},c}$ ($\mathrm{SCF{\cdot}h^{-1}}$) can be approximately calculated as follows:

$$Q_{\mathrm{ggc},c} = a^1_{\mathrm{gc},c} + a^2_{\mathrm{gc},c} HP_{\mathrm{gc},c} + a^3_{\mathrm{gc},c} \left(HP_{\mathrm{gc},c}\right)^2, \ \forall c \in \mathcal{E}_{\mathrm{ggc}} \tag{3.4}$$

where $\mathcal{E}_{\mathrm{ggc}}$ is the set of compressors driven by gas turbines. $a^1_{\mathrm{gc},c}$, $a^2_{\mathrm{gc},c}$, and $a^3_{\mathrm{gc},c}$ are compressor gas consumption coefficients.

For compressors driven by electricity, the active power $P_{\mathrm{egc},c}$ (MW) consumed by compressor c is calculated as follows [8]:

$$P_{\mathrm{egc},c} = \eta_{\mathrm{egc}} HP_{\mathrm{gc},c} \ \forall c \in \mathcal{E}_{\mathrm{egc}} \tag{3.5}$$

where $\mathcal{E}_{\mathrm{egc}}$ is the set of compressors driven by electricity. η_{egc} is constant.

A compressor can be specified by the compression ratio, inlet or outlet pressure, or flow rate. For compressor c with given compression ratio $RC_{\mathrm{gc},c}$, it is described as follows:

$$RC_{\mathrm{gc},c} = \frac{\mathcal{P}_j}{\mathcal{P}_i}, \ \forall c \in \mathcal{E}_{\mathrm{gc}} \tag{3.6}$$

Contingencies in an NG network such as component failures are not rare. Most of the time, an NG system can step into a new steady state through redispatch or adjustment without disturbance to end customers. However, in some cases, load curtailment is inevitable due to the operating constraints. In practical, optimal shedding strategies are developed with different objectives, such as minimum cost,

priority list or minimum load shedding. The OGF is used in this chapter with the objective of minimum load shedding as follows:

$$\text{Min} \sum_{i \in \mathcal{N}_{\text{gd}}} Q_{\text{lc},i} \tag{3.7}$$

subject to (3.2) to (3.4), (3.6) and

$$\Delta Q_i = \sum_{k \in \mathcal{E}^-_{\text{gp},i}} Q_{\text{gp},k} - \sum_{k \in \mathcal{E}^+_{\text{gp},i}} Q_{\text{gp},k} + \sum_{c \in \mathcal{E}^-_{\text{gc},i}} Q_{\text{gc},c} - \sum_{c \in \mathcal{E}^+_{\text{gc},i}} Q_{\text{gc},c}$$

$$+ \sum_{c \in \mathcal{E}_{\text{ggc},i}} Q_{\text{ggc},c} - \sum_{s \in \mathcal{S}_i} Q_{\text{gs},s} + Q_{\text{gd},i} = 0, \ \forall i \in \mathcal{N}_{\text{g}} \tag{3.8}$$

$$Q^{\min}_{\text{gs},s} \le Q_{\text{gs},s} \le Q^{\max}_{\text{gs},s}, \ \forall s \in \mathcal{S} \tag{3.9}$$

$$\mathcal{P}^{\min}_i \le \mathcal{P}_i \le \mathcal{P}^{\max}_i, \ \forall i \in \mathcal{N}_{\text{g}} \tag{3.10}$$

$$-Q^{\max}_{\text{gp},k} \le Q_{\text{gp},k} \le Q^{\max}_{\text{gp},k}, \ \forall k \in \mathcal{E}_{\text{gp}} \tag{3.11}$$

$$HP^{\min}_{\text{gc},c} \le HP_{\text{gc},c} \le HP^{\max}_{\text{gc},c}, \ \forall c \in \mathcal{E}_{\text{gc}} \tag{3.12}$$

$$0 \le Q_{\text{lc},i} \le Q_{\text{gd},i}, \ \forall i \in \mathcal{N}_{\text{gd}} \tag{3.13}$$

where $\mathcal{E}^-_{\text{gp},i}$ and $\mathcal{E}^+_{\text{gp},i}$ is the set of pipelines from node i. $\mathcal{E}^+_{\text{gp},i}$ is the set of pipelines to node i. $\mathcal{E}^+_{\text{gc},i}$ is the set of compressors with outlet node i. $\mathcal{E}^-_{\text{gc},i}$ is the set of compressors with inlet node i. $\mathcal{S}_i$ is the set of NG sources connected to node i. $\mathcal{E}_{\text{ggc},i}$ is the set of compressors fueled by NG extracted from node i. $\mathcal{N}_{\text{g}}$ is the set of NG nodes. $Q_{\text{gs},s}$ (SCF·h^{-1}) is the flow rate of gas source s. $Q_{\text{gd},i}$ (SCF·h^{-1}) is the NG load at node i. $\mathcal{N}_{\text{gd}}$ is the set of NG nodes with loads. $Q_{\text{lc},i}$ (SCF·h^{-1}) is the gas load curtailment at node i. $Q^{\min}_{\text{gs},s}$ and $Q^{\max}_{\text{gs},s}$ (SCF·h^{-1}) are gas supply bounds of node i. $\mathcal{P}^{\min}_i$ (psia) and $\mathcal{P}^{\max}_i$ (psia) are operation pressure bounds of node i. $Q^{\max}_{\text{gp},k}$ (SCF·h^{-1}) is the flow rate bound of pipeline k. $HP^{\min}_{\text{gc},c}$ and $HP^{\max}_{\text{gc},c}$ are minimal and maximal horsepower of compressor c.

(3.2.1) expresses the NG flow balance at each node as the algebraic sum of NG injected and extracted. (3.9) describes the bounds of NG source output. (3.10) shows the limits of node pressure. (3.11) gives the capacity bounds of pipelines. (3.12) limits the horsepower of compressors. (3.13) limits the amount of load curtailment at each node.

To simplify this optimal issue, a new variable Π is introduced where $\Pi = \mathcal{P}^2$. Then, in addition to (3.2) to (3.4), (3.6), (3.2.1) to (3.13), the objective function (3.7) is also subject to:

$$\Pi_i^{\min} \leq \Pi_i \leq \Pi_i^{\max}, \ \forall i \in \mathcal{N}_{\mathrm{g}} \tag{3.14}$$

$$\left(Q_{\mathrm{gp},k}\right)^2 = (2I_k - 1)\left(\Pi_i - \Pi_j\right) C_{\mathrm{gp},k}^2, \ \forall k \in \mathcal{E}_{\mathrm{gp}} \tag{3.15}$$

$$Q_{\mathrm{gp},k} \leq 2I_k Q_{\mathrm{gp},k}, \ \forall k \in \mathcal{E}_{\mathrm{gp}} \tag{3.16}$$

where $\Pi_i^{\min} = \left(\mathcal{P}_i^{\min}\right)^2$, $\Pi_i^{\max} = \left(\mathcal{P}_i^{\max}\right)^2$, $\Pi_i = (\mathcal{P}_i)^2$, $\Pi_j = \left(\mathcal{P}_j\right)^2$. $I_k = 0$ if $\Pi_i < \Pi_j$, otherwise $I_k = 1$.

To solve the modified optimization problem, an existed mixed integer programming solver SCIP (Solving Constraint Integer Programs) [126] is used.

3.2.2 Power System Model

The AC PF model is nonlinear and non-convex, while the DC PF extends the decoupling principle to form linear constraint sets, and only active power equations are considered.

Compared to AC PF, DC PF is more computation efficient as it reduces the computation time and iteration number by simplification. Due to this characteristic, it is widely employed in long-term planning and real-time security analysis, where calculating speed is dominant with conflict of accuracy.

The DC power flow equations are based on three assumptions: the line resistance is much smaller than the line reactance, $\left|G_{\mathrm{br},k}\right| \ll \left|B_{\mathrm{br},k}\right|$; the voltage angle difference at adjacent buses θ_{ij} is small; and all bus voltage magnitudes are approximated as 1.0 p.u., $U_i \approx U_j \approx 1.0$p.u. For a transmission branch k from bus i to j, the active power flows through is expressed as follows::

$$P_{\mathrm{br},k} = -B_{\mathrm{br},k}\theta_{ij},\ \forall k \in \mathcal{E}_{\mathrm{br}} \tag{3.17}$$

where $\mathcal{E}_{\mathrm{br}}$ is the set of power transmission branches. $P_{\mathrm{br},k}$ (MW) is the active power through branch k with the direction from bus i to j. $B_{\mathrm{br},k}$ (S) is the branch susceptance. θ_{ij} (rad) is angle difference between bus i and j.

The power bus balance equation is thus presented as follows:

$$\sum_{k\in\mathcal{E}^{-}_{\mathrm{br},i}} P_{\mathrm{br},k} - \sum_{k\in\mathcal{E}^{+}_{\mathrm{br},i}} P_{\mathrm{br},k} + P_{\mathrm{ed},i} - \sum_{g\in\mathcal{G}_i} P_{\mathrm{eg},g} = 0,\ \ \forall i \in \mathcal{N}_{\mathrm{e}} \tag{3.18}$$

where $\mathcal{E}^{-}_{\mathrm{br},i}$ is the set of power branches from node i. $\mathcal{E}^{+}_{\mathrm{br},i}$ is the set of power branches to node i. $\mathcal{G}_i$ is the set of power generators at bus i. $\mathcal{N}_{\mathrm{e}}$ is the set of power buses. $P_{\mathrm{eg},g}$ is the active power generation of generator g. $P_{\mathrm{ed},i}$ is the power load at bus i.

Except for the reference bus, all bus active power injection can be expressed in the form of (3.18). This equation set forms the modeling of DC PF.

A GFG acts as a gas consumer in the NG system. The NG it consumes can be calculated by the following equation [127]:

$$Q_{\mathrm{gfg},g} = \frac{HR_{\mathrm{gfg},g}}{GHV},\ \forall g \in \mathcal{E}_{\mathrm{gfg}} \tag{3.19}$$

where $\mathcal{E}_{\mathrm{gfg}}$ is the set of GFGs. $Q_{\mathrm{gfg},g}$ ($\mathrm{SCF{\cdot}h^{-1}}$) is NG required by GFG g. GHV ($\mathrm{BTU{\cdot}SCF^{-1}}$) is the gross heating value. $HR_{\mathrm{gfg},g}$ ($\mathrm{BTU{\cdot}h^{-1}}$) is the heat rate required by GFG g, calculated as follows:

$$HR_{\mathrm{gfg},g} = a_{\mathrm{gfg},g} + b_{\mathrm{gfg},g}P_{\mathrm{gfg},g} + c_{\mathrm{gfg},i}\left(P_{\mathrm{gfg},g}\right)^2,\ \forall g \in \mathcal{E}_{\mathrm{gfg}} \tag{3.20}$$

where $P_{\mathrm{gfg},g}$ (MW) is active power output of GFG g. $a_{\mathrm{gfg},g}$, $b_{\mathrm{gfg},g}$, and $c_{\mathrm{gfg},g}$ are heat rate coefficients of GFG g.

Generally, while acceptable system performance is maintained in terms of constraints, there are several available steady-state operating points. Determination of the most optimal state with a given objective, such as minimum fuel cost or network loss, is the OPF problem. It was firstly introduced in the 1960s by Carpentier and is a useful tool for steady-state power system analysis.

The general mathematical formulation of OPF is given as follows:

$$\min f(x) \tag{3.21}$$

subject to

$$\begin{aligned} g(x) &= 0 \\ h(x) &\leq 0 \end{aligned} \tag{3.22}$$

The equality constraint $g(x) = 0$ includes the branch power flow constraint as in (3.17), bus power balance as in (3.18), etc., while the inequality constraint $h(x) \leq 0$ includes generator output bounds, voltage magnitude bounds, transmission line capacities, and so on.

The OPF problem can be solved by the AC or DC power flow. For the AC version, the state variable vector x is the ungiven voltage angles and magnitudes, generators' active and reactive generation. For the DC version, it is the voltage angles and generators' active generation. In this chapter, the DC OPF function in Matpower 6.0b1 is employed for its calculation efficient as Monte Carlo simulation will introduce a considerable amount of calculation with a large-scale system.

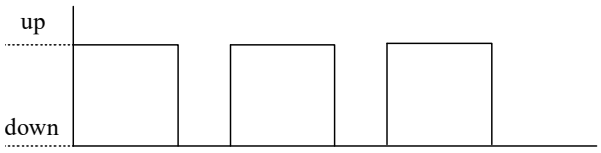

Figure 3.1: Up and down process of a repairable component [6].

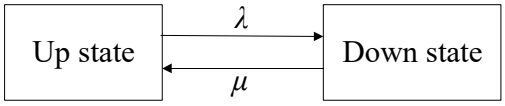

Figure 3.2: State space diagram of a repairable component [6].

3.3 Reliability Assessment

In this section, a frame of power system reliability evaluation considering the fuel supply system is put forward. The developed framework can be generally adopted in different target systems according to specific purposes and requirements.

3.3.1 Component Outage Modeling

A CI system is comprised of many interconnected components. The development of component outage models is fundamental for the system reliability assessment. Component outages can be classified according to modes, such as repairable forced outages, planned outages, aging failures, common cause failures.

The most common component failure is the repairable forced outages that can be modeled by the up-down-up cycle process illustrated by Fig.3.1. The state transition is shown in Fig.3.2.

The long term component unavailability can be expressed mathematically as

follows [6]:

$$U = \frac{\lambda}{\lambda + \mu} = \frac{MTTR}{MTTF + MTTR} \tag{3.23}$$

where λ (failures/year) is the failure rate. μ (repairs/year) is the repair rate. $MTTR$ (h) and $MTTF$ (h) are the mean time to repair and failure, respectively.

3.3.2 System State Selection

Compared with small-scale systems in which general evaluation methods can be directly employed, such as probability convolution, series and parallel networks, minimum cutsets, Markov equations, and frequency-duration approaches, for large-scale complex systems, critical processes are system state selection and system analysis.

The system state is essential for system analysis to calculate metrics. Generally, two methods are usually used for system state selection: state enumeration and Monte Carlo simulation. For large-scale and complex systems, Monte Carlo simulation is a preferred method due to its advantages, such as more accurate, easy to understand and implement, able to calculate indices expectation and distribution. Its main disadvantage is the computation burden in order to obtain accurate results. This weakness can be alleviated by advanced computer technology such as parallel computation.

Monte Carlo simulation simulates the system state based on random numbers. Basically, there are two kinds of simulation method: non-sequential Monte Carlo method and sequential Monte Carlo method.

Non-sequential Monte Carlo simulation is used in this chapter. For a two state

modeled component, its state can be determined as follows:

$$s_i = \begin{cases} 0\,(\text{success}) & \text{if } r_i > \pi_{\mathrm{d},i} \\ 1\,(\text{failure}) & \text{if } r_i < \pi_{\mathrm{d},i} \end{cases} \tag{3.24}$$

where s_i is the state of component i. $\pi_{\mathrm{d},i}$ is the failure probability of component i. r_i is a random number generated uniformly in $[0,\ 1]$.

For a component with multi states, its state can be determined similarly. For instance, for a three states component:

$$s_i = \begin{cases} 0\,(\text{success}) & \text{if } r_i > \pi_{\mathrm{dr},i} + \pi_{\mathrm{d},i} \\ 1\,(\text{failure}) & \text{if } \pi_{\mathrm{dr},i} < r_i \leq \pi_{\mathrm{dr},i} + \pi_{\mathrm{d},i} \\ 2\,(\text{derated}) & \text{if } 0 \leq r_i \leq \pi_{\mathrm{dr},i} \end{cases} \tag{3.25}$$

where $\pi_{\mathrm{dr},i}$ is the probability of the derated state. This expression can be easily expanded to components with multi derated states.

Then the system state can be presented as the combination of comprised components as follows:

$$s = (s_1, \ldots, s_i, \ldots s_n) \tag{3.26}$$

where n is the number of components in the system.

In order to obtain the estimated probability of a system state, sufficient samples are compulsory. Then the sampling frequency of the system state can be used as an unbiased estimate of its probability as follows:

$$\pi_{\mathrm{s},i} = \frac{n_{\mathrm{s},i}}{n_{\mathrm{sp}}} \tag{3.27}$$

Where $\pi_{\mathrm{s},i}$ is the estimated probability of state i. n_{sp} is the number of samples and $n_{\mathrm{s},i}$ is the number of occurrences of system state i in the sampling.

Once the probability of each system state is estimated in the sampling, the system failure probability and other indices can be calculated through the system analysis.

3.3.3 System Analysis

For a failure system state, in order to calculate indices, system analysis should be conducted. Generally, the techniques of identifying and analyzing problems in a system state are the same for different engineering systems. These include contingency analysis for problem recognition and optimization for remedial actions. In this chapter, we mainly focus on the power composite system and the NG composite system.

For both systems, when an outage causes system problems, the OPF or OGF model is used to reschedule supplies and eliminate constraint violations, and at the same time to avoid any load curtailment if possible or to minimize the total load curtailment if unavoidable. In this chapter, the objective function of the optimization models is to minimize the total load curtailment, whereas the load curtailments at power buses or NG nodes are the parts of the model solution. The indices are based on the load curtailments in selected system outage states and their probabilities of occurrence [6].

3.3.4 Reliability Indices

After analysis of the failed system states outlined in the previous steps, reliability indices can be calculated straightforward.

In this chapter, PLC and EDNS are used as performance indices to quantify the power system performance considering fuel impacts. By employment of Monte Carlo simulation, the system indices can be calculated as follows [6]:

$$\mathrm{PLC} = \sum_{i \in S_{\mathrm{lc}}} \pi_{\mathrm{s},i} \tag{3.28}$$

where S_{lc} is the set of all system states associated with load curtailment.

$$\mathrm{EDNS} = \sum_{i \in S} \pi_{\mathrm{s},i} P_{\mathrm{lc},i} \tag{3.29}$$

where $P_{\mathrm{lc},i}$ is the load curtailment of state i.

Load point indices can be obtained similarly.

3.3.5 Proposed Approach

The assessment procedure described in this chapter can be directly applied to any individual CI system. However, for an integrated energy system, it is necessary to consider recasting the model and procedure due to the emergence of independence. For instance, a GFG can be presented by the two-state model when its fuel source is always sufficient and 100% reliable. However, in the event that there is a shortage of fuel, the GFG may operate at more than one derated state where a multi-state component model is needed. Moreover, the probabilities for these derated states are related to the probabilities of fuel shortage.

In this chapter, failures of both generation and transmission components in the power system are considered while only pipeline failures in the NG system are considered.

The proposed assessment approach is described as follows.

First, assess the individual NG system reliability following the basic reliability assessment procedure by taken GFGs as NG loads. As the purpose is to evaluate how the NG fuel supply affects power system performance, special attention should be pay to the NG system nodes that are physically connected to the power system. The load point reliability indices, such as load not supplied at these objective nodes, are calculated for each different failure state of the NG system.

Table 3.1: NG Node Load Curtailment and Probability

Load Curtailment (%)	Cl_i^1	Cl_i^2	$\cdots$	Cl_i^j	$\cdots$	Cl_i^n
Probability	π_i^1	π_i^2	$\cdots$	π_i^j	$\cdots$	π_i^n

Table 3.2: Simplified NG Node Load Curtailment and Probability

Load Curtailment (%)	$\left(0,\ 1-O_{\mathrm{dr},g}^1\right]$	$\left(1-O_{\mathrm{dr},g}^1,\ 1-O_{\mathrm{dr},g}^2\right]$	$\cdots$	$\left(1-O_{\mathrm{dr},g}^{k-1},\ 1-O_{\mathrm{dr},g}^k\right]$	$\cdots$	$\left(1-O_{\mathrm{dr},g}^{n_{\mathrm{dr}}},\ 1\right]$
Probability	$\pi_{\mathrm{lc},i}^1$	$\pi_{\mathrm{lc},i}^2$	$\cdots$	$\pi_{\mathrm{lc},i}^k$	$\cdots$	$\pi_{\mathrm{lc},i}^{(n_{\mathrm{dr}}+1)}$

Then by accumulating the probabilities of system failure states with the same load curtailment, the discrete probability distribution of load not supplied can be determined for each objective node. For example, for objective node i, the distribution is illustrated in Table 3.1. Cl_i^j is the jth discrete value of load curtailment at node i with a probability of π_i^j.

For simplification purposes, load curtailments are sorted in ascending order and located to intervals distributed in [0, 1]. The number of intervals can be determined according to the corresponding GFG's characteristics in the power system. For instance, suppose in the NG system node i in Table 3.1 supplies fuel for GFG g in power system which has a number of n_{dr} derated states due to sufficient fuel resource, then it is reasonable to set $(n_{\mathrm{dr}}+1)$ intervals. The simplified distribution is presented in Table 3.2.

Where $O_{\mathrm{dr},g}^k$ is the maximum output (percentage of the GFG capacity) at the kth derated state sorted in descending. $\pi_{\mathrm{lc},i}^k$ is the probability of load curtailments falling into interval $\left(1-O_{\mathrm{dr},g}^{k-1},\ 1-O_{\mathrm{dr},g}^k\right]$, which is calculated as follows:

$$\pi_{\mathrm{lc},i}^k = \sum \pi_i^j, \quad \text{for all } j \text{ that } O_{\mathrm{dr},g}^{k-1} < Cl_i^j \leq O_{\mathrm{dr},g}^k \tag{3.30}$$

When the fuel supply is not 100% reliable, the probability of the kth derated state of GFG g, $\pi_{\mathrm{dr},g}^k$, is calculated by:

$$\pi_{\mathrm{dr},g}^k = \left(1-\pi_{\mathrm{d},g}\right)\pi_{\mathrm{lc},i}^k \qquad k = 1, 2, \cdots n_{dr} \tag{3.31}$$

where $\pi_{\mathrm{d},g}$ is the failure probability of GFG g.

It should be noticed that in (3.31) the derated states must also be sorted in descending order according to the generation output. In other words, derated states must be the counterparts of load curtailment intervals.

The probability of GFP g operating with output in $\left(1-O_{\mathrm{dr},g}^{n_{\mathrm{dr}}},\ 1\right]$ is added to $\pi_{\mathrm{f},g}$, based on the assumption that a GFG will quit when the NG fuel supply cannot support it to operate at least with the minimum output. Then considering the NG fuel uncertainty, the failure probability of GFG g is updated as follows:

$$\pi'_{\mathrm{d},g} = \pi_{\mathrm{d},g} + \left(1-\pi_{\mathrm{d},g}\right)\pi_{\mathrm{lc},i}^{(n_{\mathrm{dr}}+1)} \tag{3.32}$$

For each GFG, the process should be repeated. Then the power system reliability evaluation can be conducted to observe the system performance accounting for the uncertainty of NG fuel.

The integrated simulation shown in Fig.3.3 starts from the NG system state with known network topology, load demand and supply information. In every simulation round, the NG system operation state is generated randomly according to components' failure probabilities calculated as in (3.27). Then, if there is any NG component failed, run OGF to calculate the load curtailment at each node, record the results and turn to the next iteration. Otherwise, load curtailment is zero, record the result and turn to the next iteration. By the end of simulation of the NG system, probability distributions of NG supplied to GFGs can be calculated.

With simulation results of the NG system, the discrete distribution of NG supplied to each GFG and its associated probability can be generated. Then the multi-state model of GFGs can be established. With these models, as well as the given network topology and other component reliability data, power system simulation also starts from an initial system state with all components on. The

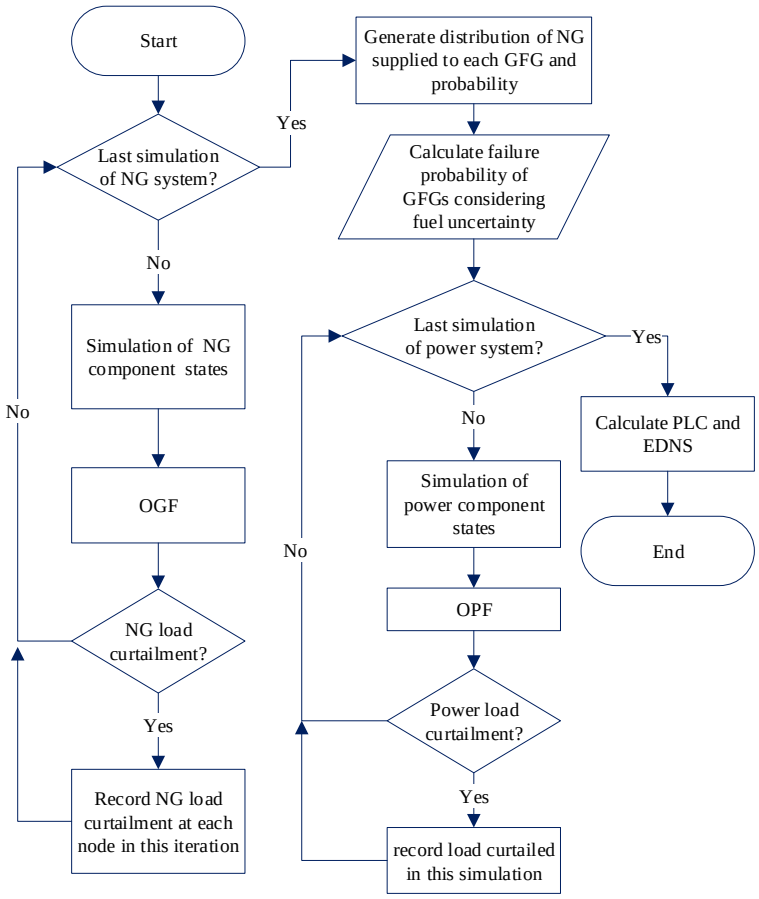

Figure 3.3: Procedure flowchart of power system reliability evaluation considering fuel impacts.

random system operation state is generated using non-sequential Monte Carlo simulation. If necessary, OPF would be run with the objective function of minimum load shedding. After completion of all simulations rounds, power system performance indices are calculated. It should be noticed the GFG outage model is shifted from two states to multi states with the impact of the associated NG supply system.

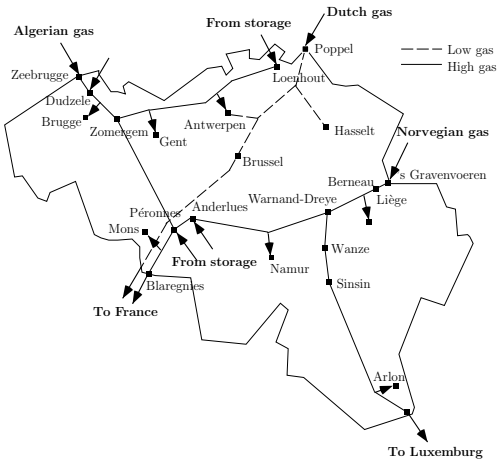

Figure 3.4: Belgian NG transmission system

3.4 Case Study

The modified Belgian NG transmission system [128] and the IEEE-24 reliability test system [129] are used for the case study.

3.4.1 Test Systems

The modified NG system, as shown in Fig.3.4, includes 24 pipelines and 20 nodes as described in Table 3.3 and Table 3.4, respectively.

It is assumed that all NG demands are interruptible and have the same priority. The failure rate and repair time of all the pipelines are assumed to be the same as $\lambda_{\text{gp}} = 0.2$ failures/year·km and $r_{\text{gp}} = 48$ hours [130]. The pipeline failure probability is calculated as follows:

$$\mu_{\text{gp}} = \frac{8760}{r_{\text{gp}}} \tag{3.33}$$

$$U_{\text{gp}} = \frac{\lambda_{\text{gp}}}{\lambda_{\text{gp}} + \mu_p} \tag{3.34}$$

Table 3.3: Nodes of Belgian Gas Transmission System

Node	Town	$\text{Supply}_{\text{min}}$ (Mm^3/day)	$\text{Supply}_{\text{max}}$ (Mm^3/day)	Demand (Mm^3/day)	$\mathcal{P}^{\text{max}}$ (Bar)	$\mathcal{P}^{\text{min}}$ (Bar)
1	Zeebrugge	17.39	8.87	0	77	0
2	Dudzele	12.6	0	0	77	0
3	Brugge	0	0	5.88	80	30
4	Zomergem	0	0	0	80	0
5	Loenhout	7.2	0	0	77	0
6	Antwerpen	0	0	6.05	80	30
7	Gent	0	0	7.88	80	30
8	Voeren	33.02	20.34	0	66.2	50
9	Berneau	0	0	0	66.2	0
10	Liège	0	0	9.55	66.2	30
11	Warnand	0	0	0	66.2	0
12	Namur	0	0	0.775	66.2	0
13	Anderlues	1.8	0	0	66.2	0
14	Péronnes	1.44	0	0	66.2	0
15	Mons	0	0	10.27	66.2	0
16	Blaregnies	0	0	23.42	66.2	50
17	Wanze	0	0	0	66.2	0

where μ_{gp}(repairs/year) is the pipeline repair rate. U_{gp} is the pipeline unavailability.

The Reliability Test System Task Force developed a test system in 1979, as shown in Fig.3.5 for better benchmarking and comparison of different methods. The details of the test system such as generator and transmission line parameters, are skipped here, and interested readers can refer to the literature [129].

Two subcases are used to assess the effect of the fuel supply system as follows:

Case I-a) Independent power system and NG system. There are no power generators fueled by NG. Besides, all gas compressors are driven by gas turbines. In other words, the power system and the NG system are not physically connected.

Case I-b) Physically connected power system and NG system through GFGs. Two 155 MW GFGs are located at bus 15 and bus 16 in the power system, and

Table 3.4: Pipelines of Belgian Gas Transmission System

Pipeline	From Node	To Node	Length (km)	$C_{\mathrm{gp},k}$	Capacity(Mm^3/day)
1	1	2	4.0	3.01169	125.08
2	1	2	4.0	3.01169	125.08
3	2	3	6.0	2.45898	102.13
4	2	3	6.0	4.91796	102.13
5	3	4	26.0	1.18128	49.06
6	5	6	43.0	0.31663	13.15
7	6	7	29.0	0.38556	16.01
8	7	4	19.0	0.47633	19.78
9	4	14	55.0	0.81219	33.73
10	8	9	5.0	2.69374	111.88
11	8	9	5.0	0.32869	13.65
12	9	10	20.0	1.34687	55.94
13	9	10	20.0	0.16434	6.83
14	10	11	25.0	1.20467	50.03
15	10	11	25.0	0.14699	6.11
16	11	12	42.0	0.92943	38.6
17	12	13	40.0	0.95238	39.56
18	13	14	5.0	2.69374	111.88
19	14	15	10.0	1.90476	79.11
20	15	16	25.0	1.20467	50.03
21	11	17	10.5	0.22681	9.42
22	17	18	26.0	0.08012	3.33
23	18	19	98.0	0.04127	1.71
24	19	20	6.0	0.16679	6.93

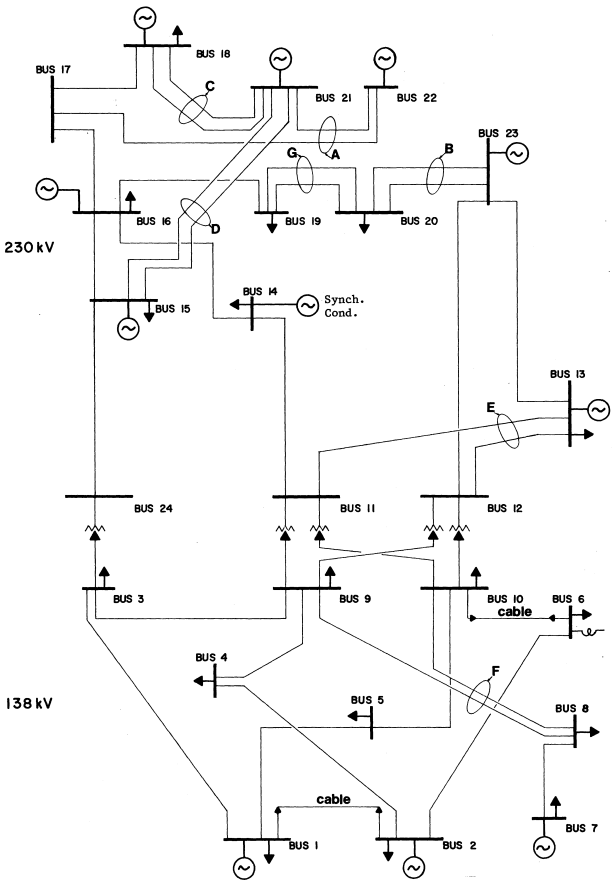

Figure 3.5: IEEE-24 reliability test system

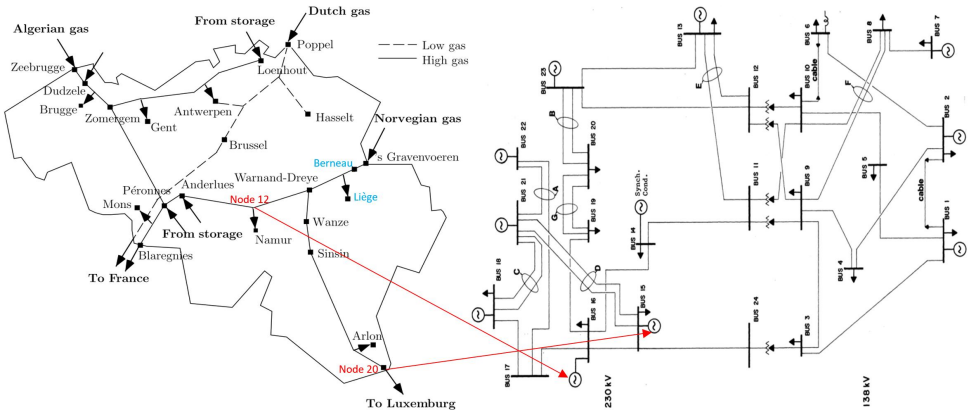

Figure 3.6: Connected power system and NG system.

Table 3.5: Heat Rate Coefficients of GFGs

GFG	Bus	Capacity (MW)	$a_{\mathrm{gfg},i}$	$b_{\mathrm{gfg},i}$	$c_{\mathrm{gfg},i}$
1	15	155	0	8.13457	0
2	16	155	0	8.13457	0

the NG is supplied by node 12 (Namur) and node 20 (Petange) of the NG system, respectively, as shown in Fig.3.6. In this chapter, it is assumed that the active power generated by a GFG has a linear relationship with the NG input [131]. The characteristics of GFGs in the modified power system are shown in Table3.5.

3.4.2 Simulation Results

Table 3.6 presents the probability distribution of NG not supplied for node 12 and 20.

The simulation results of the NG system demonstrate that contingencies in the NG system could result in a cut-off or reduction of NG supplied to GFGs. The probabilities of NG supplied without reduction at node 12 and 20 are 0.924242424 and 0.811818182, respectively, both the highest one. The probability of reduced NG supply at node 12 is as high as 0.064545454, which is almost six times of

Table 3.6: NG Network Simulation Result

Node	Gas not Supplied (%)	Probability
12	0.00%	0.924242424
	11.81%	0.038181818
	43.96%	0.023333333
	66.93%	0.003030303
	100.00%	0.011212121
20	0.00%	0.811818182
	21.27%	0.000909091
	100.00%	0.187272727

Table 3.7: Output and Probability of GFGs

GFG	Case	Generation(MW)	Probability
GFG at bus 15	Case I-b)	51.2661	0.002909091
		86.8647	0.0224
		136.6940	0.036654545
		0	0.050763636
		155	0.887272727
	Case I-a)	0	0.04
		155	0.96
GFG at bus 16	Case I-b)	122.0351	0.000872700
		0	0.219781818
		155	0.779345455
	Case I-a)	0	0.04
		155	0.96

100% NG supply reduction.

When considering the fuel supply impact, the GFGs may be constrained to operate at derated states. Table 3.7 provides a comparison of the GFGs generation output and corresponding probabilities in Case I-b) and Case I-a).

It can be seen clearly that in Case I-b) the probability of success state at full capacity of 155MW is decreased while the failure probability is increased significantly in comparison with Case I-a). It is especially obvious for the GFG

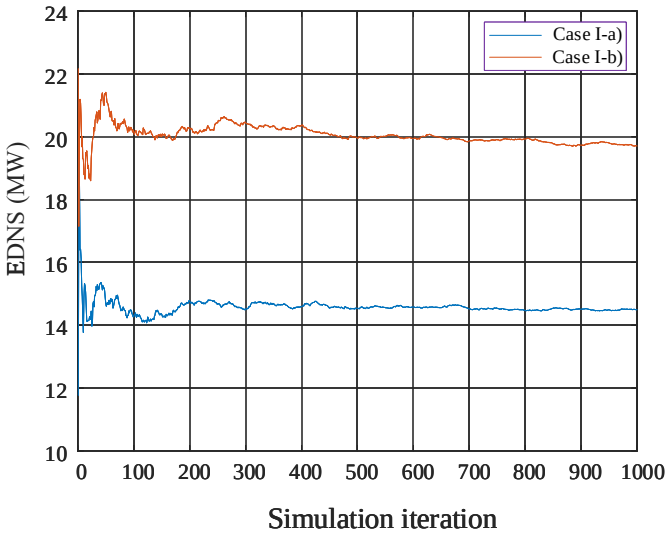

Figure 3.7: Power system EDNS.

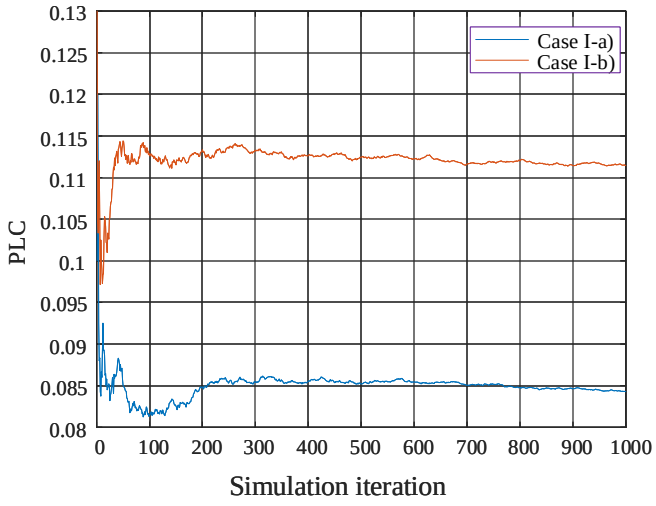

Figure 3.8: Power system PLC.

at bus 16. The reason is that its fuel is supplied by node 20 in the NG system, which has much longer distance from main NG sources. In other words, in the NG system, NG load at node 20 is more vulnerable to contingencies than NG load at node 12, which is determined by the NG network topology.

The impacts placed by the NG fuel supply system leads to reduced power

system performance, which can be displayed by the significant increase of EDNS and PLC in Case I-b) in comparison with Case I-a). EDNS increases sharply by 41.2856% from 14.5857 MW to 20.6075 MW as shown in Fig.3.7, while PLC increases by 33.3529% from 0.08527 to 0.11371, as shown in Fig.3.8. This result can be easily explained. In the combined scenario, increased GFG failure probabilities, in turn, increase the probability of the power system load curtailment. The increase is more obvious if large capacity GFGs are connected to an NG system with a weak network, for example, lack of redundancy. The power system EDNS also becomes larger due to increased failure probabilities and decreased outputs of GFGs.

Simulation results reveal two key insights: first, the interdependence impact is significant and should not be ignored; second, the interdependence worsens power system performance. Therefore, the power system becomes less reliable and resilient considering the fuel supply system. Neglecting these factors in the reliability or resilience assessment of power system would result in the underestimation of the problem.

3.5 Summary

This chapter provides a method for power system performance assessment considering the impact of NG fuel supply systems. The multi-state model is developed for GFGs incorporating the NG fuel supply uncertainty. Simulation results show that the power system reliability is affected by the reliability of the NG fuel system. The simulation results also verified the effectiveness of the approach developed in this chapter.

Chapter 4

Spatial-temporal Reliability and Damage Assessment of Transmission Networks under Hurricanes

Hurricanes can damage power transmission network structure components, e.g., towers and conductors, and threat the power system reliability. A spatial-temporal reliability and damage assessment method is proposed to evaluate the effect of hurricanes. The hurricane can be a simulated, historical or forecasting one for different application purposes, where the full track hurricane simulation model, historical records and forecasting information are used for the event construction, respectively. In the component failure analysis, the time-varying failure probability of transmission towers and conductors are modeled as functions of the time-varying hurricane intensity. In the reliability and damage assessment, the Monte Carlo simulation is adopted. The Energy Not Supplied and power outage costs caused by the hurricane event are used as operational indices, and the asset damage cost is proposed to quantify the damage of transmission networks. The modified IEEE 24-reliability test system and the two-area IEEE reliability test system -1996 affected by a simulated hurricane, respectively, are used in the case study to validate the proposed method. Simulation results show the method can quantify the hurricane impacts, identify the weak network parts, and provide information for pre-event preparedness for forecasting events.

4.1 Introduction

Transmission networks, made of interconnected transmission lines, deliver electricity from power generation plants to substations over a large area. An overhead transmission line generally comprises three kinds of components, i.e., towers, conductors, and insulating structures. These components are directly exposed to adverse weather conditions, such as hurricanes. The strong wind together with torrential rain induced by a hurricane could cause the failure of transmission lines in ways of damaging, collapsing transmission towers or blowing down conductors. The majority of weather-related transmission line failures in the U.S. have been attributed to hurricanes.

Compared with normal weather conditions, the failure probability of electrical components increases significantly under extreme weather events [132]. Reliability and damage assessment of transmission networks under hurricanes can quantify the event severity and is necessary for proactive preparation, quick response, and rapid recovery when a forecasting hurricane is approaching.

The hurricane is the tropical cyclone that develops over the Atlantic and the eastern Pacific Ocean with a minimum sustained wind speed of 74 $mi \cdot h^{-1}$ [133]. A hurricane is described by the time-varying track and intensity. The hurricane hazard impact analysis can be classified into the probabilistic method and the scenario-based method [134]. The probabilistic method is used to evaluate the aggregated effect of all possible hurricanes and is usually used for long-term design and planning purposes. The scenario-based method focuses on the study of a specific hurricane event, which can be built from simulation, historical records or forecast. For a forecasting hurricane event, a hurricane's future track and intensity is issued by the National Hurricane Center 2 to 5 days ahead according to predictions of numerical prediction models based on available observations.

For a historical hurricane event, the record can be selected from databases such as the Atlantic hurricane database. For a simulated hurricane event, the statistical model is adopted to simulate a specific hurricane event. The scenario-based method is adopted in this chapter intending to provide information for power system operators in the short term to help to make a decision.

Under a specific hurricane event, electrical component outage models are fundamental upon which power system reliability assessment techniques depend, such as analytical methods [135], [136] and Monte Carlo simulation [37]. Considerable efforts have been devoted to modeling component outage considering weather effects. In [32], [33], two and multi-state weather models are utilized to incorporate the weather effects into component outage models, where the weather conditions are divided into discrete states, in each of which the component failure rate is constant. The regional weather model [37] is used to include the regional weather effects on a transmission line traversing a large area, which is not considered in [32], [33]. Both multi-state weather models and regional weather model are developed for long-term power system reliability assessment and inadequate to represent the continuous time-varying weather conditions of hurricanes. Besides, weather conditions also change continuously over space, which has not been well reflected in models developed in [32], [33], [37].

To map the spatial-temporal hurricane impacts to transmission networks, it is necessary to model component failures as functions of both time and space changing weather conditions. When it comes to the transmission line, regarding time, at the site of the same tower or conductor segment, the wind speed experiences variation, due to combined effects of the changing distance to the hurricane center and the time-varying hurricane intensity. Regarding space, at any instant, at sites of different towers and conductor segments, wind speeds also vary due to terrain features and distances to the hurricane center. Two types of

models, i.e., data-based statistical models [40], [41], [50] and mechanism analysis based models [47], [48], [137], are widely adopted to model components failures under extreme weather events. The effectiveness of statistical models relies on the amount and quality of historical data [40], [41], [50]. In the situation of insufficient data, mechanism analysis based models are an alternative, such as fragility curves used in [51], [52]. These models can better describe the spatial-temporal impact of the hurricane by taking the continuous time-changing weather condition as an input variable of the component failure model.

Using both statistical component failure models and mechanism analysis based component failure models, a spatial-temporal reliability and damage assessment method of transmission networks under hurricanes is proposed. At sites of towers and conductor segments, time-varying wind speeds and rainfall rates are calculated using the hurricane event information. The spatial-temporal varying weather conditions are input to calculate the time-changing failure probability of spatially distributed towers and conductors. The gained time-varying component failure probabilities are used in the probability-based reliability and damage evaluation using Monte Carlo simulation. In addition to the power outage related cost, the cost induced by transmission asset damage is proposed to quantify the hurricane impact on transmission infrastructure. The contribution of this chapter can be summarized as follows: 1) The time-space varying impact of the hurricane with uncertainty on transmission network is considered through the component outage models. 2) Reliability indices, i.e., energy not supplied and asset damage indices, are integrated to quantify the performance of transmission networks under extreme weather events.

The rest of this chapter is divided into five sections. Section 4.2 introduces the hurricane hazard and its models. Section 4.3 presents transmission component failure models. Section 4.4 outlines the method for the reliability and damage

evaluation of transmission networks under hurricanes. Section 4.5 presents the case study and numerical results. Section 4.6 summarizes.

4.2 Hurricane Simulation Model

In the hurricane impact analysis, the statistical model described in the following parts in this section is adopted to simulate a specific hurricane event. The initial conditions of a hurricane including the position, date and time, intensity (specified by the central pressure difference) are determined by a stochastic approach as introduced in [138].

4.2.1 Hurricane Track Model

After the initial generation, the hurricane moves over space with time-changing direction, translation speed, and intensity, as shown in Fig. 4.1, taking hurricane Michael as an example. The assessment horizon $\mathcal{T}$ is divided into equal time intervals with a length of Δt, and $T = |\mathcal{T}|$, and $t \in \mathcal{T}$. The hurricane heading direction, translation speed, and intensity are obtained subsequently by the empirical track model developed by Vickery [139] as follows:

$$\Delta \ln \mathcal{V} = a^t_{\mathrm{hc}1} + a^t_{\mathrm{hc}2}\psi^t_{\mathrm{hc}} + a^t_{\mathrm{hc}3}\varphi^t_{\mathrm{hc}} + a^t_{\mathrm{hc}4} \ln \mathcal{V}^t_{\mathrm{hc}} + a^t_{\mathrm{hc}5}\beta^t_{\mathrm{hc}} + \varepsilon_{\mathcal{V}} \tag{4.1}$$

$$\Delta\beta = b^t_{\mathrm{hc}1} + b^t_{\mathrm{hc}2}\psi^t_{\mathrm{hc}} + b^t_{\mathrm{hc}3}\varphi^t_{\mathrm{hc}} + b^t_{\mathrm{hc}4}\mathcal{V}^t_{\mathrm{hc}} + b^t_{\mathrm{hc}5}\beta^t_{\mathrm{hc}} + b^t_{\mathrm{hc}6}\beta^{t-1}_{\mathrm{hc}} + \varepsilon_{\beta} \tag{4.2}$$

$$\begin{aligned} \ln \mathcal{I}^{t+1}_{\mathrm{hc}} = {} & d^t_{\mathrm{hc}1} + d^t_{\mathrm{hc}2} \ln \mathcal{I}^t_{\mathrm{hc}} + d^t_{\mathrm{hc}3} \ln \mathcal{I}^{t-1}_{\mathrm{hc}} + d^t_{\mathrm{hc}4} \ln \mathcal{I}^{t-2}_{\mathrm{hc}} \\ & + d^t_{\mathrm{hc}5} T^t_{\mathrm{s}} + d^t_{\mathrm{hc}6} \left({T_{\mathrm{s}}}^{t+1} - T^t_{\mathrm{s}} \right) + \varepsilon_{\mathcal{I}} \end{aligned} \tag{4.3}$$

where $\Delta \ln \mathcal{V} = \ln \mathcal{V}^{t+1}_{\mathrm{hc}} - \ln \mathcal{V}^t_{\mathrm{hc}}$. $\mathcal{V}^t_{\mathrm{hc}}$ (m·s^{-1}) is the hurricane translation speed. ψ^t_{hc} and φ^t_{hc} (degree) are the latitude and longitude of the hurricane center. $\Delta\beta =$

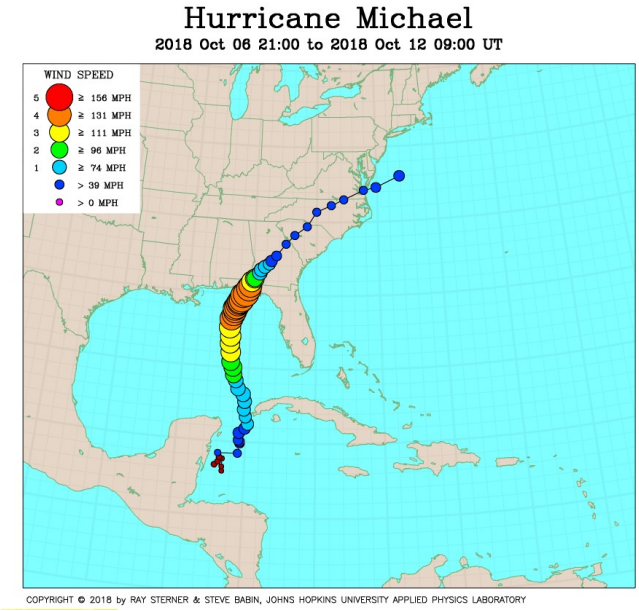

Figure 4.1: Hurricane Michael, Oct 2018 [7].

$\beta_{\mathrm{hc}}^{t+1} - \beta_{\mathrm{hc}}^{t}$. β_{hc}^{t} (in degrees from north) is the hurricane heading direction. $\mathcal{I}_{\mathrm{hc}}^{t}$ is the relative intensity. T_{s}^{t} (K) is the sea surface temperature. a_{hc1}^{t} to a_{hc5}^{t}, b_{hc1}^{t} to b_{hc6}^{t}, d_{hc1}^{t} to d_{hc6}^{t} are model coefficients derived from historical data varying with regions. $\varepsilon_{\mathcal{V}}$, ε_{β} and $\varepsilon_{\mathcal{I}}$ are random errors of the translation speed, heading direction and relative intensity, respectively.

When the hurricane center is over the ocean, the relative intensity $\mathcal{I}_{\mathrm{hc}}^{t}$ is specified as follows [140]:

$$\mathcal{I}_{\mathrm{hc}}^{t} = \frac{\Delta p_{\mathrm{hc}}^{t}}{p_{\mathrm{da}} - p_{\mathrm{dc}}} \tag{4.4}$$

$$\Delta p_{\mathrm{hc}}^{t} = p_{\mathrm{a}} - p_{\mathrm{hc}}^{t} \tag{4.5}$$

where $\Delta p_{\mathrm{hc}}^{t}$ (mb) is the central pressure difference. p_{da} (mb) is the surface value of the partial pressure of ambient dry air. p_{dc} (mb) is the minimum sustainable surface value of the central pressure of dry air. p_{hc}^{t} (mb) is the hurricane central pressure. p_{a} is the ambient pressure (1013 mb).

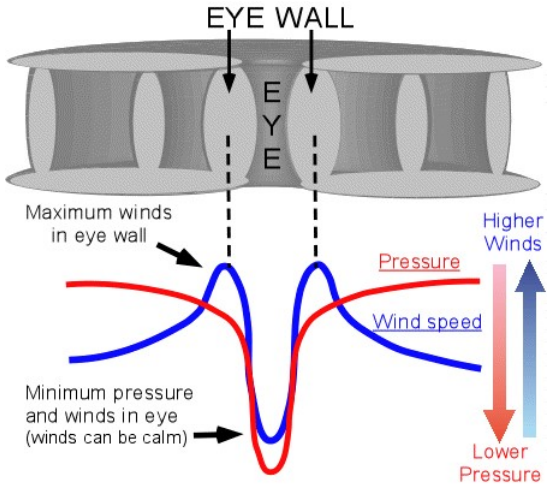

Figure 4.2: Pressure and wind distribution across a hurricane [8].

After landfall, the hurricane intensity would decay over time due to the loss of energy source. As a result, the hurricane central pressure increases over time. The changing of central pressure difference, $\Delta p_{\mathrm{hc}}^{t}$, is described by the exponential decay principle [141], as follows:

$$\Delta p_{\mathrm{hc}}^{t} = \Delta p_{\mathrm{hc}}^{t_{\mathrm{lf}}} \exp\left(-a_{\mathrm{d}}\left(t - t_{\mathrm{lf}}\right)\right),\ t > t_{\mathrm{lf}} \tag{4.6}$$

$$a_{\mathrm{d}} = a_{\mathrm{d0}} + a_{\mathrm{d1}}\left(\frac{\Delta p_{\mathrm{c}}^{t_{\mathrm{lf}}} \mathcal{V}_{\mathrm{hc}}^{t_{\mathrm{lf}}}}{\mathcal{R}_{\mathrm{wm}}^{t_{\mathrm{lf}}}}\right) + \varepsilon_{a_{\mathrm{d}}} \tag{4.7}$$

where t_{lf} is the time when the hurricane makes landfall. a_{d} is the decay constant. $\Delta p_{\mathrm{hc}}^{t_{\mathrm{lf}}}$ (mb), $\mathcal{V}_{\mathrm{hc}}^{t_{\mathrm{lf}}}$ (m·s^{-1}) and $\mathcal{R}_{\mathrm{wm}}^{t_{\mathrm{lf}}}$ (km) are the central pressure difference, the translation speed and the radius of maximum wind speed at t_{lf}, respectively. a_{d0} and a_{d1} are decay constants derived from historical data. $\varepsilon_{a_{\mathrm{d}}}$is the zero-mean normally distributed error.

4.2.2 Wind Field Model

At the gradient height and above, the gradient wind speed is a function of radius, as shown in Fig.4.2. According to Holland [142], at radius $\imath$ (km) to the hurricane

center, the gradient wind speed $\mathcal{V}^t_{\mathrm{G},\imath}$ (m·s^{-1}) is calculated as follows:

$$\mathcal{V}^t_{\mathrm{G},\imath} = \left(\left(\frac{\mathcal{R}^t_{\mathrm{wm}}}{\imath} \right)^{\mathcal{B}^t} \mathcal{B}^t \Delta p^t_{\mathrm{hc}} \frac{\exp\left(- \left(\frac{\mathcal{R}^t_{\mathrm{wm}}}{\imath} \right)^{\mathcal{B}^t} \right)}{\rho} + \frac{f_\imath{}^2 \imath^2}{4} \right)^{\frac{1}{2}} - \frac{\imath f_\imath}{2} \tag{4.8}$$

$$\mathcal{B}^t = 1.881 - 0.00557 \mathcal{R}^t_{\mathrm{wm}} - 0.01295 \psi^t_{\mathrm{hc}} + \varepsilon_{\mathcal{B}} \tag{4.9}$$

$$\ln \mathcal{R}^t_{\mathrm{wm}} = 3.859 - 7.7001 \times 10^{-5} \left(\Delta p^t_{\mathrm{hc}} \right)^2 + \varepsilon_{\ln \mathcal{R}_{\mathrm{wm}}} \tag{4.10}$$

$$f_\imath = 2\Omega \sin \varphi_\imath \tag{4.11}$$

where $\mathcal{R}^t_{\mathrm{wm}}$ (km) is the radius of maximum wind speed, which is a function of Δ^t_{hc} and ψ^t_{hc} [143]. $\mathcal{B}^t$ is the Holland pressure profile shape parameter [138]. ρ is the air density (1.15kg·m^{-3}). $f_\imath$ is the Coriolis coefficient. Ω is the earth rotation rate (7.2921×10^{-5} rad/s). $\varphi_\imath$ (degree) is the site latitude. $\varepsilon_{\mathcal{B}}$ and $\varepsilon_{\ln \mathcal{R}_{\mathrm{wm}}}$ are normally distributed random errors [138], [143].

The wind speed below the gradient height varies vertically due to ground surface roughness. At radius $\imath$ (km) to the hurricane center and height h (m), the mean wind speed $\mathcal{V}^t_{h,\imath}$ (m·s^{-1}) is calculated using widely accepted power-law profile model [144], as follows:

$$\mathcal{V}^t_{h,\imath} = \mathcal{V}^t_{\mathrm{G},\imath} \left(\frac{h}{h_{\mathrm{G}}} \right)^{\alpha_\imath} \tag{4.12}$$

where $\alpha_\imath$ is the power-law exponent related to local terrain roughness. h_{G} (m) is the gradient height.

4.2.3 Rainfall Model

The rainfall model is used to calculate site rainfall rate determined by the hurricane intensity, the central pressure changing rate, and the translation speed [145], as

follows:

$$Rf_{\tau}^{t} = k_1^t k_2^t k_{\mathcal{V}}^t k_{\tau}^t \tag{4.13}$$

$$k_1^t = 0.0319\Delta p_{\mathrm{hc}}^t - 0.0395,\ k_1^t \geq 1 \tag{4.14}$$

$$k_2^t = 1.0 - 0.01\frac{\mathrm{d}p_{\mathrm{hc}}^t}{\mathrm{d}t} \tag{4.15}$$

$$k_{\tau}^t = -5.5 + 110\frac{\mathcal{R}_{\mathrm{wm}}^t}{\tau} - 390\left(\frac{\mathcal{R}_{\mathrm{wm}}^t}{\tau}\right)^2 + 550\left(\frac{\mathcal{R}_{\mathrm{wm}}^t}{\tau}\right)^3 - 250\left(\frac{\mathcal{R}_{\mathrm{wm}}^t}{\tau}\right)^4 \tag{4.16}$$

where Rf_{τ}^t (mm·h^{-1}) denotes the site rainfall rate at radius τ (km). k_{τ}^t is the auxiliary variable. $\mathrm{d}_{\mathrm{hc}}^t/\mathrm{d}t$ (mb·h^{-1}) is the central pressure changing rate. k_1^t, k_2^t and $k_{\mathcal{V}}^t$ are correction coefficients for the hurricane intensity, the central pressure changing rate, and the translation speed, respectively.

4.3 Component Failure Model

Under hurricanes, some components, e.g., transmission towers and conductors, are directly exposed to the hurricane wind and rainfall, while some are not, e.g., components underground and shielded in buildings. In this work, the hurricane impact caused by intense wind and strong rainfall is considered, while the flood effect is not included. Thus, the failures of underground gas components under hurricanes, which are mainly related to the flood, are not taken into account. This section maps hurricane impacts on failure probabilities of exposed transmission towers and conductors, using mechanism analysis based and data based models, respectively.

The impact of hurricanes can be represented by using some defined parameters that indicate their severity. When a hurricane moves on land, its effects are mainly strong winds and heavy rainfall. Thus, in this chapter, wind speed and rainfall are

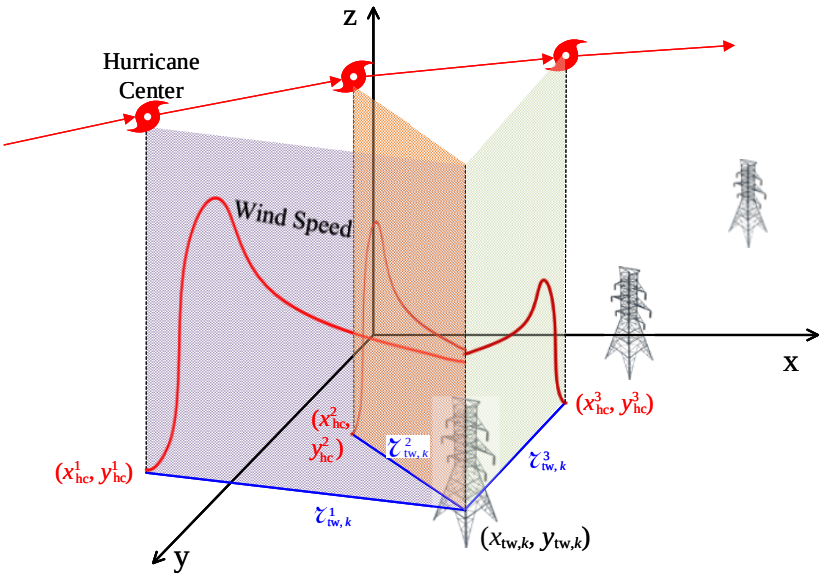

Figure 4.3: Transmission towers under a hurricane.

selected as two hurricane parameters.

4.3.1 Hurricane Intensity at Component Locations

As illustrated in Fig .4.3, from $t = 1$, the hurricane begins to affect tower k located at $\left(x_{\text{tw},k}, y_{\text{tw},k}\right)$ (km). The tower suffers the strongest wind at time slot 2. After time slot 3, the hurricane imposes no impact on the tower. Red solid curves describe the site gradient wind speed that changes with the distance from the hurricane center.

With given information of hurricane location and intensity, the distance between the hurricane center and the location of tower k at t, $\tau^t_{\text{tw},k}$, is calculated first to calculate the hurricane wind speed and rainfall rate at the tower site, as follows:

$$\tau^t_{\text{tw},k} = \left(\left(x_{\text{tw},k} - x^t_{\text{hc}}\right)^2 + \left(y_{\text{tw},k} - y^t_{\text{hc}}\right)^2\right)^{0.5}, \ \forall t \in \mathcal{T}, k \in \mathcal{E}_{\text{tw}} \tag{4.17}$$

where $\left(x^t_{\text{hc}}, y^t_{\text{hc}}\right)$ (km) is the hurricane center location at t. $\mathcal{E}_{\text{tw}}$ is the set of

transmission towers.

Substitute $\iota^t_{\mathrm{tw},k}$ into (4.8), the gradient wind speed at the location of tower k, $\mathcal{V}^t_{\mathrm{G},\iota^t_{\mathrm{tw},k}}$, is obtained. However, in the U.S., the basic wind speed is 3-second gust wind speed at a height of 10 meters [146]. Therefore, $\mathcal{V}^t_{\mathrm{G},\iota^t_{\mathrm{tw},k}}$ is converted by (4.12) and the gust factor, as follows:

$$\mathcal{V}^t_{\mathrm{tw},k} = G_\tau \mathcal{V}^t_{\mathrm{G},\iota^t_{\mathrm{tw},k}} \left(\frac{h_\mathrm{d}}{h_\mathrm{G}}\right)^{\alpha_{\mathrm{tw},k}}, \ \forall t \in \mathcal{T}, k \in \mathcal{E}_\mathrm{tw} \tag{4.18}$$

where $\mathcal{V}^t_{\mathrm{tw},k}$ (m·s^{-1}) and $\alpha_{\mathrm{tw},k}$ are the 3-second, 10-meter wind speed and the power-law exponent at the location of tower k. h_d= 10m. G_τ is the gust factor.

4.3.2 Failure Model of Transmission Towers

The effect of hurricanes on a tower is closely related to the tower structure responses. The analytical fragility function [51] based on structural characteristics is used to evaluate the probability that a tower collapses under hurricanes. The fragility curve is defined as the cumulative distribution function of the capacity of a tower to resist an undesirable limit state.

In addition to strong wind, hurricanes also introduce heavy rain. The rain load on a transmission tower is related the wind speed. To include the rainfall impact, the concept of equivalent wind speed[1] in [51] is used, as follows:

$$\mathcal{V}^{*t}_{\mathrm{tw},k} = \mathcal{V}^t_{\mathrm{tw},k} + a_\mathrm{tw}\left(Rf^t_{\mathrm{tw},k}\right)^{b_\mathrm{tw}} \exp\left(c_\mathrm{tw}\mathcal{V}^t_{\mathrm{tw},k}\right) - d_\mathrm{tw}\exp\left(e_\mathrm{tw}\mathcal{V}^t_{\mathrm{tw},k}\right), \ \forall t \in \mathcal{T}, k \in \mathcal{E}_\mathrm{tw} \tag{4.19}$$

where $Rf^t_{\mathrm{tw},k}$ (mm·h^{-1}) is the rainfall rate at the location of tower k. $\mathcal{V}^{*t}_{\mathrm{tw},k}$ (m·s^{-1}) is the equivalent wind speed at the location of tower k. a_tw, b_tw, c_tw, d_tw and e_tw

[1]Wind speed in the following part of this thesis refers to the 3-second gust at 10m height.

are constants. The equation indicates equivalent wind speed is a fusion of the basic wind speed and rain intensity.

The failure probability $\pi^t_{\mathrm{tw},k}$ of tower k, is mathematically described by the lognormal fragility curve [108] as follows:

$$\pi^t_{\mathrm{tw},k} = \frac{1}{\sqrt{2\pi}\sigma_{\mathrm{tw},k}} \int_{-\infty}^{x^t_{\mathrm{tw},k}} \exp\left(\frac{-\left(\tau - \mu^t_{\mathrm{tw},k}\right)^2}{2\left(\sigma_{\mathrm{tw},k}\right)^2} \right) d\tau \ \forall t \in \mathcal{T}, k \in \mathcal{E}_{\mathrm{tw}} \tag{4.20}$$

where $x^t_{\mathrm{tw},k} = \ln \mathcal{V}^{*t}_{\mathrm{tw},k}$ is the natural logarithm of the equivalent wind speed. $\mu_{\mathrm{tw},k}$ and $\sigma_{\mathrm{tw},k}$ are the logarithmic mean and standard deviation, respectively.

The attacking angle of hurricane wind on towers also has an impact on the tower failure probability. Various of $\mu_{\mathrm{tw},k}$ and $\sigma_{\mathrm{tw},k}$ in (4.20) are used to reflect the influence of wind attacking angle [51].

4.3.3 Failure Model of Conductors

The regression method proposed in [147] is extended to formulate the time-varying failure rate of conductors under hurricanes. The transmission conductor is divided into segments, each of which is assumed to be in the same terrain and exposed to the hurricane intensity at the central location of each segment. The failure rate $\lambda^t_{\mathrm{cs},k}$ (failure·km^{-1}·h^{-1}) of conductor segment k is expressed as follows:

$$\lambda^t_{\mathrm{cs},k} = L_{\mathrm{cs},k} \exp\left(\frac{a_{\mathrm{cs},k} \mathcal{V}^t_{\mathrm{cs},k}}{\mathcal{V}_{\mathrm{dcs},k}} + \frac{b_{\mathrm{cs},k} Rf^t_{\mathrm{cs},k}}{Rf_{\mathrm{dcs},k}} + c_{\mathrm{cs},k} \right), \ \forall t \in \mathcal{T}, k \in \mathcal{E}_{\mathrm{cs}} \tag{4.21}$$

where $L_{\mathrm{cs},k}$ (km) is the segment length. $\mathcal{V}^t_{\mathrm{cs},k}$ (m·s^{-1}) and $Rf^t_{\mathrm{cs},k}$ (mm·h^{-1}) are the wind speed and rainfall rate at the location of segment k, respectively. $\mathcal{V}_{\mathrm{dcs},k}$ (m·s^{-1}) and $Rf_{\mathrm{dcs},k}$ (mm·h^{-1}) are the design wind speed and design rainfall rate of segment k, respectively. $a_{\mathrm{cs},k}$, $b_{\mathrm{cs},k}$, and $c_{\mathrm{cs},k}$ are segment parameters derived from historical data. $\mathcal{E}_{\mathrm{cs}}$ is the set of transmission conductor segments.

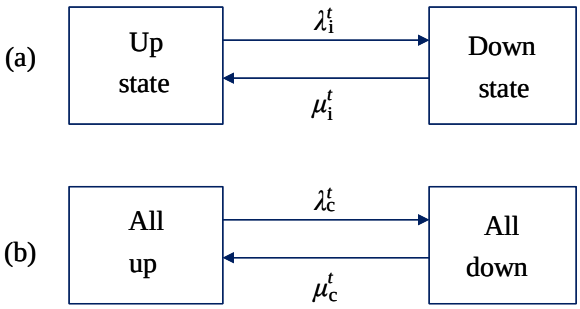

Figure 4.4: Two state model for common cause failure under hurricanes.

Then, without considering repairs, according to the discrete-time Markov process with constant failure rate at time slot t, the failure probability $\pi^t_{\text{cs},k}$ of segment k is calculated as follows [148]:

$$\pi^t_{\text{cs},k} = (1 - \pi^{t\text{-}1}_{\text{cs},k})(1 - \exp\left(-\lambda^t_{\text{cs},k}\Delta t\right)) + \pi^{t\text{-}1}_{\text{cs},k},\ \forall t \in \mathcal{T}, k \in \mathcal{E}_{\text{cs}} \tag{4.22}$$

In this thesis, failures of towers and conductor segments are assumed to be independent. The transmission line fails if at least one of its conductor segments or towers fail. Based on the series model, the failure probability of the transmission line k with n_{tw} towers and n_{sg} conductor segments, $\pi^t_{\text{ln},k}$, is calculated as follows:

$$\pi^t_{\text{ot},k} = 1 - \prod_{i=1}^{n_{\text{tw}}}(1 - \pi^t_{\text{tw},i}) \prod_{j=1}^{n_{\text{cs}}}(1 - \pi^t_{\text{cs},j}),\ \forall t \in \mathcal{T}, k \in \mathcal{E}_{\text{ot}} \tag{4.23}$$

where $\mathcal{E}_{\text{ot}}$ is the set of overhead transmission lines.

4.3.4 Common-cause Failure under Hurricanes

As defined in [37], a common cause outage is an event having an external cause with multiple failure effects where the effects are not consequences of each other. The individual two-state models are used for the common-cause outage and each independent outage, as shown in Fig. 4.4.

The two-state model in Fig. 4.4(a) is applied to independent outages of each component and that in Fig. 4.4(b) to their common-cause outage. Each independent outage and the common-cause outage are independent and not exclusive of each other [6].

The associated probability of the j-th system state (a combination of independent outages and common-cause outage) can be calculated by the following equation:

$$\pi^t_{\mathrm{ss},\,j} = \prod_{i \subset su_i} \pi^t_{\mathrm{u},\,i} \cdot \prod_{i \subset sd_i} \pi^t_{\mathrm{d},\,i} \cdot \max\left\{ I^t_{\mathrm{cd}} \pi^t_{\mathrm{cd}},\ \left(1 - I^t_{\mathrm{cd}}\right) \pi^t_{\mathrm{cu}} \right\},\ i = (1, 2, \cdots n_{\mathrm{co}}) \quad (4.24)$$

where n_{co} is the number of components that may suffer a common-cause outage. su_i and sd_i are the set of components without and with independent outages, respectively. $\pi^t_{\mathrm{d},\,i}$ and $\pi^t_{\mathrm{u},\,i}$ are the independent outage occurrence and nonoccurrence probability of component i, respectively. π^t_{cd} and π^t_{cu} are the probability of common-cause outage occurrence and nonoccurrence, respectively. I^t_{cd} is the common-cause outage indicator (if common cause outage occurs, $I^t_{\mathrm{cd}} = 1$; otherwise, $I^t_{\mathrm{cd}} = 0$). For two transmission circuits sharing the same supporting towers, $n_{\mathrm{co}} = 2$, π^t_{cd} is the probability that at least one tower fails, π^t_{cu} is the probability that all towers are up.

4.4 Reliability and Damage Assessment

Based on component failure models in Section 4.3, power system reliability assessment can be conducted by analytical or simulation methods. In analytical methods, all possible system states should be enumerated in theory, which is computationally expensive for large-scale systems. In practice, only limited system states are enumerated by probability criterion or order criterion. The drawback is that it underestimates the situation and leads to conservative results,

especially under extreme conditions, such as hurricanes. Therefore, the Monte Carlo simulation is adopted to evaluate the spatial-temporal hurricane impact on transmission networks.

Reliability indices and damage indices are used to reflect the hurricane impact on the system reliability and physical network damage, respectively.

4.4.1 Assessment Method

An overview of the assessment procedure is illustrated in Fig.4.5. The detailed description of the procedure is shown in the following steps:

Step 1) Data collection.

Step 1.1) Power system information acquisition, including network topology information, load forecast data, component electrical parameters, component value, structure feature, system operation constraints, such as the bounds of power generators, transmission lines and so on. Besides, the historical records of power system damage caused by hurricanes are also required.

Step 1.2) Geographic data collection, including geographic locations and local terrain information of components, which can be gained from the geographic information system. This data are used to calculate the wind and rainfall intensity at component sites.

Step 1.3) Hurricane event data, such as the time-varying hurricane center location, translation speed, moving direction, central pressure deficiency and coefficients needed in the hurricane wind field model. According to different application purposes, the hurricane information can be gained from the meteorological department, generated using the hurricane simulation model developed in Section 4.2 or selected from historical hurricane records.

Step 2) Discretize the studied time span and transmission lines into a proper number of intervals. At time slot t, determine the hurricane center location and intensity. Then, calculate the distances from component locations to the hurricane center. Next, calculate the site wind speed and rainfall rate for components exposed to the hurricane. After that, determine the component failure probability in t using the models developed in Section 4.3.

Step 3) Monte Carlo simulation. At the beginning of a new iteration, check if it is converged. At the end of each iteration, calculate the power system reliability and asset damage indices.

If it is not converged, generate new system states[2]. The power system is assumed to be in the normal state at the beginning, which means all components are up. Then in time slot t, pick a component, check if it is down. If so, turn to the next component; else, determine the component state by comparing the component failure probability in t with a randomly generated number uniformly distributed in [0, 1]. If the randomly generated number is larger than the component failure probability, the component is determined to be up in t, record it and turn to the next time interval. Otherwise, the component is simulated to fail in the left time. When all component states over $\mathcal{T}$ are gained, the power system state in t is determined by the combination of all component states in t.

Step 4) Reliability assessment commitment. In $\mathcal{T}$, with a simulated system state, check if any component fails. If no, start the next iteration as described in step 3. If yes, record the number of damaged components, calculate and update asset damage cost. Then, conduct the reliability assessment commitment

[2]A power system comprises of buses, branches, and generators. Buses, generators and underground cables are assumed to be reliable under hurricanes. Towers and conductors comprising overhead transmission lines have two states, as up and down. The overhead transmission line is down at least one of the towers or conductors is down. The system state is the combination of transmission lines on σ-algebra space.

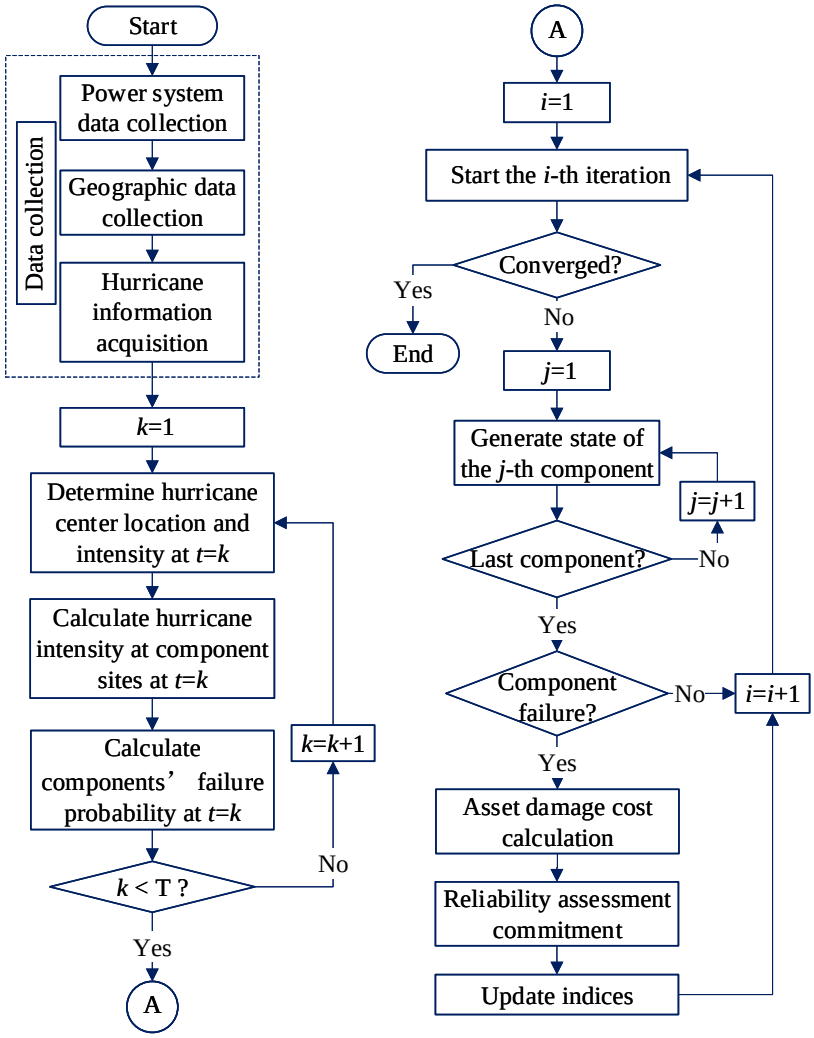

Figure 4.5: Flowchart of transmission network reliability and damage assessment under hurricanes.

(RAC) described in the following to determine if all load can be satisfied with generation redispatch and generator curtailment in $\mathcal{T}$. If all required loads can be satisfied, load curtailments are zero, start the next iteration as described in step 3. Otherwise, the time-varying optimal load curtailments at load buses are output results given by the RAC. Then, update load curtailments to the results and turn to the next iteration as described in step 3.

Considering the market processes in ERCOT [30], PJM [31] etc., the load curtailment model is formulated as a RAC problem as follows:

$$\min C_{\text{cost}} = \sum_{t\in\mathcal{T}} \left\{ \underbrace{VOLL \sum_{i\in\mathcal{N}_{\text{e}}} P^t_{\text{lc},i}}_{\text{Load shedding cost}} + \underbrace{C_{\text{pen}} \sum_{g\in\mathcal{G}_{\text{DA}}} |u^t_g - u^t_{\text{DA},g}|}_{\text{Penalty cost of unit status adjustment}} \right\} \tag{4.25}$$

$$\sum_{g\in\mathcal{G}_{\text{DA},i}} P^t_{\text{eg},g} + \sum_{g\in\mathcal{G}_{\text{RT},i}} P^t_{\text{eg},g} + \sum_{k\in\mathcal{E}^+_{\text{br},i}} P^t_{\text{br},k} - \sum_{k\in\mathcal{E}^-_{\text{br},i}} P^t_{\text{br},k}$$

$$= P^t_{\text{ed},i} - P^t_{\text{lc},i},\ \forall t \in \mathcal{T},\ i \in \mathcal{N}_{\text{e}} \tag{4.26}$$

$$\left(I^t_{\text{br},k} - 1\right) P^{\max}_{\text{br},k} \le P^t_{\text{br},k} - B_{\text{br},k}\left(\theta^{+\,t}_{\text{br},k} - \theta^{-,t}_{\text{br},k}\right)$$

$$\le \left(1 - I^t_{\text{br},k}\right) P^{\max}_{\text{br},k},\ \forall t \in \mathcal{T},\ k \in \mathcal{E}_{\text{br}} \tag{4.27}$$

$$-I^t_{\text{br},k} P^{\max}_{\text{br},k} \le P^t_{\text{br},k} \le I^t_{\text{br},k} P^{\max}_{\text{br},k},\ \forall t \in \mathcal{T},\ k \in \mathcal{E}_{\text{br}} \tag{4.28}$$

$$P^t_{\text{eg},g} + r^t_{\text{R+},g} + r^t_{\text{S},g} \le P^{\max}_{\text{eg},g} u^t_g,\ \forall t \in \mathcal{T},\ g \in \mathcal{G}_{\text{DA}} \cup \mathcal{G}_{\text{RT}} \tag{4.29}$$

$$P^{\min}_{\text{eg},g} u^t_g \le P^t_{\text{eg},g} - r^t_{\text{R-},g},\ \forall t \in \mathcal{T},\ g \in \mathcal{G}_{\text{DA}} \cup \mathcal{G}_{\text{RT}} \tag{4.30}$$

$$r^t_{\text{R+},g} \le R^{5+}_g u^t_g,\ \forall t \in \mathcal{T},\ g \in \mathcal{G}_{\text{DA}} \cup \mathcal{G}_{\text{RT}} \tag{4.31}$$

$$r^t_{\text{R-},g} \le R^{5-}_g u^t_g,\ \forall t \in \mathcal{T},\ g \in \mathcal{G}_{\text{DA}} \cup \mathcal{G}_{\text{RT}} \tag{4.32}$$

$$r^t_{\text{S},g} \le R^{10+}_g u^t_g,\ \forall t \in \mathcal{T},\ g \in \mathcal{G}_{\text{DA}} \cup \mathcal{G}_{\text{RT}} \tag{4.33}$$

$$u^t_g = u^0_g,\ \forall t \in \left[1,\ \text{UT}_{\text{R},g} + \text{DT}_{\text{R},g}\right],\ g \in \mathcal{G}_{\text{DA}} \cup \mathcal{G}_{\text{RT}} \tag{4.34}$$

$$\text{UT}_{\text{R},g} = \max\left\{0,\ \left(\text{UT}_g - \text{UT}_{0,g}\right) u^0_g\right\},\ \forall g \in \mathcal{G}_{\text{DA}} \cup \mathcal{G}_{\text{RT}} \tag{4.35}$$

$$\mathrm{DT}_{\mathrm{R},g} = \max\left\{0,\ \left(\mathrm{DT}_g - \mathrm{DT}_{0,g}\right)\left(1 - u_g^0\right)\right\},\ \forall g \in \mathcal{G}_{\mathrm{DA}} \cup \mathcal{G}_{\mathrm{RT}} \tag{4.36}$$

$$\sum_{h=t-\mathrm{UT}_g+1}^{t} v_g^h \le u_g^t,\ \forall t \in \left\{\mathrm{UT}_g, ..., T\right\},\ g \in \mathcal{G}_{\mathrm{DA}} \cup \mathcal{G}_{\mathrm{RT}} \tag{4.37}$$

$$\sum_{h=t-\mathrm{DT}_g+1}^{t} \omega_g^h \le 1 - u_g^t,\ \forall t \in \left\{\mathrm{DT}_g, ..., T\right\},\ g \in \mathcal{G}_{\mathrm{DA}} \cup \mathcal{G}_{\mathrm{RT}} \tag{4.38}$$

$$v_g^t - w_g^t = u_g^t - u_g^{t\text{-}1},\ \forall t \in \mathcal{T},\ g \in \mathcal{G}_{\mathrm{DA}} \cup \mathcal{G}_{\mathrm{RT}} \tag{4.39}$$

$$P_{\mathrm{eg},g}^t - P_{\mathrm{eg},g}^{t\text{-}1} \le R_g^{60+} u_g^{t\text{-}1} + R_g^{\mathrm{SU}} v_g^t,\ \forall t \in \mathcal{T},\ g \in \mathcal{G}_{\mathrm{DA}} \cup \mathcal{G}_{\mathrm{RT}} \tag{4.40}$$

$$P_{\mathrm{eg},g}^{t\text{-}1} - P_{\mathrm{eg},g}^t \le R_g^{60\text{-}} u_g^t + R_g^{\mathrm{SD}} w_g^t,\ \forall t \in \mathcal{T},\ g \in \mathcal{G}_{\mathrm{DA}} \cup \mathcal{G}_{\mathrm{RT}} \tag{4.41}$$

$$\sum_{g \in \mathcal{G}_{\mathrm{DA}} \cup \mathcal{G}_{\mathrm{RT}}} r_{\mathrm{R}+,g}^t \ge 0.02 \sum_{i \in \mathcal{N}_{\mathrm{e}}} \left(P_{\mathrm{ed},i}^t - P_{\mathrm{lc},i}^t\right),\ \forall t \in \mathcal{T} \tag{4.42}$$

$$\sum_{g \in \mathcal{G}_{\mathrm{DA}} \cup \mathcal{G}_{\mathrm{RT}}} r_{\mathrm{R}\text{-},g}^t \ge 0.02 \sum_{i \in \mathcal{N}_{\mathrm{e}}} \left(P_{\mathrm{ed},i}^t - P_{\mathrm{lc},i}^t\right),\ \forall t \in \mathcal{T} \tag{4.43}$$

$$\sum_{g \in \mathcal{G}_{\mathrm{DA}} \cup \mathcal{G}_{\mathrm{RT}}} r_{\mathrm{S},g}^t \ge 0.1 \sum_{i \in \mathcal{N}_{\mathrm{e}}} \left(P_{\mathrm{ed},i}^t - P_{\mathrm{lc},i}^t\right),\ \forall t \in \mathcal{T} \tag{4.44}$$

$$P_{\mathrm{ed},i}^t \ge P_{\mathrm{lc},i}^t \ge 0,\ \forall t \in \mathcal{T},\ i \in \mathcal{N}_{\mathrm{e}} \tag{4.45}$$

where $\mathcal{G}_{\mathrm{DA}}$ is the set of generators committed on the day-ahead market. $\mathcal{G}_{\mathrm{RT}}$ is the set of generators can be scheduled in the operating day. $\mathcal{N}_{\mathrm{e}}$ is the set of buses. $\mathcal{E}_{\mathrm{br}}$ is the set of branches. *VOLL* ($\cdot$MWh^{-1}) is the value of load loss. $B_{\mathrm{br},k}$ (S) is the susceptance of transmission line k. $P_{\mathrm{br},k}^{\max}$ (MW) is the rate of the transmission line k. $\mathcal{E}_{\mathrm{br},i}^{+}$ and $\mathcal{E}_{\mathrm{br},i}^{-}$ are the set of transmission lines to and from bus i, respectively. v_g^t, w_g^t, u_g^t are the start-up command, shut-down command, on/off status of unit g during time slot t, respectively. $P_{\mathrm{eg},g}^t$ (MW), $r_{\mathrm{S},g}^t$ (MW), $r_{\mathrm{R}+,g}^t$ (MW) and $r_{\mathrm{R}\text{-},g}^t$ (MW) are the set-point, spinning reserve, up regulation

reserve and down regulation reserve of unit g during time slot t, respectively. $P^{\min}_{\mathrm{eg},g}$(MW) and $P^{\max}_{\mathrm{eg},g}$ (MW) are the minimal and maximal real power output of unit g, respectively. $\mathrm{UT}_{\mathrm{R},g}$ (h) and $\mathrm{DT}_{\mathrm{R},g}$ (h) are the minimum up and down duration of unit g, respectively. UT_g (h) and DT_g (h) are the minimum up and down duration of unit g, respectively. $\mathrm{UT}_{0,g}$ (h) and $\mathrm{DT}_{0,g}$ (h) are the number of time slots the unit g has been up and down before the assessment horizon, respectively. R_g^{5+} (MW·h^{-1}), R_g^{10+} (MW·h^{-1}), and R_g^{60+} (MW·h^{-1}) are the maximum 5-min, 10-min and 60-min ramp-up rate of unit g, respectively. R_g^{5-} (MW·h^{-1}) and R_g^{60-} (MW·h^{-1}) are the maximum 5-min and 60-min ramp down rate of unit g, respectively. R_g^{SD} (MW) and R_g^{SU} (MW) are the shut-down and start-up capacity of unit g, respectively. $P^t_{\mathrm{ed},i}$ (MW) and $P^t_{\mathrm{lc},i}$ (MW) are the forecast load and shedding load at bus i during the assessment horizon. $P^t_{\mathrm{br},k}$ (MW) is the power flow on transmission line k during time slot t. $\theta^{+,t}_{\mathrm{br},k}$ and $\theta^{-,t}_{\mathrm{br},k}$ are the bus angle of the from bus and to bus of transmission line k, respectively. $I^t_{\mathrm{br},k}$ is the operating status of transmission line k (1 for operation, 0 otherwise).

In (4.25), the objective function is to minimize the load shedding cost together with the adjustment cost of committed units. The node power balance equation is given in constraint (4.26). The DC power flow on each transmission line considering the operation status is shown in constraints (4.27) and (4.28). The capacity limitation of each unit is depicted by constraints (4.29) – (4.33), respectively. The initial status of each unit is limited by constraints (4.34) – (4.36) [149]. The on/off duration of each unit is shown in constraints (4.37) – (4.39) [149], [150]. The ramp-up and ramp-down rate of each unit are bounded by constraints (4.40) and (4.41), respectively [149], [150]. The regulation up, regulation down and spinning reserve requirements are shown in constraints (4.42) – (4.44) [150]. The load shedding at each bus is limited by constraint (4.45).

In this chapter, the day-ahead unit commitment is solved using the method

proposed in [150], considering the uncertainty of loads, while without the battery energy storage systems, to generate the commitment status of unit $g \in \mathcal{G}_{\mathrm{DA}}$.

4.4.2 Assessment Indices

Power operational indices related to power load shedding are used to reflect the ability power systems to provide adequate service to customers under hurricanes. Besides, infrastructure indices are employed to describe power network physical damages. Overall indices are proposed to quantify the total cost of power load interruption and component damage.

4.4.2.1 Power Operational Indices

At the power load point level, time-varying power demand not supplied and related cost at buses are used to reveal the hurricane impact over time and space, calculated as follows:

$$DNS^{t}_{\mathrm{e},j} = \sum_{i \in S^{t}_{\mathrm{elc}}} \pi^{i,t}_{\mathrm{elc}} \cdot DNS^{i,t}_{\mathrm{e},j} \tag{4.46}$$

$$C^{t}_{\mathrm{elc},j} = \Delta t \cdot DNS^{t}_{\mathrm{e},j} \cdot C^{t}_{\mathrm{e},j} \tag{4.47}$$

where $DNS^{t}_{\mathrm{e},j}$ (MW) is the expected power demand not supplied at bus j during time slot t. S^{t}_{elc} is the set of power system states with power load curtailment during time slot t. $\pi^{i,t}_{\mathrm{elc}}$ is the associated probability of power system state i. $DNS^{i,t}_{\mathrm{e},j}$ (MW) is the power demand not supplied at the bus j associated with system state i during time slot t. It is equal to $P^{t}_{\mathrm{lc},j}$ in (4.25) associated with system state i. $C^{t}_{\mathrm{elc},j}$ and $C^{t}_{\mathrm{e},j}$ (M$) are the cost of power load shedding and the per-unit interruption cost at bus j, respectively.

4.4.2.2 Power Infrastructure Indices

The impact of hurricanes cannot be reflected only by load curtailment related indices, because component failures do not necessarily result in the load curtailment. Therefore, an index named asset damage cost is proposed to take the time-varying power infrastructure damage into account as follows:

$$C_{\mathrm{ad}}^{t} = \sum_{i \in S_{\mathrm{ad}}^{t}} \left(\pi_{\mathrm{ad}}^{i,t} \cdot \sum_{j=1}^{n_{\mathrm{ad}}} C_{\mathrm{cm},\,j}^{t} \right) \tag{4.48}$$

where C_{ad}^{t} (M$) is asset damage cost during t. S_{ad}^{t} is the set of system states with components that are damaged during t. $\pi_{\mathrm{ad}}^{i,t}$ is the associated probability of system state i. n_{ad} is the number of components that are damaged during t associated with system state i. $C_{\mathrm{cm},\,j}^{t}$ (M$) is the repair or replacement cost of damaged component j, which is modeled as follows:

$$C_{\mathrm{cm},\,j}^{t} = \begin{cases} w_{\mathrm{cm},\,j}^{t} \cdot C_{\mathrm{cv},\,j}, & \mathcal{V}_{\mathrm{cm},\,j}^{t} < \mathcal{V}_{\mathrm{thr}} \\ C_{\mathrm{rp},\,j}, & \mathcal{V}_{\mathrm{cm},\,j}^{t} \geq \mathcal{V}_{\mathrm{thr}} \end{cases} \tag{4.49}$$

$$w_{\mathrm{cm},\,j}^{t} = f\left(\mathcal{V}_{\mathrm{cm},\,j}^{t} \right) \tag{4.50}$$

where $w_{\mathrm{cm},\,j}^{t}$ is the factor describing the damage extent of damaged component j, which is a function of the hurricane intensity at the location of component j as shown in (4.50). $\mathcal{V}_{\mathrm{cm},\,j}^{t}$ (m·s^{-1}) is the equivalent wind speed (for towers) or wind speed (for conductor segments) at the location of component j. $\mathcal{V}_{\mathrm{thr}}$ (m·s^{-1}) is the wind speed threshold above which the component is considered to be entirely damaged. $C_{\mathrm{cv},\,j}$ (M$) and $C_{\mathrm{rp},\,j}$ (M$) are the component value and replacement cost of the damaged component j, respectively.

4.4.2.3 Power Overall Indices

At the system level, hourly-varying demand not supplied, total power energy not supplied, $TENS_{\mathrm{e}}$ (MWh), as well as total cost $TCOST_{\mathrm{e}}$ (M$) are used to offer a summarized view of the hurricane impact, as follows:

$$DNS_{\mathrm{e}}^{t} = \sum_{j \in \mathcal{N}_{\mathrm{ed}}} DNS_{\mathrm{e},j}^{t} \tag{4.51}$$

$$TENS_{\mathrm{e}} = \sum_{t \in \mathcal{T}} \Delta t \cdot DNS_{\mathrm{e}}^{t} \tag{4.52}$$

$$TCOST_{\mathrm{e}} = \sum_{t \in \mathcal{T}} \left(C_{\mathrm{ad}}^{t} + \sum_{i \in \mathcal{N}_{\mathrm{ed}}} C_{\mathrm{elc},i}^{t} \right) \tag{4.53}$$

where DNS_{e}^{t} (MW) is the power system demand not supplied during time slot t. $\mathcal{N}_{\mathrm{ed}}$ is the set of power buses with loads.

4.5 Case Studies

The IEEE 24-reliability test system and the two-area IEEE reliability test system-1996 under a simulated hurricane are used to validate the proposed method.

4.5.1 Simulated Hurricane

A hurricane that makes landfall at the Gulf of Mexico is simulated using the model in Section 4.2. Its initial location is decided randomly within the area (29.31°N-30.21°N, 86.64°W-90.29°W). The date and time it is generated are randomly selected from hurricane season (June 1 to November 30). The initial pressure deficit is assumed to be log-normally distributed with a mean value of 55 and a variance of 25. The translation speed is assumed to conform log-normally distribution with a mean value of 6 and a variance of 4. The hurricane

approaching direction is assumed to satisfy normal distribution N(0, 4) degree. The initial hurricane conditions can be flexibly replaced with Meteorological hurricane forecast data or historical data if the application purpose is different. Besides, the hurricane is assumed to move at a constant transition speed along a straight line, which is reasonable within the relatively small studied power system area. The energy loss is not considered when the hurricane makes landfall. Moreover, the pressure deficit is assumed not to decrease when the hurricane center is over the ocean. The a_{d0}, a_{d1} in (4.7) are taken as 0.006 and 0.00046 while the standard deviation is set to 0.0025 [151]. The assignment of $k_{\mathcal{V}}$ in (4.13) is the same as in [145]. The power system is supposed to be out of the hurricane impact when the hurricane is at latitudes north of the 33.22°N or its pressure deficient is less than 25mb.

The simulated hurricane summarized in Table 4.1 is generated at 8:00 am, the 231st day of a year. It is a category 2 hurricane according to the Saffir-Simpson Hurricane Wind Scale. The hurricane is considered to have no impact on the power system when it enters the north area of 33.22°N at 21:00 of the same day.

4.5.2 IEEE 24-Reliability Test System

4.5.2.1 Test System Information

The power system is projected to a $150 * 200$ km area approximately located within (30.52°N-32.32°N, 87.68°W-89.25°W) while the hurricane is considered to start to threaten the power system when it is generated or firstly appears within the area of (29.31°N-30.21N, 86.64°W-90.29°W). Readers are referred to [129] for detailed information of the IEEE 24-reliability test system. Generators, transformers, and underground cables are supposed to be reliable under the hurricane.

Table 4.1: Simulated Hurricane Data

Time	t	Location	Maximum sustained wind ($m \cdot s^{-1}$)	Central pressure (mb)
08:00	1	29.7484°N, 88.2827°W	45.9140	964.1570
09:00	2	29.9807°N, 88.3199°W	45.8743	964.1570
10:00	3	30.2131°N, 88.3571°W	45.8311	964.1570
11:00	4	30.4454°N, 88.3944°W	45.5299	964.6767
12:00	5	30.6778°N, 88.4318°W	44.9763	965.6997
13:00	6	30.9101°N, 88.4693°W	44.1809	967.1938
14:00	7	31.1425°N, 88.5069°W	43.1586	969.1127
15:00	8	31.3748°N, 88.5446°W	41.9278	971.3987
16:00	9	31.6072°N, 88.5823°W	40.5102	973.9852
17:00	10	31.8395°N, 88.6202°W	38.9297	976.8003
18:00	11	32.0719°N, 88.6582°W	37.2114	979.7697
19:00	13	32.3043°N, 88.6962°W	35.3810	982.8202
20:00	13	32.5366°N, 88.7344°W	33.4645	985.8823
21:00	14	32.7690°N, 88.7726°W	31.4868	988.8930

The power system component geographic locations are extracted in forms of latitude and longitude. Buses at the same station are supposed to have the same location, such as bus 3 and 24, bus 9, 10, 11 and 12. The power system under the hurricane marked by center locations at the hourly interval from 08:00 to 21:00 in flat Earth coordinates with the origin (29°42'N, 89.24°W) is shown in Fig. 4.6. The angular direction of the flat Earth x-axis (degrees clockwise from north) is 270°.

The power system area is divided into ten regions marked as R1 to R10 with different colors from south to north. The design wind speed (50-year return period) of R1 to R10 decrements by one from 50 $m \cdot s^{-1}$ according to ASCE7 windspeed map. $\mu_{\text{tw},k}$ and $\sigma_{\text{tw},k}$ in (4.20) for different wind attack angles and $\mathcal{V}_{\text{thr}}$ in (4.49) for the ten regions are also different. The design rainfall rate for all regions is set to 30 $mm \cdot h^{-1}$.

The power system area terrain is assumed to be an open country. For the open

country, the gust factor G_τ in (4.18) is taken as 1.75 [152]. $1/\alpha$ and h_G in (4.18) are set as 1/7 and 275m, respectively [144]. The transmission line span length is set to a typical value as 350m. Conductor segments length in (4.21) is taken the same as the span length. $a_{cs,k}$, $b_{cs,k}$ and $c_{cs,k}$ in (4.21) are set to 10.5497, 3.0385, and -31.0087, respectively. $C^t_{e,j}$ in (4.47) is set to 29.41 KW^{-1} [22] with the assumption that all loads are composite customers. In (4.49), the value of towers and conductors are set to 0.25 M$ and 0.052 M$ ·km^{-1}, respectively. w^t_{cm} is assumed to change linearly with hurricane wind speed at the component location. The replacing cost of an entirely damaged tower and conductor are set to 0.45 M$ and 0.072 M$·km^{-1}, respectively.

4.5.2.2 Component Failure Probability

The failure probabilities of the transmission lines during the hurricane are shown in Fig.4.7. It can be seen that the hurricane starts to affect the power system from time slot 3.

During the simulation, line 7-8 (from bus 7 to bus 8), 13-23 and 16-17 are almost not affected by the hurricane because they are too far from the hurricane. The failure probabilities of line 1-3, 1-5, 2-4 and 2-6 are relatively lower because the design value of R1 is the highest and the wind attack angles are not the most unfavorable. Line 15-21 crosses the hurricane maximum wind radius during time lot 7 to 9 but still has very low failure probability due to the large wind attack angle. The failure probabilities of transmission lines display a downward trend after the rise as the hurricane moves near first and then far away. The highest transmission line failure probability appears in during time slot 6 to 9, in which line 11-14, 16-19 and 20-23 have the top 3 failure probabilities because they cross the hurricane maximum wind radius and have unfavorable wind attack

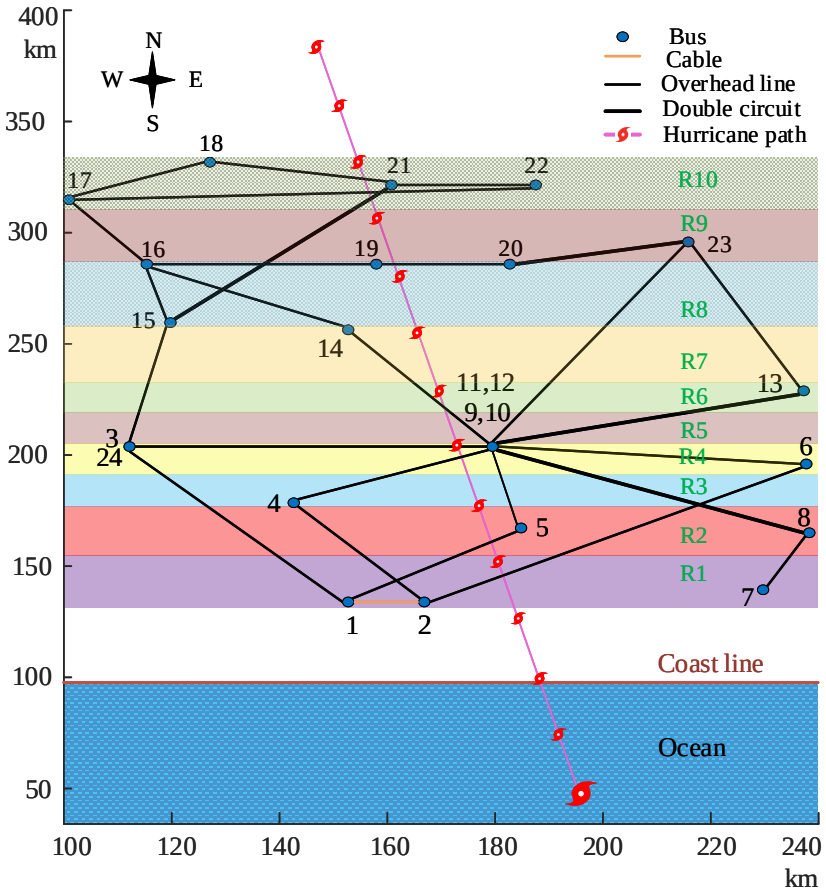

Figure 4.6: IEEE 24-Reliability Test System under the hurricane.

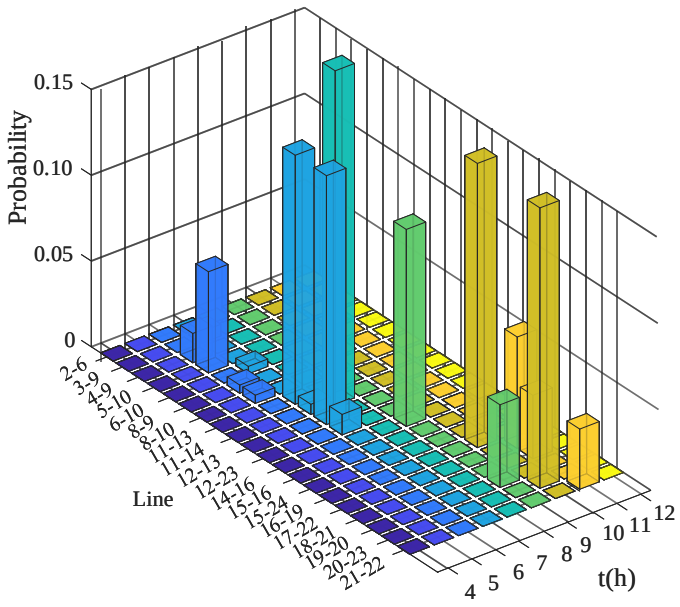

Figure 4.7: Failure probability of transmission lines during the hurricane.

angles. The time-varying component failure probabilities indicate that constant component failure probability is not appropriate for the power system reliability assessment under the hurricane.

Regarding space, failure probabilities associated with different transmission lines vary significantly in a specific interval, as shown in Fig.4.7. Lines in R1 and R2 perform better than lines in other regions. The different performance is due to that the region near the coastline has a higher design wind criteria than those further away. Line 11-13, 12-13, 11-14, 14-16, 16-19, 20-23 located mostly in Area 5 to 8 are the most vulnerable lines. It indicates that R5 to R8 are not as resistant as other parts to the simulated hurricane. It should be noted line 15-21 is located in R8 to R10 but of low failure probability due to the impact of wind attack angle.

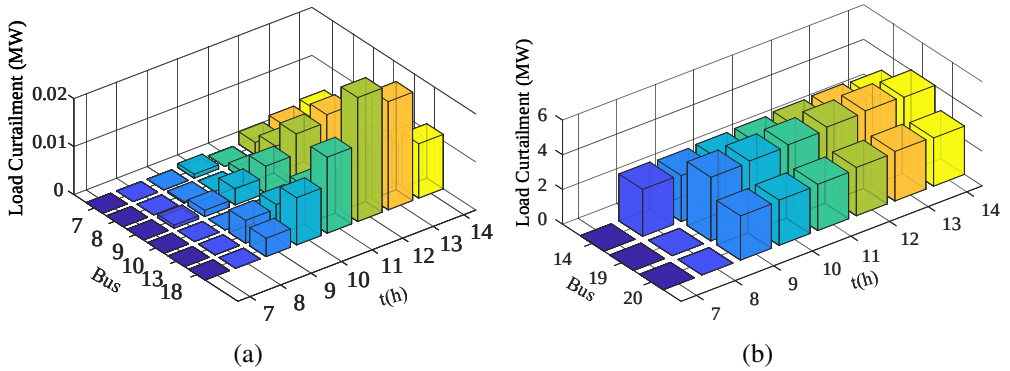

(a) (b)

Figure 4.8: Load curtailments at buses.

4.5.2.3 Reliability and Damage Assessment Results

Under the simulated hurricane, the system suffers $TENS_e$ as 59.2848 MWh and *TCOST* as 7.5969 M$ caused by the event.

In addition to the overall system index, time-varying individual bus load curtailments are given in Fig.4.8 to describe the hurricane impacts over time and space. Bus 7 to 10, 13, 14, and 18 to 20 experience load shedding during the hurricane while the load on the left buses are rarely affected by the hurricane. Among the affected buses, bus 19 has the highest load curtailment, followed by bus 20 and 14. It implies that the three buses are of higher risk under the hurricane threat which is consistent with the simulation result analysis of line failure probabilities. The vulnerability of line 11-14, 14-16, 16-19, 19-20, and 20-23 results in the relatively high load curtailment of bus 14, 19, and 20.

Besides, the time-varying number of failed components and system load curtailment as shown in Fig.4.9 are used to describe the system performance over time. The expected total number of failed components increases from $t = 4$ and keeps unchanged from the 10th hour. It costs 5.8533 M$ to repair or replace the damaged components. However, the failure of components does not necessarily

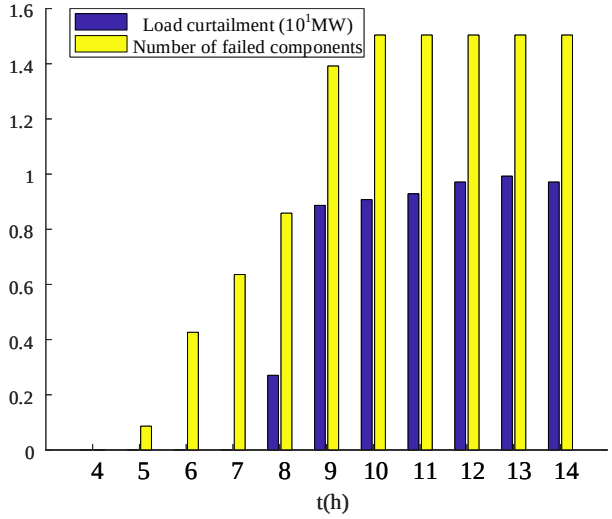

Figure 4.9: The total number of failed components and load curtailment.

have a consistent trend with the load curtailment due to the failure sequence and conditional system states as well as the importance of the components. The load curtailment over time increases first, then partly decreases because the time-varying load levels throughout the time span are taken into consideration. The load profile is extracted from the test system load data, according to the occurring time, date and duration of the hurricane.

4.5.2.4 Suggestions

The simulation results enable the awareness of potential problems. According to the simulation results, suggestions can be provided to the system operators to allow a directed action to be planned and carried out before the hurricane arrives. From the short-term review, for the simulated hurricane, deployment of the energy storage and the portable power generation at bus 14, 19 and 20 can help to reduce the risk of load curtailment and promote system reliability. Besides, the adjustment of unit commitment status is also a potential strategy. For example, due to the line failures, some committed generators might be shut down to meet the

power balance and security requirements. Some generators will be committed to minimize the load shedding cost. From a long-term view, the upgrade of the weak transmission lines with much strict design criteria and optimization of generation capacity and relocation can help to build a more resilient power system.

4.5.3 IEEE Reliability Test System-1996

The two-area IEEE reliability test system-1996 [153] is used as a large test system. The information of area 1 and area 2 is the same as the IEEE 24-reliability test system as introduced in 4.5.2, except area 2 is 60 km far from area 1 in the positive direction of the x-axis as shown in Fig.4.10.

All transmission lines in area 2, as well as the three tie lines between the two areas, are entirely not affected by the hurricane because of their far distances from the hurricane. Therefore, no electrical components are damaged by the hurricane in area2. The expected number of damaged components and asset damage cost are the same as the results in 4.5.2.3.

Under the simulated hurricane, the system suffers $TENS_e$ as 58.3269 MWh and *TCOST* as 7.5909 M$ caused by the event, decreasing by 1.6157% and 0.0790%, respectively, compared to the results in 4.5.2.3. Loads at buses in area 2 are not shed during the hurricane event. The load curtailments at buses in area 1 are a little smaller than the result in 4.5.2.3. The reason is that the load shedding at bus 14 is mainly due to the failure of line 11-14 and 14-16, which results in the isolation of bus 14. Connection with area 2 cannot decrease the loading shedding when isolation happens. Bus 19 and 20 face similar situations when line 16-19, 19-20, 20-23 fail. As a result, the spare generation capacity in area 2 cannot promote system reliability significantly.

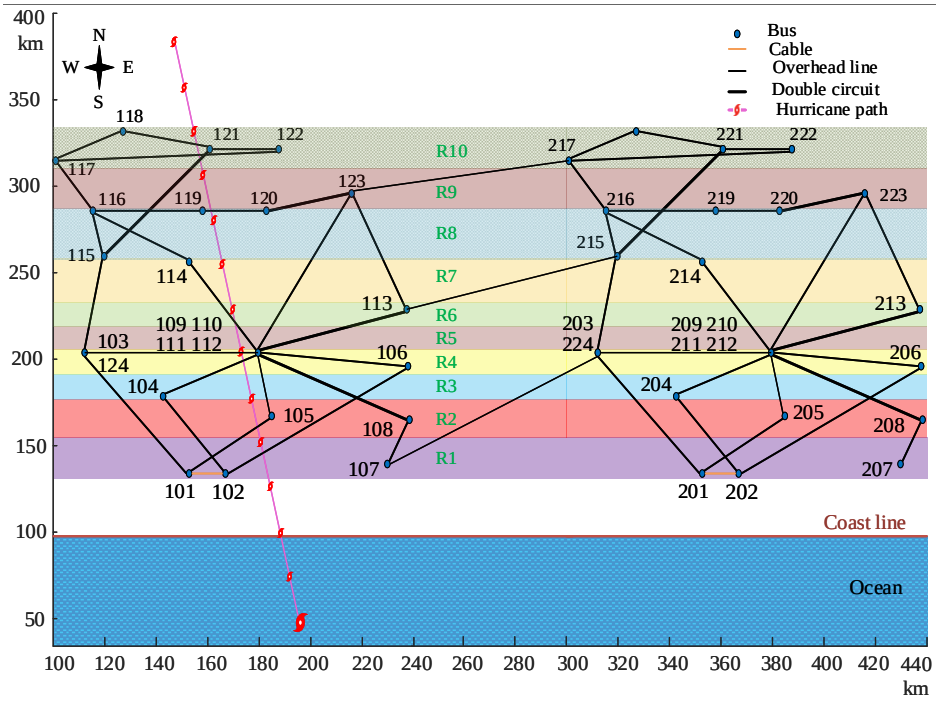

Figure 4.10: Two-area IEEE reliability test system-1996 under the hurricane.

4.6 Summary

This chapter proposes a method to assess the short-term reliability of power systems subject to the spatial-temporal impact of hurricanes. The validation of the method is conducted through the modified IEEE 24-reliability test system and the two-area IEEE reliability test system-1996 under the simulated hurricane. The simulation results reveal that the proposed method can evaluate the hurricane impact on power systems over time and space. Besides, the technique can help to identify the weak parts of power systems for the approaching hurricane and give indices to quantify its impact from both time and space dimensions. It can also provide information for pre-event decision making to prepare power systems adequately for hurricanes. Based on the simulation results, proactive strategies, such as the allocation of external energy sources, can be taken to mitigate the

hurricane impact and reduce the cost of hazards.

Chapter 5

Resilience Assessment of Interdependent Energy Systems under Hurricanes

Energy systems, e.g., power systems and NG systems, are increasingly interdependent, which brings benefits under normal conditions and introduces risks under extreme weather events, e.g., hurricanes. A comprehensive method is proposed to reflect the spatial-temporal hurricane impacts on interdependent power and NG systems. Mechanism analysis based and data based component failure models are used to map hurricane effects on exposed component failure probabilities based on which system states are generated using Monte Carlo simulation. For system states with failed components, the integrated energy flow is developed to determine minimum joint load shedding considering the inherent properties of each system and characteristics of interdependence coordinately. Operational metrics and infrastructure metrics are employed to quantify the service adequacy and network resistance of the interdependent energy systems, respectively. The modified IEEE 24-reliability test system and the 12-node NG system under a simulated hurricane are used to validate the effectiveness of the proposed method. Simulation results show the method can identify weak parts and quantify the performance of interdependent power and natural gas systems under hurricanes to provide information for effective and coordinative preparedness.

5.1 Introduction

Along with the evolution of energy systems, power systems and NG systems have become highly interdependent due to the increasing connections among them. For example, the utilization of NG for power generation has grown steadily [1] while gas facilities are also preferably driven by electricity [17]. Interdependence provides environmental, economic, and operational benefits under normal conditions [77], [78]. However, risks associated with interdependence might emerge under EWEs [26]. Mitigating the threats from EWEs, resilience-oriented research on energy systems has gained growing attention from independent systems to interdependent ones.

The resilience of a system under EWEs is directly related to the system features and the characteristics of the extreme event it suffers [154]. In the context of the power system, various works have been done in components failure models under EWEs, resilience assessment methods, resilience metrics as well as resilience enhancement strategies. Under EWEs, the failure probability of exposed components, e.g., power transmission towers, is closely related to the evolving weather conditions. Traditional models, e.g., the two or multi-state weather models [33] and the regional weather model [37], are not adequate to capture the impact of time-space-changing weather conditions on component failure probabilities. Data based statistical models [40], [41] and mechanism analysis based models [47], [48] take continuously changing weather conditions as an input variable to component failure functions, thus can better reflect the spatial-temporal weather impact on component failure probabilities. [61] develops a conceptual framework to provide fundamentals to model and quantify the power system resilience. [64] presents a probabilistic method to assess the resilience of power distribution systems under different weather scenarios. [62], [63] propose

resilience metrics from different perspectives, e.g., operation, infrastructure, and topology, etc., to quantify the power system resilience specifically. [155], [156] introduce resilience enhancement strategies.

Coordination of interdependent power and NG systems under normal conditions has been well studied in e.g., co-optimal planning [69], optimal energy flow [73], and operation scheduling [77], [78], to utilize interdependence to achieve benefits. Under EWEs, interdependence could introduce risks as disruptions in one system can permeate to the connected ones and may loop back through coupling links. For example, quit of gas compressors due to electricity cut off caused by EWEs may lead to gas load shedding, which could result in reduction even cut off of NG supplied to GFGs. A shortage of fuel could further contribute to the outage in the power system. However, little work is done to explore the performance of interdependent power and NG systems under EWEs considering individual system properties and interdependence characteristics coordinately. [157] proposes a proactive method to enhance the preparedness of multiple energy carrier microgrids by energy storage, using the steady-state gas flow model without modeling compressors. [86] proposes a resilience-constrained unit commitment model to enhance the resilience of the integrated power distribution and NG system without modeling the hurricane impact on component failures directly. The background highlights the necessity to investigate, understand, model, and quantify the performance of interdependent power and NG systems under EWEs for coordinative and proactive preparedness.

Under this background, this chapter proposes a comprehensive method to quantify the performance of interdependent power and NG systems under hurricanes. Mechanism analysis based and data based component failure models are used to reflect hurricane effects on the component failure probabilities, which are input to the Monte Carlo simulation to simulate component states. When

components are simulated to fail, integrated energy flow is developed to determine the optimal joint load shedding over time. Operational and infrastructure indices are used to describe the performance of the interdependent systems. The contribution of this chapter can be summarized as follows: 1) Develop a method that evaluates hurricane impacts on the performance of interdependent power and NG systems. 2) Propose the integrated energy flow taking into account individual system properties and interface characteristics to minimize the joint load shedding. 3) Integrate operational and infrastructure indices to quantify the performance of interdependent systems.

The remainder of this chapter is divided into five sections. Section 5.2 models interdependent energy systems. Section 5.3 presents the resilience assessment method and indices. Section 5.4 conducts case studies. Section 5.5 summarizes.

5.2 Interdependent Energy System Models

The interdependent power system and NG system are physically connected, as shown in Fig.5.1, through GFGs and gas compressors driven by electricity. When exposed transmission towers or conductors failed under hurricanes, disruptions in the power system may permeate to the NG system and further loop back. To sufficiently explore the behavior of the interdependent power and NG systems with components failures caused by hurricanes, inherent properties of each system and interdependence characteristics need to be modeled coordinately.

5.2.1 Power System Model

After generation, the power is transmitted to substations through transmission networks consisting of branches, circuit breakers, switches, etc. Considering the

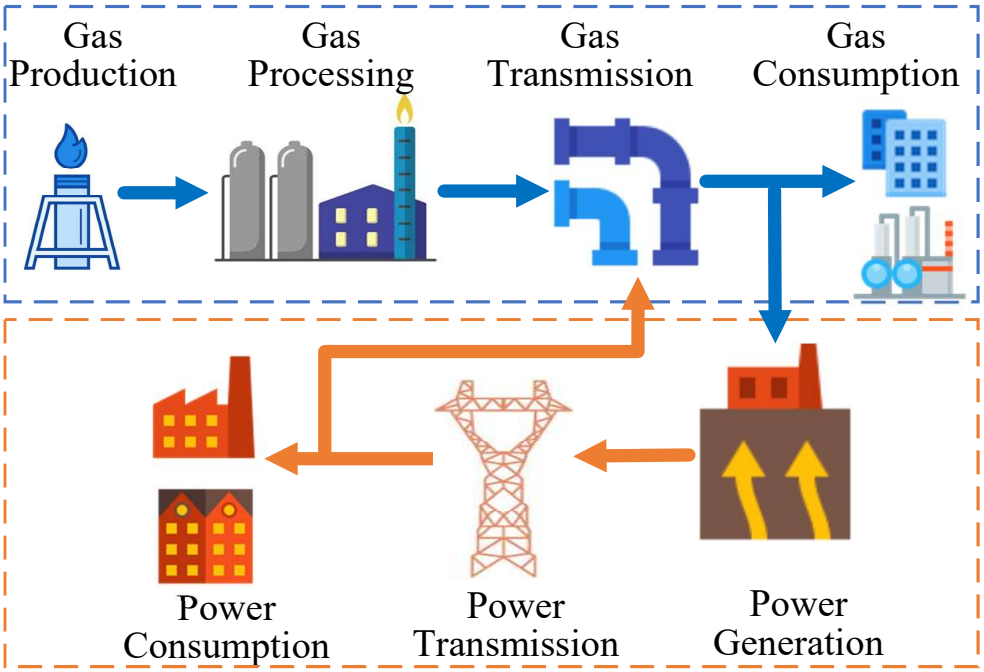

Figure 5.1: Interdependent power system and NG system.

status, the ramp constraints of each generation unit are presented as follows:

$$P^{t}_{\mathrm{eg},g} - P^{t\text{-}1}_{\mathrm{eg},g} \le R^{60+}_{g}\Delta t u^{t}_{g},\ \forall t \in \mathcal{T}, g \in \mathcal{G} \tag{5.1}$$

$$P^{t\text{-}1}_{\mathrm{eg},g} - P^{t}_{\mathrm{eg},g} \le R^{60\text{-}}_{g}\Delta t u^{t\text{-}1}_{g},\ \forall t \in \mathcal{T}, g \in \mathcal{G} \tag{5.2}$$

$$p^{t}_{\mathrm{eg},g} - R^{t}_{g} \le P^{t}_{\mathrm{eg},g} \le p^{t}_{\mathrm{eg},g} + R^{t}_{g}, \forall t \in \mathcal{T}, g \in \mathcal{G} \tag{5.3}$$

where $\mathcal{G}$ is the set of generators. R^{60+}_{g} (MW·h^{-1}) and R^{60-}_{g} (MW·h^{-1}) are the maximum 60-min ramp-up and ramp-down rate of unit g. $P^{t}_{\mathrm{eg},g}$ (MW) is the active power output of generator g. u^{t}_{g} is the on ($u^{t}_{g} = 1$) / off ($u^{t}_{g} = 0$) status of unit g. $p^{t}_{\mathrm{eg},g}$ (MW) is the set-point of unit g during time slot t. R^{t}_{g} (MW) is the reserve capacity of unit g. u^{t}_{g}, $p^{t}_{\mathrm{eg},g}$ and R^{t}_{g} are first stage decision variables determined by the two-stage robust unit commitment model for integrated energy systems as described in the Appendix.

To depict the power flow on transmission branches, the DC power flow is introduced as follows:

$$\left(I^t_{\mathrm{br},k}-1\right)M \le P^t_{\mathrm{br},k} - B_{\mathrm{br},k}\left(\theta^{+,t}_{\mathrm{br},k}-\theta^{-,t}_{\mathrm{br},k}\right) \le \left(1-I^t_{\mathrm{br},k}\right)M,\ \forall t\in\mathcal{T}, k\in\mathcal{E}_{\mathrm{br}} \tag{5.4}$$

$$-I^t_{\mathrm{br},k}P^{\max}_{\mathrm{br},k} \le P^t_{\mathrm{br},k} \le I^t_{\mathrm{br},k}P^{\max}_{\mathrm{br},k},\ \forall t\in\mathcal{T}, k\in\mathcal{E}_{\mathrm{br}} \tag{5.5}$$

where $\mathcal{E}_{\mathrm{br}}$ is the set of power transmission branches. $B_{\mathrm{br},k}$ (S) is the susceptance of branch k. M is a large number. $P^t_{\mathrm{br},k}$ (MW) is the power flow on branch k during time slot t. $\theta^{+,t}_{\mathrm{br},k}$ (°) and $\theta^{-,t}_{\mathrm{br},k}$ (°) are the bus angle of the from bus and to bus of branch k, respectively. $I^t_{\mathrm{br},k}$ is the operating status of branch k (1 for operation, 0 otherwise). $P^{\max}_{\mathrm{br},k}$ (MW) is the rate of branch k.

The amount of power load shedding at each bus is constrained as follows:

$$P^t_{\mathrm{ed},j} \ge P^t_{\mathrm{lc},j} \ge 0,\ \forall t\in\mathcal{T}, j\in\mathcal{N}_{\mathrm{ed}} \tag{5.6}$$

where $P^t_{\mathrm{ed},j}$ (MW) and $P^t_{\mathrm{lc},j}$ (MW) are the power load forecast and load shedding at bus j during time slot t, respectively. $\mathcal{N}_{\mathrm{ed}}$ is the set of power buses with loads.

Including the power consumed by gas compressors, the node power balance equation is described as follows:

$$\sum_{g\in\mathcal{G}_j} P^t_{\mathrm{eg},g} + \sum_{k\in\mathcal{E}^+_{\mathrm{br},j}} P^t_{\mathrm{br},k} - \sum_{k\in\mathcal{E}^-_{\mathrm{br},j}} P^t_{\mathrm{br},k} = P^t_{\mathrm{ed},j} + \sum_{c\in\mathcal{E}_{\mathrm{egc},j}} P^t_{\mathrm{egc},c} - P^t_{\mathrm{lc},j},\ \forall t\in\mathcal{T}, j\in\mathcal{N}_{\mathrm{e}} \tag{5.7}$$

where $\mathcal{G}_j$ is the set of generation units connected to bus j. $\mathcal{E}^+_{\mathrm{br},j}$ and $\mathcal{E}^-_{\mathrm{br},j}$ are the set of branches to and from bus j, respectively. $P^t_{\mathrm{egc},c}$ (MW) is the power consumed by gas compressor c. $\mathcal{E}_{\mathrm{egc},j}$ is the set of gas compressors fed by power bus j. $\mathcal{N}_{\mathrm{ed}}$ is the set of power buses.

5.2.2 Gas System Model

A transmission NG system consists of sources, pipelines, compressors, etc. With consideration of the operating status, the capacity bounds of each gas source are expressed as follows:

$$Q_{\mathrm{gs},s}^{\min} I_{\mathrm{gs},s}^{t} \leq Q_{\mathrm{gs},s}^{t} \leq Q_{\mathrm{gs},s}^{\max} I_{\mathrm{gs},s}^{t},\ \forall t \in \mathcal{T}, s \in \mathcal{S} \tag{5.8}$$

where $\mathcal{S}$ is the set of gas sources. $Q_{\mathrm{gs},s}^{\min}$ (MMSCF·h^{-1}) and $Q_{\mathrm{gs},s}^{\max}$ (MMSCF·h^{-1}) are the minimal and maximal output of gas resource s, respectively. $I_{\mathrm{gs},s}^{t}$ is the on ($I_{\mathrm{gs},s}^{t} = 1$)/off ($I_{\mathrm{gs},s}^{t} = 0$) status of NG source s. $Q_{\mathrm{gs},s}^{t}$ (MMSCF·h^{-1}) is the set-point of source s during time slot t, respectively.

Compared with the power flow, the gas flow changes much slower when disruptions occur. For ideal gas in horizontal isothermal pipelines, flow dynamics are controlled by partial differential equations, namely the continuity equation representing the mass conservation law and the momentum equation derived from the second Newton law. A popular way to solve partial differential equations is to discrete them over time and space into algebraic equations. Considering the operating status, the dynamic NG flow in a pipeline segment is constrained as follows:

$$\begin{aligned} &L_{\mathrm{gp},k}\left(\left(\mathcal{P}_{\mathrm{gp},k}^{+,t} + \mathcal{P}_{\mathrm{gp},k}^{-,t}\right) - \left(\mathcal{P}_{\mathrm{gp},k}^{+,t\text{-}1} + \mathcal{P}_{\mathrm{gp},k}^{-,t\text{-}1}\right)\right) \\ &= 2\Delta t C_{\mathrm{gp},k}^{1}\left(Q_{\mathrm{gp},k}^{-,t} - Q_{\mathrm{gp},k}^{+,t}\right),\ \forall t \in \mathcal{T}, k \in \mathcal{E}_{\mathrm{gp}} \end{aligned} \tag{5.9}$$

$$\begin{aligned} &\left(I_{\mathrm{gp},k}^{t} - 1\right) M \leq \frac{1}{4} L_{\mathrm{gp},k} C_{\mathrm{gp},k}^{2}\left(Q_{\mathrm{gp},k}^{-,t} + Q_{\mathrm{gp},k}^{+,t}\right)\left|Q_{\mathrm{gp},k}^{-,t} + Q_{\mathrm{gp},k}^{+,t}\right| \\ &-\left(\mathcal{P}_{\mathrm{gp},k}^{+,t}\right)^{2} + \left(\mathcal{P}_{\mathrm{gp},k}^{-,t}\right)^{2} \leq \left(1 - I_{\mathrm{gp},k}^{t}\right) M,\ \forall t \in \mathcal{T}, k \in \mathcal{E}_{\mathrm{gp}} \end{aligned} \tag{5.10}$$

$$-I_{\mathrm{gp},k}^{t} Q_{\mathrm{gp},k}^{\max} \leq Q_{\mathrm{gp},k}^{+,t} \leq I_{\mathrm{gp},k}^{t} Q_{\mathrm{gp},k}^{\max},\ \forall t \in \mathcal{T}, k \in \mathcal{E}_{\mathrm{gp}} \tag{5.11}$$

$$-I^t_{\mathrm{gp},k} Q^{\max}_{\mathrm{gp},k} \le Q^{-,t}_{\mathrm{gp},k} \le I^t_{\mathrm{gp},k} Q^{\max}_{\mathrm{gp},k},\ \forall t \in \mathcal{T}, k \in \mathcal{E}_{\mathrm{gp}} \tag{5.12}$$

where $\mathcal{E}_{\mathrm{gp}}$ is the set of gas pipelines. $\mathcal{P}^{+,t}_{\mathrm{gp},k}$ (psia) and $\mathcal{P}^{-,t}_{\mathrm{gp},k}$ (psia) are the pressure at from and to node of pipeline segment k, respectively. $Q^{-,t}_{\mathrm{gp},k}$ (MMSCF·h^{-1}) and $Q^{+,t}_{\mathrm{gp},k}$ (MMSCF·h^{-1}) are the volume flow rate injected to pipeline k at the from node and out of pipeline segment k at the to node, respectively. $I^t_{\mathrm{gp},k}$ is the operating status of gas pipeline k (1 for operation, 0 otherwise). $L_{\mathrm{gp},k}$ (mile) and $Q^{\max}_{\mathrm{gp},k}$ (MMSCF·h^{-1}) are the length and capacity rate of pipeline segment k. $C^1_{\mathrm{gp},k} = 2.7273 \times 10^4 \times 4\mathcal{P}_{\mathrm{sc}} T_{\mathrm{ka}} Z_{\mathrm{a}} / \pi D^2_{\mathrm{gp},k} T_{\mathrm{sc}}$, $C^2_{\mathrm{gp},k} = 1.0138 \times 10^{14} f \mathrm{M_g} T_{\mathrm{ka}} Z_{\mathrm{a}} / 9\pi^2 D^5_{\mathrm{gp},k} \mathrm{g_c} \mathbb{R}_{\mathrm{g}}$. $\mathcal{P}_{\mathrm{sc}}$ and T_{sc} are the pressure and temperature of standard condition (14.65 psia, 520 R), respectively. T_{ka} (R) is the average temperature of the gas in pipeline segment k. Z_{a} is the average gas compressibility factor. $D_{\mathrm{gp},k}$ (in) is the pipeline diameter. f is the Darcy friction factor. $\mathrm{M_g}$ is the specific natural gas molemass (17.4). $\mathrm{g_c}$ is the gravitational constant (32.1 lbm·ft·s^{-2}). $\mathbb{R}_{\mathrm{g}}$ is the universal gas constant (10.73 psia·ft^3·lb^{-1}·mole^{-1}).

Compressors are installed to boost the pressure because NG suffers pressure loss in transmission due to friction. Considering the compressor operating status, the pressure ratio of each compressor is modeled as follows:

$$\left(I^t_{\mathrm{gc},c} - 1\right) M \le \mathcal{P}^{+,t}_{\mathrm{gc},c} - RC^t_{\mathrm{gc},c} \mathcal{P}^{-,t}_{\mathrm{gc},c} \le \left(1 - I^t_{\mathrm{gc},c}\right) M,\ \forall t \in \mathcal{T}, c \in \mathcal{E}_{\mathrm{gc}} \tag{5.13}$$

where $\mathcal{P}^{-,t}_{\mathrm{gc},c}$ (psia) and $\mathcal{P}^{+,t}_{\mathrm{gc},c}$ (psia) are the pressure of the compressor inlet and outlet node, respectively. $RC^t_{\mathrm{gc},c}$ is the compression ratio of compressor c. $I^t_{\mathrm{gc},c}$ is the operating status of gas compressor c (1 for operation, 0 otherwise). $\mathcal{E}_{\mathrm{gc}}$ is the set of gas compressors.

The horsepower of each compressor is calculated as follows:

$$HP^t_{\mathrm{gc},c} = \frac{a_{\mathrm{hp}} \mathcal{P}_{\mathrm{sc}} Q^t_{\mathrm{gc},c} T_{\mathrm{za}} c_{\mathrm{k}}}{T_{\mathrm{sc}} \eta_{\mathrm{gc},c} (c_{\mathrm{k}} - 1)} \left(\left(RC^t_{\mathrm{gc},c} \right)^{\frac{c_{\mathrm{k}}-1}{c_{\mathrm{k}}}} - 1 \right),\ \forall t \in \mathcal{T}, c \in \mathcal{E}_{\mathrm{gc}} \tag{5.14}$$

$$0 \leq HP^{t}_{\mathrm{gc},c} \leq I^{t}_{\mathrm{gc},c} HP^{\max}_{\mathrm{gc},c},\ \forall t \in \mathcal{T}, c \in \mathcal{E}_{\mathrm{gc}} \tag{5.15}$$

where $HP^{t}_{\mathrm{gc},c}$ (hp) is the horsepower of gas compressor c during time slot t. $HP^{\max}_{\mathrm{gc},c}$ (hp) is the maximum horsepower of compressor c. $Q^{t}_{\mathrm{gc},c}$ (MMSCF·h^{-1}) is the volume flow rate from the compressor inlet to the outlet. a_{hp} is constant. c_{k} is the gas specific heat ratio. $\eta_{\mathrm{gc},c}$ is the compressor efficiency.

At each gas node, the pressure is constrained as follows:

$$\mathcal{P}^{\min}_{j} \leq \mathcal{P}^{t}_{j} \leq \mathcal{P}^{\max}_{j},\ \forall t \in \mathcal{T},\ j \in \mathcal{N}_{\mathrm{g}} \tag{5.16}$$

where $\mathcal{N}_{\mathrm{g}}$ is the set of gas nodes. $\mathcal{P}^{\min}_{j}$ (psia) and $\mathcal{P}^{\max}_{j}$ (psia) are minimal and maximal allowed pressure at node j, respectively. $\mathcal{P}^{t}_{j}$ (psia) is the pressure at node j during time slot t.

Load shedding at each node is constrained as follows:

$$Q^{t}_{\mathrm{gd},j} \geq Q^{t}_{\mathrm{lc},j} \geq 0,\ \forall t \in \mathcal{T},\ j \in \mathcal{N}_{\mathrm{gd}} \tag{5.17}$$

where $Q^{t}_{\mathrm{gd},j}$ (MMSCF·h^{-1}) and $Q^{t}_{\mathrm{lc},j}$ (MMSCF·h^{-1}) are the gas load forecast and gas load shedding at node j during time slot t, respectively. $\mathcal{N}_{\mathrm{gd}}$ is the set of gas nodes with loads.

Including the gas consumed by GFGs, the node gas balance equation is expressed as follows:

$$\sum_{s \in \mathcal{S}_j} Q^{t}_{\mathrm{gs},s} + \sum_{k \in \mathcal{E}^{+}_{\mathrm{gp},j}} Q^{+,t}_{\mathrm{gp},k} - \sum_{k \in \mathcal{E}^{-}_{\mathrm{gp},j}} Q^{-,t}_{\mathrm{gp},k} + \sum_{c \in \mathcal{E}^{+}_{\mathrm{gc},j}} Q^{t}_{\mathrm{gc},c} - \sum_{c \in \mathcal{E}^{-}_{\mathrm{gc},j}} Q^{t}_{\mathrm{gc},c} = Q^{t}_{\mathrm{gd},j}$$

$$+ \sum_{g \in \mathcal{G}_{\mathrm{gfg},j}} Q^{t}_{\mathrm{gfg},g} - Q^{t}_{\mathrm{lc},j},\ \forall t \in \mathcal{T},\ j \in \mathcal{N}_{\mathrm{g}} \tag{5.18}$$

where $\mathcal{S}_j$ is the set of gas sources located at node j. $\mathcal{E}^{+}_{\mathrm{gp},j}$ and $\mathcal{E}^{-}_{\mathrm{gp},j}$ are the set of gas pipelines to and from node j, respectively. $\mathcal{E}^{+}_{\mathrm{gc},j}$ and $\mathcal{E}^{-}_{\mathrm{gc},j}$ are the set of gas compressors to and from node j, respectively. $\mathcal{G}_{\mathrm{gfg},j}$ is the set of GFGs fed by node j. $Q^{t}_{\mathrm{gfg},g}$ (MMSCF·h^{-1}) is the gas required by gas-fired generator g.

5.2.3 Interdependence Model

The dependence among the power system and the NG system is bi-directional. GFGs converter energy stored in NG into electrical energy and participate in the NG system as loads. The NG consumed by each gas-fired generator is determined by its output and efficiency as follows:

$$Q^t_{\mathrm{gfg},g} = C_{\mathrm{g2e},g}\eta_{\mathrm{g2e},g}P^t_{\mathrm{eg},g},\ \forall t \in \mathcal{T},\ g \in \mathcal{G}_{\mathrm{gfg}} \tag{5.19}$$

where $\mathcal{G}_{\mathrm{gfg}}$ is the set of GFGs. $C_{\mathrm{g2e},g}$ is a constant. $\eta_{\mathrm{g2e},g}$ is the energy conversion efficiency of GFG g.

Similarly, gas compressors driven by electricity act as power consumers in the power system. The power required by each compressor is determined by its horsepower as follows:

$$P^t_{\mathrm{egc},c} = 7.457 \times 10^{-4} HP^t_{\mathrm{gc},c},\ \forall t \in \mathcal{T},\ c \in \mathcal{E}_{\mathrm{egc}} \tag{5.20}$$

where $\mathcal{E}_{\mathrm{egc}}$ is the set of gas compressors driven by electricity.

5.3 Resilience Assessment method and indices

This section introduces the resilience assessment method and indices based on the integration of the models built in Chapter 4 Section 4.3 and Section 5.2.

5.3.1 Assessment Method

The detailed procedure shown in Fig.5.2 is described in the following steps:

Step 1) Data collection. In addition to the data listed in Section 4.4, Chapter 4, the NG system information is also needed, including the system topology, load forecast, and constraint limitations, etc.

Step 2) Component failure probability calculation as described in Section 4.4, Chapter 4 using the models built in Section 4.3, Chapter 4.

Step 3) Two state robust UC as described in the Appendix .

Step 4) System state generation by Monte Carlo simulation. It is assumed no component fails at the beginning of a new iteration. Then from time slot $t = 1$, take an exposed component (tower or conductor segment), if it has been simulated to be down, proceed to the next exposed component; else, simulate the component operating state by Monte Carlo simulation. A random number r_i distributed uniformly in $[0, 1]$ is generated first, then it is compared with the component failure probability at time slot t. If the component failure probability is smaller than r_i, the component is simulated to be up during t, record the simulation result and proceed to time slot $t+1$. Otherwise, record the component state as failed t, and it would keep failed during the left time. Continue the simulation until the states in $\mathcal{T}$ of all exposed components are generated. In this paper, it is assumed that failures of towers and conductor segments are independent. The failure probability and state of a transmission line can be determined according to the series theory with given failure probability and state of towers and conductor segments in this line. The power system state is determined by the combination of transmission lines' states.

Step 5) Resilience indices calculation. In $\mathcal{T}$, with a system state generated in Step 4), check if any exposed component fails. If no, turn to step 3 to start the next iteration. If yes, calculate and update infrastructure indices. Then, conduct the integrated energy flow to determine if the power and gas loads can be satisfied in $\mathcal{T}$. If yes, turn to step 4). If no, record the optimal power and gas load curtailments in every time interval of $\mathcal{T}$. Update operational indices and check if converged. If no, start the next iteration. If yes, end the simulation.

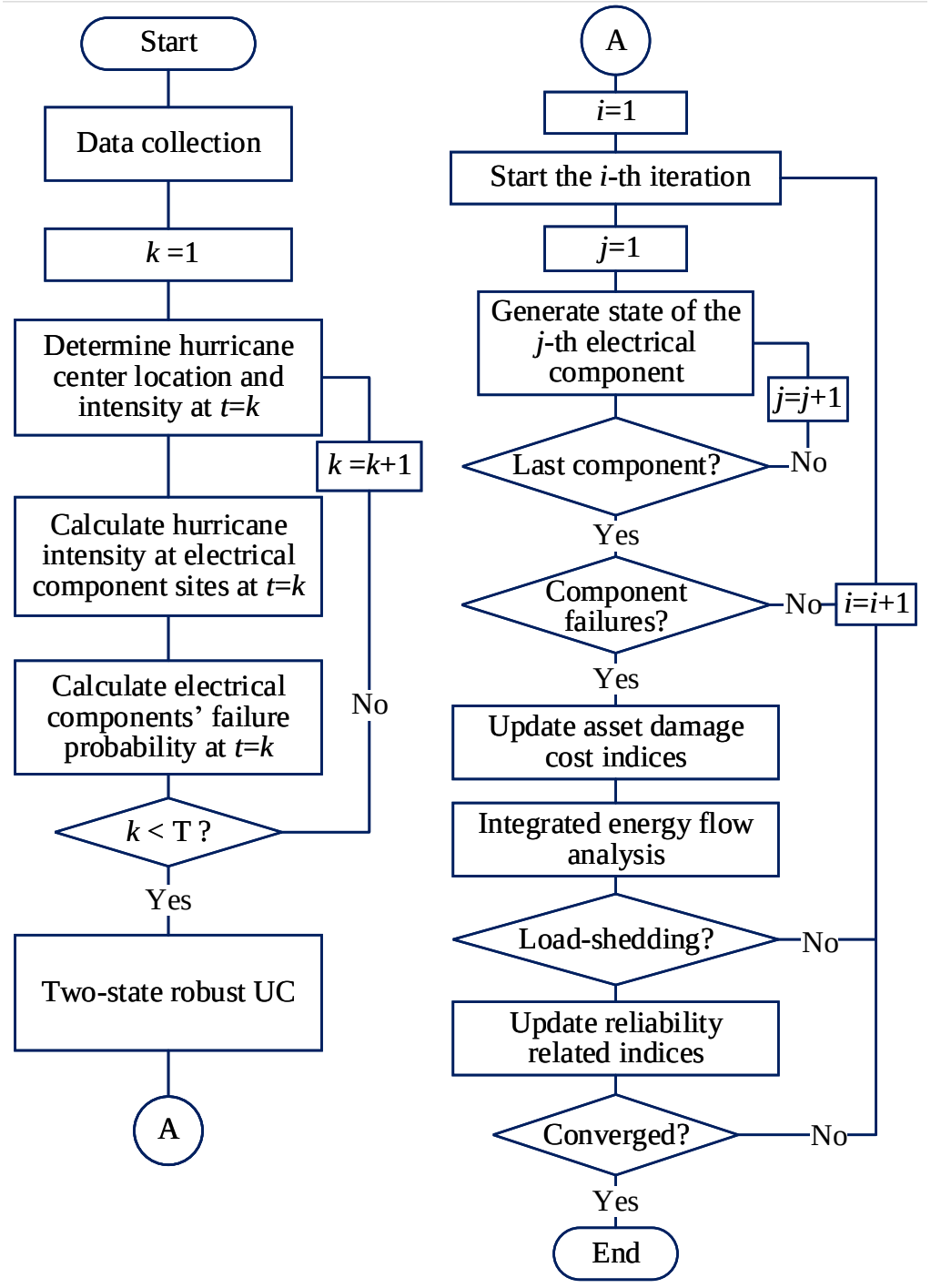

Figure 5.2: Flowchart of resilience assessment of integrated energy systems under hurricanes.

In step 5, the integrated energy flow is formulated as an optimization problem with the objective of minimum joint load shedding as follows:

$$\min_{\mathbf{y}\in\mathbf{Y}} \mathbf{d}^{\mathrm{T}}\mathbf{y} = \sum_{t\in\mathcal{T}} \left\{ \underbrace{\sum_{j\in\mathcal{N}_{\mathrm{ed}}} P^{t}_{\mathrm{lc},j}}_{\text{Power Load Shedding}} + \underbrace{\sum_{j\in\mathcal{N}_{\mathrm{gd}}} w_{\mathrm{gd},j} Q^{t}_{\mathrm{lc},j}}_{\text{Gas Load Shedding}} \right\} \tag{5.21}$$

where $w_{\mathrm{gd},j}$ is the weight factor of the gas load at node j. $\mathbf{y} = \{P^{t}_{\mathrm{eg},g}, P^{t}_{\mathrm{br},k}, \theta^{+,t}_{\mathrm{br},k}, \theta^{-,t}_{\mathrm{br},k}, Q^{t}_{\mathrm{gs},s}, \mathcal{P}^{+,t}_{\mathrm{gp},k}, \mathcal{P}^{-,t}_{\mathrm{gp},k}, Q^{+,t}_{\mathrm{gp},k}, Q^{-,t}_{\mathrm{gp},k}, \mathcal{P}^{+,t}_{\mathrm{gc},c}, \mathcal{P}^{-,t}_{\mathrm{gc},c}, HP^{t}_{\mathrm{gc},c}, Q^{t}_{\mathrm{gfg},g}, P^{t}_{\mathrm{egc},c}, P^{t}_{\mathrm{lc},j}, Q^{t}_{\mathrm{lc},j}, I^{t}_{\mathrm{gc},c}, I^{t}_{\mathrm{gp},k}, I^{t}_{\mathrm{gs},s}\}$ is the decision variables. Y is the constraint set for real-time operation of the interdependent energy system as described in (5.1) - (5.20).

Problem (5.21) is a non-convex mixed-integer optimization problem, due to the non-convexity of (5.10). The piece-wise linear method [158] is adopted to approximate (5.10) into a set of linear constraints with auxiliary variables, formulating a mixed-integer linear programming counterpart of (5.21), which can be solved efficiently by off-shore solvers, e.g., Gurobi [159].

5.3.2 Assessment Indices

In addition to the power operational indices and infrastructure indices introduced in 4.4.2 of Chapter 4, NG operational indices related to load shedding are used to reflect the ability of interdependent power and NG systems to provide adequate service to customers under hurricanes. Overall indices are proposed to quantify the hurricane impact on the integrated energy systems.

5.3.2.1 NG Operational Indices

At load point level, time-varying gas demand not supplied and related cost at gas nodes are used to reveal the hurricane impact over time and space, as follows:

$$DNS^{t}_{\mathrm{g},j} = \sum_{i \in S^{t}_{\mathrm{glc}}} \pi^{i,t}_{\mathrm{glc}} \cdot DNS^{i,t}_{\mathrm{g},j} \tag{5.22}$$

$$C^{t}_{\mathrm{glc},j} = \Delta t \cdot DNS^{t}_{\mathrm{g},j} \cdot C^{t}_{\mathrm{g},j} \tag{5.23}$$

where $DNS^{t}_{\mathrm{g},j}$ (MMSCF·h^{-1}) is the expected gas demand not supplied at node j during time slot t. S^{t}_{glc} is the set of power system states with gas load curtailment during time slot t. $\pi^{i,t}_{\mathrm{glc}}$ is the associated probability of power system state i. $DNS^{i,t}_{\mathrm{g},j}$ (MMSCF·h^{-1}) is the gas demand not supplied at node j associated with system state i. It is equal to $Q^{t}_{\mathrm{lc},j}$ in (5.21) associated with system state i. $C^{t}_{\mathrm{glc},j}$ and $C^{t}_{\mathrm{g},j}$(M$) are the cost of gas load shedding and per-unit interruption cost at node j, respectively.

At the system level, hourly-varying gas demand not supplied are expressed as follows:

$$DNS^{t}_{\mathrm{g}} = \sum_{j \in \mathcal{N}_{\mathrm{gd}}} DNS^{t}_{\mathrm{g},j} \tag{5.24}$$

where DNS^{t}_{g} (MMSCF·h^{-1}) is the gas system demand not supplied during t.

5.3.2.2 Overall Indices

Total power energy not supplied introduced in 4, total gas energy not supplied, $TENS_{\mathrm{g}}$ (BTU), as well as total cost $TCOST$ (M$) of the interdependent power and

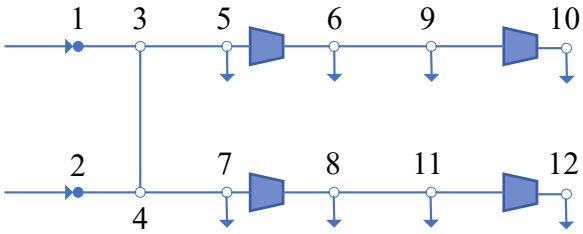

Figure 5.3: The 12-Node NG transmission system.

NG systems are used to offer a summarized view, as follows:

$$TENS_{\mathrm{g}} = \sum_{t=1}^{\mathrm{T}} \Delta t \cdot DNS_{\mathrm{g}}^{t} \tag{5.25}$$

$$TCOST = TCOST_{\mathrm{e}} + \sum_{t=1}^{\mathrm{T}} \sum_{j \in \mathcal{N}_{\mathrm{gd}}} C_{\mathrm{glc},\,j}^{t} \tag{5.26}$$

5.4 Case Studies

Under a simulated hurricane, the IEEE 24-reliability test system and the 12-node NG transmission system are used to validate the effectiveness of the proposed method.

5.4.1 Test Systems

5.4.1.1 12-Node NG Transmission System

The 12-node NG test system as shown in Fig. 5.2 is modified from the 15-node NG transmission system in [50]. It has 12 nodes, 7 pipelines and 4 compressors as described in Table 5.1, Table 5.2 and Table 5.3, respectively. The daily gas load profile is referred to [160].

Table 5.1: Nodes in the 12-Node Gas System

Node	Q_{gs}^{max} (MMSCF·h^{-1})	Q_{gs}^{min} (MMSCF·h^{-1})	Q_{gd} (MMSCF·h^{-1})	$\mathcal{P}^{max}$ (psia)	$\mathcal{P}^{min}$ (psia)
1	50	0	0	1200	600
2	50	0	0	1200	600
3	0	0	1.438	1200	500
4	0	0	0.818	1200	500
5	0	0	1.3248	1200	400
6	0	0	1.0424	1200	400
7	0	0	1.3450	1200	400
8	0	0	1.1363	1200	400
9	0	0	2.7253	1200	400
10	0	0	2.0787	1200	400
11	0	0	1.0424	1200	400
12	0	0	4.4385	1200	400

Table 5.2: Pipelines in the 12-Node Gas System

Compressor	From node	To node	C_{gp}^{1}	C_{gp}^{2}	Q_{br}^{max} (MMSCF·h^{-1})
1	1	3	1196.6885	88.56261	12.9196
2	2	4	1196.6885	88.56261	12.9357
3	3	4	1196.6885	88.56261	15.5040
4	3	5	1189.3805	87.12770	15.5062
5	4	7	1189.3805	87.12770	14.7093
6	6	9	1189.3805	87.12770	12.5349
7	8	11	1643.6379	206.4352	8.8203

Table 5.3: Compressors in the 12-Node Gas System

Compressor	From node	To node	Fed by power bus	RC_{gc}	HP_{gc}^{max}
1	5	6	8	1.37	6206.7185
2	7	8	19	1.378	5928.89065
3	9	10	20	1.37	5017.3863
4	11	12	14	1.378	3555.2062

Table 5.4: GFGs in the Power System in Case I-b)

GFG	Power Bus	Capacity (MW)	Fed by Gas Node	η_{g2e}
1	7	100	8	0.5
2	7	100	8	0.5
3	7	100	8	0.5
3	13	197	6	0.5
4	13	197	6	0.5
5	13	197	6	0.5
6	15	12	10	0.5
7	15	12	10	0.5
8	15	12	10	0.5
9	15	12	10	0.5
10	15	12	10	0.5
11	15	155	10	0.5
12	21	400	10	0.5
13	22	50	8	0.5
14	22	50	8	0.5
15	22	50	8	0.5
16	22	50	8	0.5
17	22	50	8	0.5
18	22	50	8	0.5

5.4.1.2 IEEE 24-Reliability Test System

The basic information of the IEEE 24-reliability test system has been introduced in Chapter 4. In this chapter, the total power load is enlarged by 1.4 times for all the three subcases. The power system load profile is extracted from [129] according to the hurricane date, time and duration.

Three subcases are used to validate the proposed method as follows:

Case I-a) Independent power system and NG system under the simulated hurricane. There are no power generators fueled by gas. Besides, all gas compressors are driven by gas turbines.

Case I-b) Interdependent power and NG systems under the simulated hurri-

cane. All gas compressors are driven by electricity as described in Table 5.3. Besides, all generators at power bus 7, 13, 15, 21 and 22 are assumed to be GFGs and fed by gas node 8, 6, 10, 10 and 8, respectively, as listed in Table 5.4.

Case I-c) Reduced capacity of GFGs. All generators with a total capacity of 215MW at power bus 15 are no longer fueled by NG. The total capacity of GFGs is reduced from 1806MW in case I-b) to 1591MW in this case.

5.4.2 Simulation Results

The overall comparison of the three subcases is shown in Table 5.5. Under the simulated hurricane, the independent power system in case I-a) suffers $TENS_{\mathrm{e}}$ as 104.3545MWh and *TCOST* as 8.9307M$. In comparison with case I-a, the interdependent power and NG systems in case I-b) suffer $TENS_{\mathrm{e}}$ as 265.3054MWh, increasing sharply by 154.2347%, $TENS_{\mathrm{g}}$ from 0 to 1.1794×10^{9}BTU and *TCOST* as 13.6984M$. The results indicate that the interdependence amplifies the hurricane impact by introducing the disruptions originally occurring in the power system to the connected NG system and further increasing the amount of power load shedding. When the capacity of GFGs is reduced in case I-c), there is an apparent decline in the power load shedding while the gas load shedding increases slightly in comparison with that in case I-b).

Besides, the expected number of damaged power components and the cost to repair or replace these components are with a slight difference in the three subcases due to the effect of the simulation process.

5.4.2.1 Impact of the Hurricane

The variation of bus load curtailments over $\mathcal{T}$ is shown in Fig.5.4. Load shedding occurs at bus 1 to 5, 8 to 10, 14 to 16, and 18 to 20, while loads on the left buses

Table 5.5: Comparison of 3 Subcases

Results		case I-a)	case I-b)	case I-c)
Objective values (M$)	Asset damage cost	5.8616	5.8616	5.9074
	Power load curtailment cost	3.0691	7.8026	6.8396
	Gas load curtailment cost	0	0.0342	0.0360
	Total cost	8.9307	13.6984	12.7829
Energy not supplied	Power (MWh)	104.3545	265.3054	232.5601
	Gas (Btu)	0	1.1794×10^9	1.2412×10^9
	Total (MWh)	104.3545	610.95334	596.3241

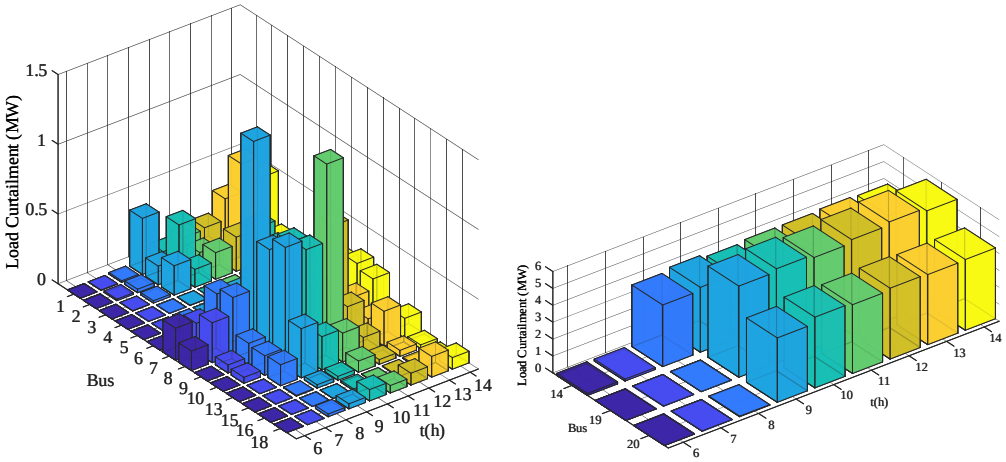

(a) (b)

Figure 5.4: Load curtailments at power buses in case I-a).

are rarely affected by the hurricane. Bus 19,14 and 20 have the top 3 highest load curtailment which is consistent with the results of transmission line failure probabilities. Line 11-14, 14-16, 16-19, 19-20, and 20-23 are with a greater likelihood to be damaged by the hurricane, which leads to the relatively high load curtailment at bus 14, 19, and 20.

The impact of the hurricane on the overhead transmission line failure probabilities has been analyzed in 4. In this chapter, the focus is on the impact of interdependence and the combined impacts of hurricanes and interdependence.

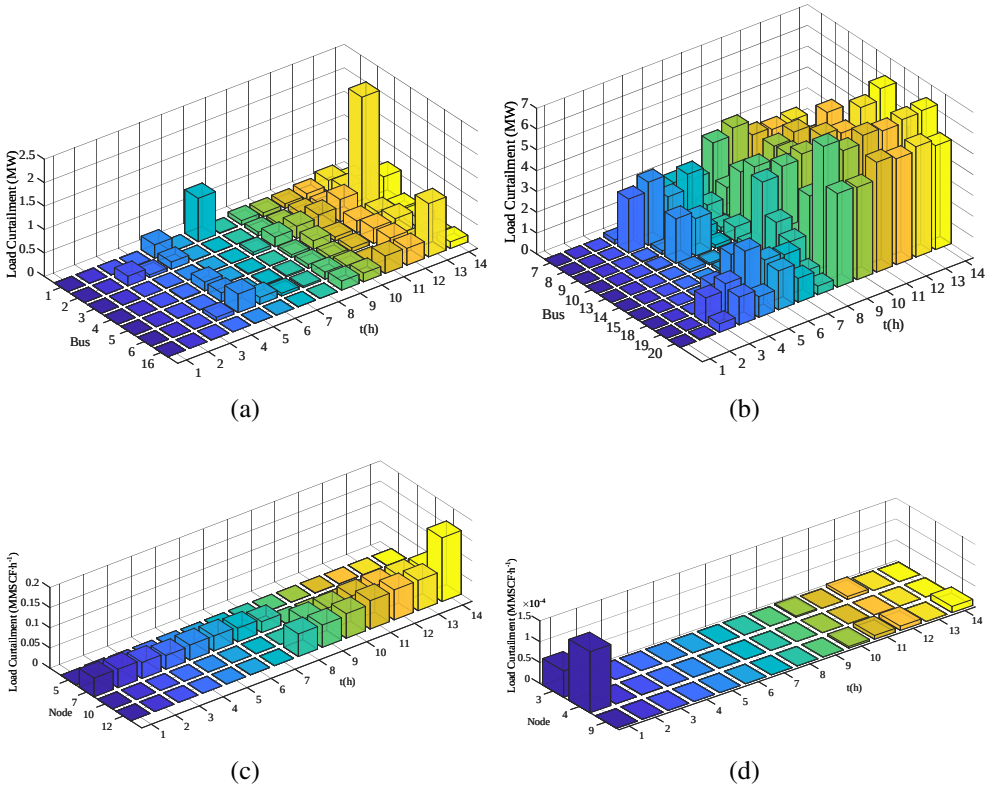

Figure 5.5: Load curtailments at power buses and gas nodes in case I-b).

5.4.2.2 Combined Impact of Hurricane and Interdependence

The time-varying load curtailment at power buses and gas nodes is given in Fig.5.5. It can be seen from Fig.5.5a and Fig.5.5b that load shedding is inevitable at all power buses with load[1]. Load curtailment at bus 14, 19 and 20 are significantly higher than others as in case I-a). In comparison with case I-a), all power load buses experience more load shedding in case I-b) due to the insufficient power generation caused by the shortage of gas fuel. By comparing Fig.5.4a and Fig.5.5a, it can be seen load shedding at bus 7 to 10, 13 to 16, and 18 to 20 increases sharply.

Besides, power load shedding in case I-a) starts from $t = 5$, while in case I-b),

[1]In IEEE-24 Reliability Test System, there are 17 power buses with load out of 24 buses

both the power system and the NG system experience load shedding over the whole $\mathcal{T}$ due to the negative impact of interdependence. The difference demonstrates the different characteristics of electricity and NG. NG can be stored in pipelines for later use to achieve optimal objectives.

Node 12, 10 and 7 have the top three high load shedding. NG supplied to 12 has to be through compressor 11-12, which gains electricity from power bus 14. However, bus 14 is easy to be isolated with failures of power line 11-14 and 14-16. Unfortunately, the isolation of bus 14 interrupts power supplied to compressor 11-12, forces the compressor out and results in load shedding at node 12. Node 10 is the fuel source for 7 GFGs with a total capacity of 615MW. Although 5 GFGs with a capacity of 12MW at bus 15 are committed to be down according to the UC result, node 12 still affords fuel for 555MW power generation capacity, which puts much stress on node 12 and challenges its ability to satisfy all loads connected to it. Node 7 suffers the third high load shedding because it is set to have much lower weight factor than other nodes except node 5 which has the same weight factor as node 7.

Take an example to explain how the interdependence amplifies the adverse hurricane impact. For a power system state with transmission line 4-9 failed from time slot 5, 16-19 and 20-23 failed from time slot 9, 18-21 failed from time slot 10, bus 19 and 20 are isolated from time slot 9. Loads at power bus 19 and 20 are totally shed from time slot 9 due to bus isolation. As a result, gas compressor 7-8 (from node 7 to node 8) and 9-10 are forced out immediately, indicating that interruptions in the power system have spread to the NG system. When compressor 9-10 is out of service from time slot 9, all load at gas node 10 has to be shed immediately, which leads to cut off of gas fuel supplied to GFGs at power bus 15 and 21 and they are forced out from time slot 9. The impact of load shedding in the NG system loops back to the power system. From time slot 9, the

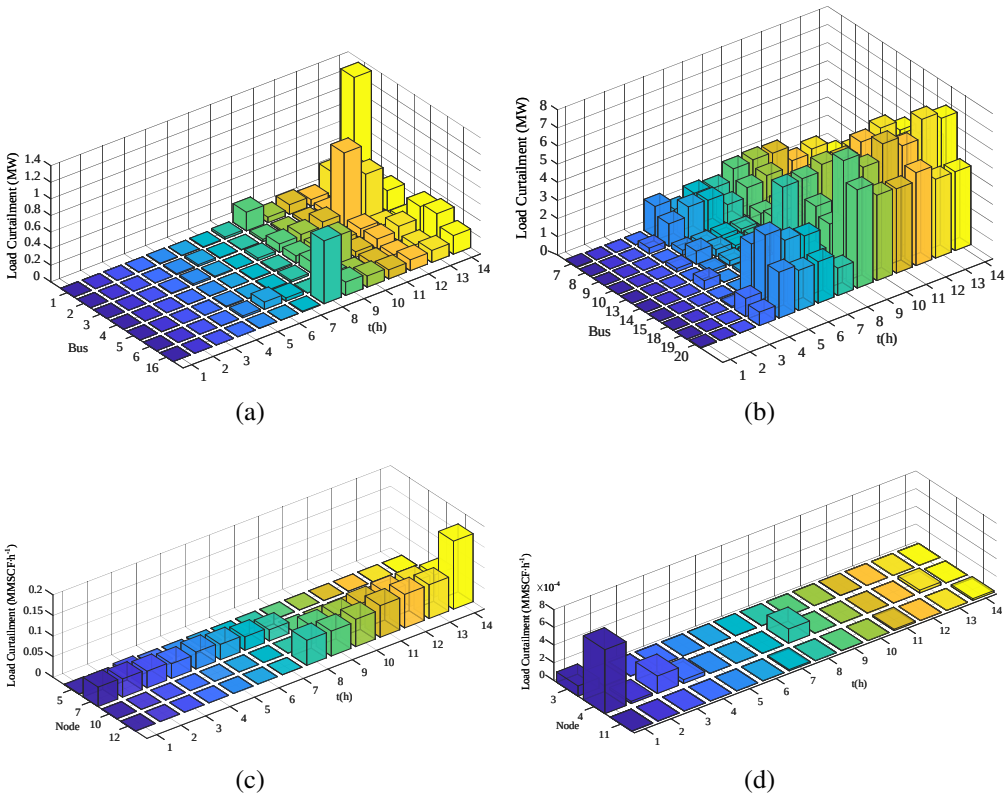

Figure 5.6: Load curtailments at power buses and gas nodes in case I-c).

NG stored at pipeline 8-11 is extracted to satisfy loads at node 8, 11 and 12. In order to store as much as NG in the pipeline 8-11, the NG system is optimized to increase the gas pressure at node 8, 11 and 12 from time slot 1 to 9. However, the gas stored is limited and due to the lower bound of node pressure constraint, the load at node 12 cannot be fully satisfied from time slot 13. Besides, in order to satisfy gas loads with higher priority, gas node 8 cannot provide gas to GFGs as much as required. As a result, GFGs fed by gas node 8 are with low output even out of service most of the time. Power generation shortage results in power load shedding at bus 13, 16, and 18.

5.4.2.3 Impact of the Interdependence

In comparison with case I-b), the total capacity of the GFGs is reduced by 215 MW, all 6 generators at power bus 15 are no longer fueled by NG in case I-c). As a result, as shown in Table 5.5, $TENS_{\mathrm{e}}$ decreases by 12.3425% from 265.3054MWh in case I-b) to 232.5601MWh, while $TENS_{\mathrm{g}}$ increases slightly by 5.2400% from 1.1794×10^{9}Btu in case I-b) to 1.2412×10^{9}Btu. *TCOST* is reduced by 6.6833% from 13.6984M$ in case I-b) to 12.7829M$ due to different factors of gas loads. Detailed time-varying load shedding at power buses and gas nodes is given in Fig.5.6. It is obvious the higher the interdependence is, the higher risk it may introduce. To prepare the connected system more effectively, more attention should be paid to the crucial interfaces.

5.4.2.4 Suggestions

According to the simulation results, suggestions can be provided to the system operators to allow directed actions to be planned and carried out before the advent of hurricanes. From the short-term perspective, for the simulated hurricane, deployment of the energy storage and the portable power generation at buses with load shedding, e.g., 14, 19 and 20, can help to reduce the risk of load curtailment and promote system resilience. Besides, the interlinks should be paid with special attention. For example, place backup generators at the location of electricity-driven gas compressors and use gas storage facilities at power plants to store gas for emergency use. For example, in case I-b) if compressor 7-8 and 11-12 are equipped with backup generators, the $TENS_{\mathrm{e}}$ would decrease significantly by 25.2700% from 114.3546MWh to 85.4572 MWh, while $TENS_{\mathrm{g}}$ would decrease dramatically by 76.0049% from 1.3074×10^{9}Btu to 3.1370×10^{8}Btu. Line pack storage could be considered as a helpful tool for enhancing the system

preparedness in emergency conditions. The adjustment of unit commitment status is also a potential strategy. Some generators will be committed to minimize the load shedding cost. From a long-term view, the upgrade of weak transmission lines with much strict design criteria and optimization of generation capacity and relocation can help to build a more resilient energy system.

5.5 Summary

This chapter proposes a jointed data and model approach for resilience assessment integrating component failure models under hurricanes and interdependent energy system models to quantify the hurricane impacts on the performance of interdependent power and NG systems. The simulation results reveal that the interdependence could amplify the adverse impacts of hurricanes on the power system and transfer the disturbance to the NG system.

Chapter 6

Resilience Assessment of Power Systems Under Hurricanes Considering Frequency Control

Under EWEs, e.g., hurricanes, failures of transmission lines can cause serious power imbalance and result in significant frequency deviation. An assessment method is proposed to reflect the negative hurricane impacts on the frequency performance of transmission networks in this chapter. The day ahead UC is obtained using the two-stage RO model developed in Chapter 5. For each system state with component failures generated by Monte Carlo simulation, at each time slot, the frequency regulation process is modeled including the primary, secondary and tertiary frequency control considering the physical constraints. The amount of load shedding in tertiary control at each time slot is determined based on the day ahead UC using the model developed in Chapter 4. In addition to the infrastructure and operational indices proposed in Chapter 4, frequency indices are used to reflect the system frequency performance. The modified IEEE 24-reliability test system under a simulated hurricane is used to validate the effectiveness of the proposed method. Simulation results show the hurricanes could cause frequency nadir or peak out of the required range and neglect of the frequency regulation process would lead to underestimation of the hurricane impacts. The method developed could be used as guidance of UC and regulation reserve under EWEs.

6.1 Introduction

The power system frequency which depends on the active power balance is a basic indicator of power quality. A large deviation of frequency from nominal value harms electrical devices, disturbs loads, threatens system stability even causes system collapse [161]. To maintain reliable and stable service, the power system frequency must be regulated to be within the allowed range through frequency control including primary, secondary and tertiary control. However, due to the increasing system size and complexity, as well as the changing structure, the operational conditions of power systems are changing widely.

Many studies have recognized the changing operation conditions and propose frequency control schemes, methods and strategies to solve problems arising. For example, energy storage is used for quick response [53], [54]; active load management is proposed to deviate the imbalance of generation and load to improve the system frequency performance [55]; load shedding strategies are developed to prevent system frequency out of range [56]. The majority of these studies particularly consider the effects of high penetration of renewable resources on frequency regulation, such as wind turbines and solar panels due to their intermittency and uncertainty features [57]–[60]. However, EWEs that frequently occur in recent years, such as hurricanes, also pose great challenges to power system operation by extreme adverse environments under which exposed electrical components fail with higher probabilities than in normal conditions, as stated in Chapter 4. For example, the failures of transmission lines display spatial-temporal features under hurricanes due to the moving of hurricanes and the changing hurricane intensity. Sequential failures of transmission lines could isolate loads or generations and results in a sudden imbalance between load and generation. Some work can be found in power system resilience assessment under EWEs with

indices from the perspective of infrastructure and load shedding [61]–[64], which cannot describe the degradation of system performance caused by the isolation of generators or loads. However, much less work has been done to include the frequency regulation process and its impact on the system performance under EWEs. [65] proposes an islanding strategy considering the frequency constraints when splitting the system into islands.

In addition to the indices proposed in the literature, frequency deviation indices are necessary to describe and quantify the system frequency performance to provide guidance for regulation reserve requirements and resilience improvement from the perspective of frequency. Under this background, this chapter proposes a comprehensive method to quantify the performance of transmission networks under hurricanes taking account of the frequency regulation process. To mitigate the hurricane impacts on the day-ahead market from a probabilistic perspective, a resilient UC problem is formulated as a two-stage RO problem solved using a column-and-constraint generation scheme. System states are generated using Monte Carlo simulation. For each system state with component failures, the hourly UC is run at each time slot based on the results of the day ahead two-stage robust UC. For any time slot with generation and load imbalance, the frequency regulation process is modeled including the primary, secondary and tertiary frequency control with proper consideration of physical constraints such as regulation reserve capacity and generation ramp rate. In addition to the infrastructure indices and operational indices proposed in Chapter 4, frequency indices are used to reflect the system frequency performance and its impacts on operational indices. The contribution of this chapter can be summarized as follows: 1) Develop a method that evaluates hurricane impacts on the frequency performance of power systems. 2) Propose the two-stage robust UC to mitigate the hurricane impacts on the day-ahead market from a probabilistic perspective.

3) employment of frequency indices to quantify the system performance.

The remainder of this chapter is divided into five sections. Section 6.2 introduces the power system frequency control models. Section 6.3 presents the resilience assessment method and indices. Section 6.4 conducts case studies. Section 6.5 summarizes.

6.2 Power System Frequency Control Models

When a sudden imbalance of generation and load occurs, the system frequency deviates from the nominal value. The primary control response first to try to restore the system frequency to the nominal value. However, due to the characteristic of droop, there would be a difference between the new system frequency after primary control. The secondary control is activated on selected generators to restore the system frequency by changing the reference output setpoints of generators. If the system frequency is still out of the allowed range, load shedding or unit cut off is necessary to keep stable operation.

6.2.1 Primary Frequency Response Model

The primary control function is provided locally by speed governors on all generators, which take participate in the generation adjust automatically in response to the frequency change caused by a power imbalance between load and generation.

After a disturbance, the primary control adjusts the turbine valve or gate to balance the power mismatch in a time frame of seconds. When a new steady state is reached, the power output is changed according to their droop characteristics and the frequency is a new value, which is usually different from the nominal value due to the nature of droop.

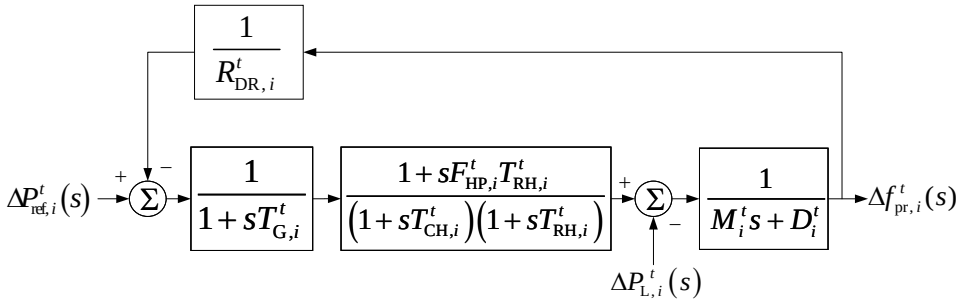

Figure 6.1: Block diagram of primary frequency control loop.

In the frequency control analysis, the collective performance of all generators in the system is represented by an equivalent generator with equivalent parameters. For a system state i at time slot t, the block diagram of the primary frequency control loop with a reheat steam turbine is shown in Fig.6.1.

The equivalent parameters are calculated as follows:

$$T^t_{\mathrm{G},i} = \sum_{g\in\mathcal{G}^t_{\mathrm{PR},i}} T_{\mathrm{G},g},\ \forall t \in \mathcal{T} \tag{6.1}$$

$$T^t_{\mathrm{CH},i} = \sum_{g\in\mathcal{G}^t_{\mathrm{PR},i}} T_{\mathrm{CH},g},\ \forall t \in \mathcal{T} \tag{6.2}$$

$$T^t_{\mathrm{RH},i} = \sum_{g\in\mathcal{G}^t_{\mathrm{PR},i}} T_{\mathrm{RH},g},\ \forall t \in \mathcal{T} \tag{6.3}$$

$$F^t_{\mathrm{HP},i} = \sum_{g\in\mathcal{G}^t_{\mathrm{PR},i}} F_{\mathrm{HP},g},\ \forall t \in \mathcal{T} \tag{6.4}$$

$$M^t_i = 2\sum_{g\in\mathcal{G}^t_{\mathrm{PR},i}} M_g,\ \forall t \in \mathcal{T} \tag{6.5}$$

$$R^t_{\mathrm{DR},i} = \sum_{g\in\mathcal{G}^t_{\mathrm{PR},i}} \frac{1}{R_{\mathrm{DR},g}},\ \forall t \in \mathcal{T} \tag{6.6}$$

where $\mathcal{T}$ is the assessment horizon divided into equal time intervals with a length

of Δt, and $T = |\mathcal{T}|$. $\mathcal{G}^t_{\mathrm{PR},i}$ is the set of units that respond to the frequency change in the primary loop. $T^t_{\mathrm{G},i}$, $T^t_{\mathrm{CH},i}$ and $T^t_{\mathrm{RH},i}$ are the system equivalent governor, steam chest and reheat turbine time constant of state i at time slot t, respectively. $F^t_{\mathrm{HP},i}$ denotes the equivalent high pressure power fraction of reheat turbine. M^t_i is the equivalent system inertia constant. $R^t_{\mathrm{DR},i}$ is the system equivalent droop. D^t_i represents the damping constant of system loads. $T_{\mathrm{G},g}$, $T_{\mathrm{CH},g}$, $T_{\mathrm{RH},g}$, $F_{\mathrm{HP},g}$, M_g and $R_{\mathrm{DR},g}$ are governor time constant, steam chest time constant, reheat turbine time constant, high pressure power fraction of reheat turbine, inertia constant and droop of unit g, respectively.

When the speed setting unchanged, $\Delta P^t_{\mathrm{ref},i} = 0$. The transfer function of the primary frequency response loop is given as follows:

$$G^t_{\mathrm{L},i}(s) = \frac{\left(1+sT^t_{\mathrm{G},i}\right)\left(1+sT^t_{\mathrm{CH},i}\right)\left(1+sT^t_{\mathrm{RH},i}\right)}{\left(1+sT^t_{\mathrm{G},i}\right)\left(1+sT^t_{\mathrm{CH},i}\right)\left(1+sT^t_{\mathrm{RH},i}\right)\left(M^t_i s+D^t_i\right)+R^t_{\mathrm{DR},i}\left(1+sF^t_{\mathrm{HP},i}T^t_{\mathrm{RH},i}\right)}, \quad \forall t \in \mathcal{T} \tag{6.7}$$

For system state i, following a load change $\Delta P^t_{\mathrm{L},i}$ at t, the frequency deviation is written as follows:

$$\Delta f^t_{\mathrm{pr},i}(s) = -G^t_{\mathrm{L},i}(s)\,\Delta P^t_{\mathrm{L},i}(s), \ \forall t \in \mathcal{T} \tag{6.8}$$

where $\Delta f^t_{\mathrm{pr},i}(s)$ and $P^t_{\mathrm{L},i}(s)$ are the frequency deviation and load change in s-domain, respectively.

The steady-state frequency deviation $\Delta f^t_{\mathrm{pr},i}$ is calculated as follows:

$$\Delta f^t_{\mathrm{pr},i} = \frac{\Delta P^t_{\mathrm{L},i}}{1/R^t_{\mathrm{DR},i} + D^t_i}, \ \forall t \in \mathcal{T} \tag{6.9}$$

It can be seen the steady state frequency deviation following a load change depends on the droop characteristic of the equivalent generator and the composite system load frequency characteristic.

The dynamic response of primary frequency control, $\Delta f^t_{\mathrm{pr},i}(t)$ can be found by straight forward inverse Laplace transform of $\Delta f^t_{\mathrm{pr},i}(s)$, which is expressed as follows:

$$\Delta f^t_{\mathrm{pr},i}(t) = \mathcal{L}^{-1}\left(f^t_{\mathrm{pr},i}(s)\right) = \mathcal{L}^{-1}\left(\frac{-G^t_{\mathrm{L},i}(s)\,\Delta P^t_{\mathrm{L},i}}{s}\right),\ \forall t \in \mathcal{T} \tag{6.10}$$

Due to the high order feature of (6.10), numerical methods can be used to yield $\Delta f^t_i(t)$.

6.2.2 Secondary Frequency Response Model

According to the primary frequency response model, following a load change, there is still a considerable frequency deviation for a power system installed with speed governors when the speed changer setting is fixed at a given value. When the frequency deviation is out of the pre-defined range, the secondary control is responsible to restore the frequency to the nominal value.

The secondary control is centralized and accomplished by speed changer motors automatically to adjust the load reference setpoints of generators in a time frame of few seconds to minutes after a distance. If the load increases, more generation is required; otherwise, some generation capacity is cut. The secondary control is directly affected by the available power spinning reserve, constrained physically by the amount and the rate of change of power generation. The method developed in [58] is employed to consider the effects of the spinning reserve on the secondary control loop as shown in Fig.6.2.

Different from the control loop developed in [162] where load reference settings are accomplished by an integral control, the control loop in 6.2 has two inputs: the load change $\Delta P^t_{\mathrm{L},i}$ and the power automatic generation control (AGC) regulation curve of the equivalent generation unit $\Delta P^t_{\mathrm{sc},i}$, which is expressed as

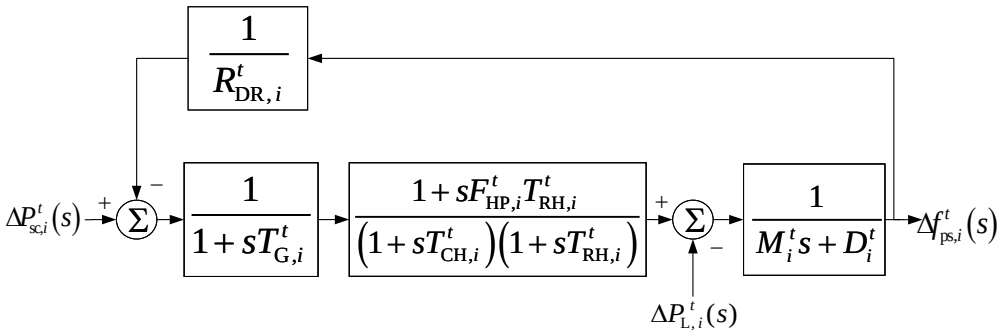

Figure 6.2: Block diagram of primary and secondary frequency control loop.

follows:

$$\Delta P^t_{\mathrm{sc},i}(t)=\begin{cases} K^t_{\mathrm{sc},i}t, & 0\le t\le t^t_{\mathrm{s2s},i} \\ \Delta P^t_{\mathrm{s2s},i}, & t^t_{\mathrm{s2s},i}\le t \end{cases},\ \forall t\in\mathcal{T} \tag{6.11}$$

$$K^t_{\mathrm{sc},i}=\frac{1}{2}\left(\left(1+\mathrm{sign}\left(\Delta P^t_{\mathrm{L},i}\right)\right)\sum_{g\in\mathcal{G}^t_{\mathrm{sc},i}}R^{+,t}_{\mathrm{sc},i}+\left(\mathrm{sign}\left(\Delta P^t_{\mathrm{L},i}\right)-1\right)\sum_{g\in\mathcal{G}^t_{\mathrm{sc},i}}R^{-,t}_{\mathrm{sc},g}\right),$$

$$\forall t\in\mathcal{T} \tag{6.12}$$

$$\Delta P^t_{\mathrm{s2s},i}=\begin{cases} \Delta P^t_{\mathrm{L},i}, & -\Delta P^{\min,t}_{\mathrm{sc},i}\le\Delta P^t_{\mathrm{L},i}\le\Delta P^{\max,t}_{\mathrm{sc},i} \\ \Delta P^{\min,t}_{\mathrm{sc},i}, & \Delta P^{\min,t}_{\mathrm{sc},i}<\Delta P^t_{\mathrm{L},i} \\ \Delta P^{\max,t}_{\mathrm{sc},i}, & \Delta P^t_{\mathrm{L},i}<\Delta P^{\max,t}_{\mathrm{sc},i} \end{cases},\ \forall t\in\mathcal{T} \tag{6.13}$$

$$t^t_{\mathrm{s2s},i}=\frac{\Delta P^t_{\mathrm{s2s},i}}{K^t_{\mathrm{sc},i}},\ \forall t\in\mathcal{T} \tag{6.14}$$

$$\Delta P^{\min,t}_{\mathrm{sc},i}=\sum_{g\in\mathcal{G}^t_{\mathrm{sc},i}}\left(P^{\min}_g-P^t_g\right),\ \forall t\in\mathcal{T} \tag{6.15}$$

$$\Delta P_{\mathrm{sc},i}^{\max,t} = \sum_{g \in \mathcal{G}_{\mathrm{sc},i}^{t}} \left(P_g^{\max} - P_g^t \right), \ \forall t \in \mathcal{T} \tag{6.16}$$

where t is the time duration from the beginning of time slot t. $\Delta P_{\mathrm{sc},i}^{t}(t)$ is the power regulation curve at the time-domain of AGC units considering the ramp rate and spinning reserve capacity. $K_{\mathrm{sc},i}^{t}$ is the equivalent ramp rate of AGC units contributing to the secondary control loop. $t_{\mathrm{s2s},i}^{t}$ is the time required for the AGC units to reach the new load reference setpoints. $\Delta P_{\mathrm{s2s},i}^{t}$ is the generation change of AGC units. $\mathcal{G}_{\mathrm{sc},i}^{t}$ is the set of AGC units contributing to the secondary control with state i at time slot t. $R_{\mathrm{sc},g}^{+,t}$ and $R_{\mathrm{sc},g}^{-,t}$ are the ramp up rate and ramp down rate of generation unit g, respectively. $\Delta P_{\mathrm{sc},i}^{\min,t}$ and $\Delta P_{\mathrm{sc},i}^{\max,t}$ are minimal and maximal adjustment capacity of AGC units when the system load decreases or increases, respectively. $P_g^{\min}$ and $P_g^{\max}$ are minimal and maximal output of unit g, respectively. P_g^t is the setpoint of unit g before the load change.

The output of the control loop in Fig.6.3 with two input is expressed as follows:

$$\Delta f_{\mathrm{ps},i}^{t}(s) = \Delta P_{\mathrm{L},i}^{t}(s)\, G_{\mathrm{L},i}^{t}(s) + \Delta P_{\mathrm{sc},i}^{t}(s)\, G_{\mathrm{sc},i}^{t}(s), \ \forall t \in \mathcal{T} \tag{6.17}$$

where $\Delta P_{\mathrm{sc},i}^{t}(s)$ is the Laplace transform of $\Delta P_{\mathrm{sc},i}^{t}(t)$, expressed as follows:

$$\Delta P_{\mathrm{sc},i}^{t}(s) = \frac{K_{\mathrm{sc},i}^{t}\left(1 - e^{-t_{\mathrm{s2s},i}^{t}}\right)}{s^2}, \ \forall t \in \mathcal{T} \tag{6.18}$$

$G_{\mathrm{sc},i}^{t}(s)$ is the transfer function with input $\Delta P_{\mathrm{sc},i}^{t}(s)$ and output $\Delta f_{\mathrm{ps},i}^{t}(s)$, described as follows:

$$G_{\mathrm{sc},i}^{t}(s) = \frac{1 + sF_{\mathrm{HP},i}^{t} T_{\mathrm{RH},i}^{t}}{\left(1+sT_{\mathrm{G},i}^{t}\right)\left(1+sT_{\mathrm{CH},i}^{t}\right)\left(1+sT_{\mathrm{RH},i}^{t}\right)\left(M_i^t s + D_i^t\right) + R_{\mathrm{DR},i}^{t}\left(1+sF_{\mathrm{HP},i}^{t}T_{\mathrm{RH},i}^{t}\right)}, \quad \forall t \in \mathcal{T} \tag{6.19}$$

The steady state frequency deviation is calculated as follows:

$$\Delta f_{\mathrm{ps},i}^{t} = \frac{\Delta P_{\mathrm{s2s},i}^{t} - \Delta P_{\mathrm{L},i}^{t}}{1/R_{\mathrm{DR},i}^{t} + D_i^t}, \ \forall t \in \mathcal{T} \tag{6.20}$$

The dynamic response of primary and secondary control loop considering the limits of spinning reserve capacity and unit ramp rates is the inverse Laplace transform of $\Delta f^t_{\mathrm{ps},i}(s)$ as follows:

$$\Delta f^t_{\mathrm{ps},i}(t) = \mathcal{L}^{-1}\left(\Delta f^t_{\mathrm{ps},i}(s)\right),\ \forall t \in \mathcal{T} \tag{6.21}$$

where $\Delta f^t_{\mathrm{ps},i}(t)$ is the dynamic frequency deviation following a load change.

6.2.3 Tertiary Frequency Response Model

Following a considerable imbalance associated with serious load or generation change, the secondary frequency control loop may inadequate to restore the system frequency to the nominal value due to the insufficiency of the spinning reserve.

In this situation, an emergency control plan or the tertiary control, which can be achieved by load or generation shedding, load management, etc., must be applied to bring back the frequency to the specified value and reduce the cascading risk. The tertiary control can be activated automatically or manually according to activation criteria, such as the frequency nadir, the frequency changing rate. The timescale of the tertiary control is tens of minutes up to hours after a disturbance.

In this chapter, the focus is not on the strategy of the tertiary control; thus the model developed in Chapter 4, Section 4.4 is used in this chapter. It should be noted that in Chapter 4, the assessment time horizon is the hurricane event duration $\mathcal{T}$, and the optimization of load shedding is over $\mathcal{T}$, while in this Chapter, the shedding of load or generation is formulated as a rolling optimization problem using the model in Chapter 4, Section 4.4 with a look-ahead time. For each time slot t, the load or generation shedding is optimized over the next 6 hours from t if the secondary control is unable to restore the system frequency to the nominal value, but only the optimal load or generation result of t and the generation

scheduling of $t + 1$ are used. The detailed procedure is described in the next section.

6.3 Assessment Method and Frequency Indices

6.3.1 Assessment Method

The detailed procedure illustrated in Fig.6.3 is described as follows:

Step 1) and Step 2) are the same as Step 1) and Step 2) described in Chapter 4, Section 4.4.

Step 3) Day-ahead UC considering the hurricane impacts. To mitigate these impacts on the day-ahead market from a probabilistic perspective, the resilient UC problem is formulated as a two-stage RO problem as described in Appendix (no NG system included) solved using a column-and-constraint generation scheme.

Step 4) is the same as Step 3) described in Chapter 4, Section 4.4.

Step 5) Resilience indices calculation. For a system state generated in Step 4), check if any exposed component fails in $\mathfrak{T}$. If no, turn to step 3 to start the next iteration. If yes, calculate and update infrastructure indices proposed in Chapter 4.

Then calculate the dynamic frequency response from time slot $t = 1$. Record the frequency indices at t. If the steady state system frequency after the primary and secondary control is out of the allowed range, load or generation shedding at t and the generation scheduling at $t + 1$ is determined hourly with a looking ahead time of 6 hours using the model developed in Chapter 4, Section 4.4 with the day-ahead UC and system state at t as inputs, record and update the load shedding related indices at t and turn to $t + 1$ when $t < T$.

When $t = T$, check if converged. If no, turn to Step 4). If yes, end the simulation.

6.3.2 Assessment Indices

In addition to the operational indices, infrastructures indices and overall indices developed in Chapter 4 (detailed expressions are not repeated in this chapter), frequency indices are employed to describe the system frequency performance under hurricane impacts.

6.3.2.1 Frequency Indices

For each time slot t, four kinds of indices are used to quantify the system frequency behavior: the expected maximal frequency deviation, the expected time duration when the frequency is out of the allowed range, the expected number of frequency out of the allowed range, and expected indirect energy not supplied, which are calculated as follows:

$$\Delta f_{\mathrm{pk}}^{t} = \sum_{i \in S_{\mathrm{pk}}^{t}} \pi_{i}^{t} \cdot \Delta f_{\mathrm{pk},i}^{t} \tag{6.22}$$

$$\Delta f_{\mathrm{nr}}^{t} = \sum_{i \in S_{\mathrm{nr}}^{t}} \pi_{i}^{t} \cdot \Delta f_{\mathrm{nr},i}^{t} \tag{6.23}$$

$$n_{\mathrm{abf}}^{+,t} = \sum_{i \in S_{\mathrm{abf}}^{+,t}} \pi_{i}^{t} \tag{6.24}$$

$$n_{\mathrm{abf}}^{-,t} = \sum_{i \in S_{\mathrm{abf}}^{-,t}} \pi_{i}^{t} \tag{6.25}$$

$$t_{\mathrm{abf}}^{+,t} = \sum_{i \in S_{\mathrm{abf}}^{+,t}} \pi_{i}^{t} \cdot t_{\mathrm{abf},i}^{+,t} \tag{6.26}$$

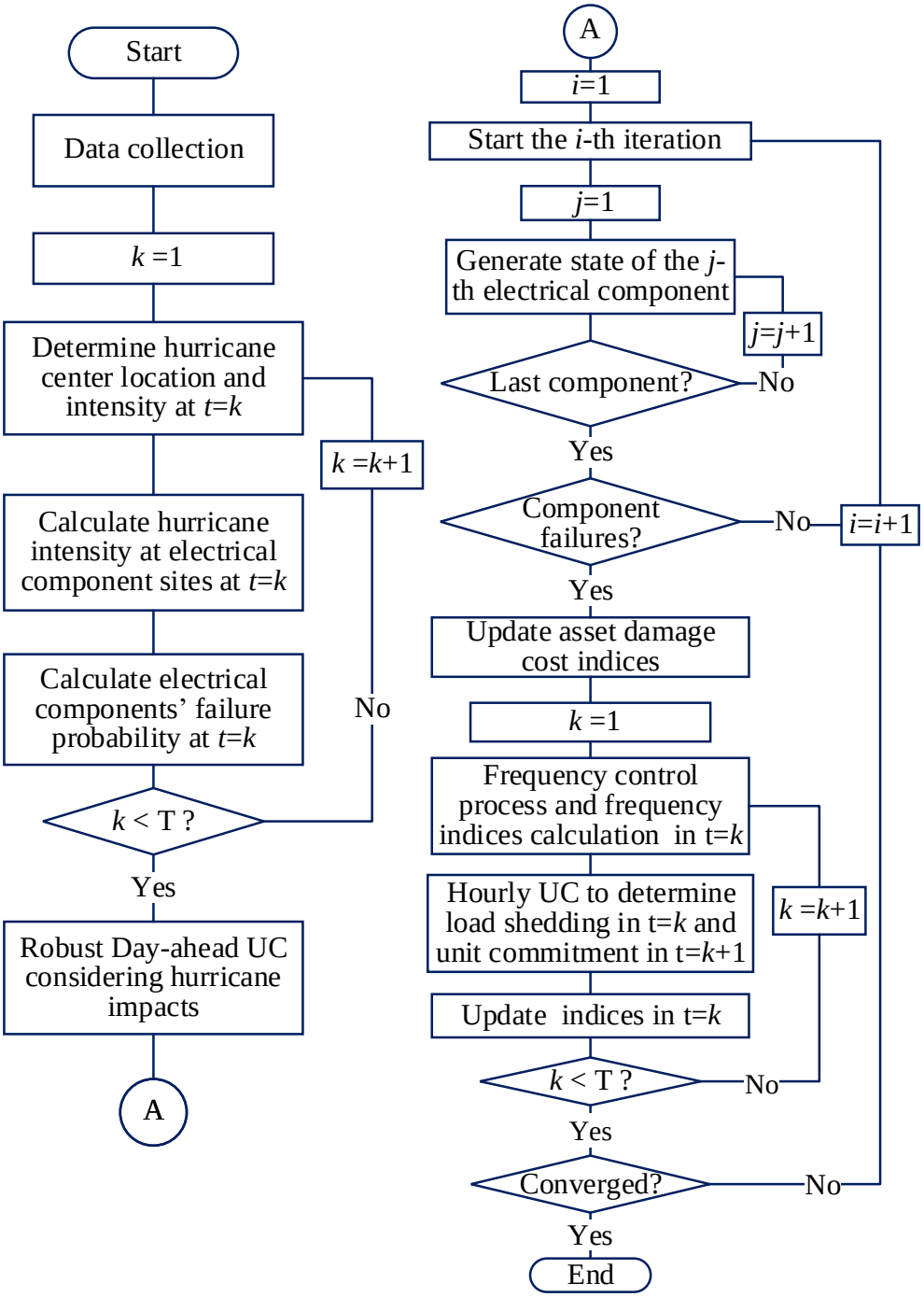

Figure 6.3: Procedure of power system resilience assessment under hurricanes considering frequency control process .

$$t_{\text{abf}}^{-,t} = \sum_{i \in S_{\text{abf}}^{-,t}} \pi_i^t \cdot t_{\text{abf},i}^{-,t} \tag{6.27}$$

$$ENS_{\text{pst}}^t = \sum_{i \in S_{\text{abf}}^{-,t}} \pi_i^t \cdot I_{\text{rs},i}^t \left(\frac{\Delta P_{\text{sc},i}^{\max,t}}{2} \left(t_{\text{pr},i}^t + t_{\text{ps},i}^t \right) + \left(\Delta P_{\text{L},i}^t - \Delta P_{\text{sc},i}^{\max,t} \right) \Delta t \right)$$

$$+ \sum_{i \in S_{\text{abf}}^{-,t}} \pi_i^t \cdot \left(1 - I_{\text{rs},i}^t \right) \frac{\Delta P_{\text{L},i}^t}{2} \left(t_{\text{pr},i}^t + t_{\text{ps},i}^t \right) \tag{6.28}$$

where Δf_{pk}^t and Δf_{nr}^t are the expected peak and nadir value of frequency deviation at time slot t, respectively. S_{pk}^t and S_{nr}^t are the set of system states with positive and negative frequency deviation, respectively. $\Delta\pi_i^t$ is the associated probability of state i at time slot t. $\Delta f_{\text{pk},i}^t$ and $\Delta f_{\text{nr},i}^t$ are the peak and nadir value of the frequency deviation associated with system state i at time slot t. $n_{\text{abf}}^{+,t}$ and $n_{\text{abf}}^{-,t}$ are the expected number of frequency deviation that exceeds the up and low limit during time slot t, respectively. $S_{\text{abf}}^{+,t}$ and $S_{\text{abf}}^{-,t}$ are the set of system states with frequency deviation exceeding the up and low limit during time slot t, respectively. $t_{\text{abf}}^{+,t}$ and $t_{\text{abf}}^{-,t}$ are the expected time duration of frequency deviation that exceeds the up and low limit during time slot t, respectively. $t_{\text{abf},i}^{+,t}$ and $t_{\text{abf},i}^{-,t}$ are the time duration of frequency deviation that exceeds the up and low limit of system state i during time slot t, respectively. $I_{\text{rs},i}^t$ is the indicator of frequency restoration, and $I_{\text{rs},i}^t = 1$ when $\Delta P_{\text{L},i}^t < \Delta P_{\text{ps},i}^{\max,t}$, otherwise $I_{\text{rs},i}^t = 0$. ENS_{pst}^t is the expected energy not supplied considering the frequency control process during time slot t as proposed in [58]. $t_{\text{pr},i}^t$ is the time duration of the primary control process. $t_{\text{ps},i}^t$ is the total time duration of the primary and secondary control process. $t_{\text{pr},i}^t$ and $t_{\text{ps},i}^t$ are calculated using the iteration method proposed in [58].

6.3.2.2 Overall Indices

The calculation of $TCOST_{\mathrm{e}}$ is the same as that in Chapter 4, while the total power energy not supplied, $TENS_{\mathrm{e}}$ (MWh) considering the frequency control process is recalculated as follows:

$$TENS_{\mathrm{e}} = \sum_{t=1}^{\mathrm{T}} ENS_{\mathrm{pst}}^{t} \tag{6.29}$$

6.4 Case Studies

6.4.1 Test System

Under a simulated hurricane, the IEEE 24-reliability test system is used to validate the effectiveness of the proposed method. The test system is the same as in Chapter 4 which is not described in detail in this chapter. It is assumed that all generator units in the system take participate in the primary and secondary frequency control with the same parameters as in [58]. The normal system frequency is 60 Hz. The maximal and minimal allowed frequency deviation is 0.2 Hz and -0.2 Hz, respectively.

Two subcases are used to validate the proposed method as follows:

Case I-a) Power system resilience assessment under the simulated hurricane without considering the frequency control process.

Case I-b) Power system resilience assessment under the simulated hurricane considering the primary, secondary and tertiary frequency control process.

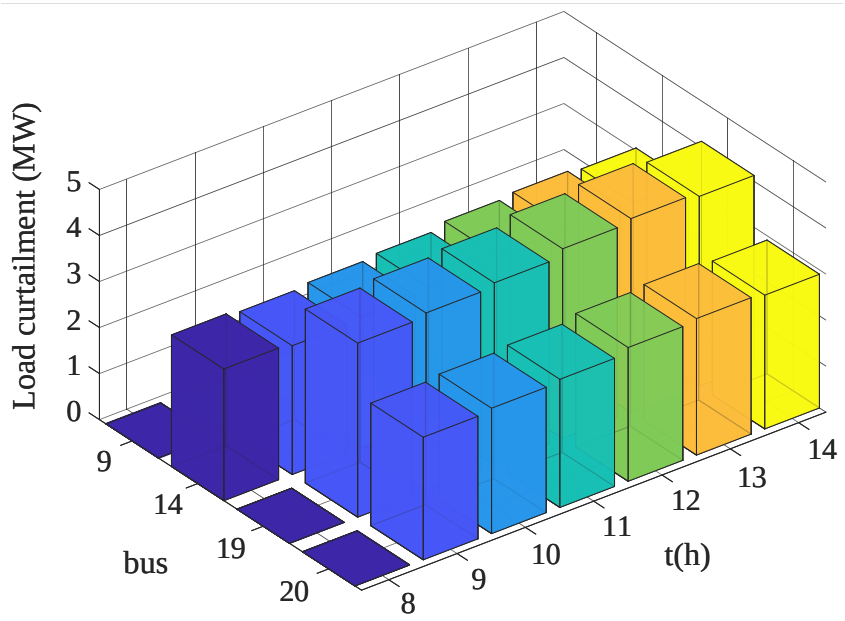

Figure 6.4: Load curtailment at buses in case I-a) and I-b).

6.4.2 Simulation Results

In case I-a), the load curtailment is optimized using the model developed in Chapter 4 while no frequency control process is considered. The amount of load curtailment at each load bus at time slot t associated with system state i in case I-a) is equal to the load curtailment determined in the tertiary control in case I-b). The time-varying load curtailments at buses are shown in 6.4.

Consistent with the simulation results in Chapter 4, bus 9, 14, and 19 to 20 are facing the highest risk of load curtailments due to the vulnerability of line 11-14, 14-16, 16-19, 19-20, and 20-23. The difference is that some buses in Chapter 4 with slight load curtailments are no longer suffer load curtailments in this chapter due to the different settings of the optimization problem, although the same model is used in these two chapters. In Chapter 4, the load shedding optimization is over the whole hurricane event duration $\mathcal{T}$ for each simulated

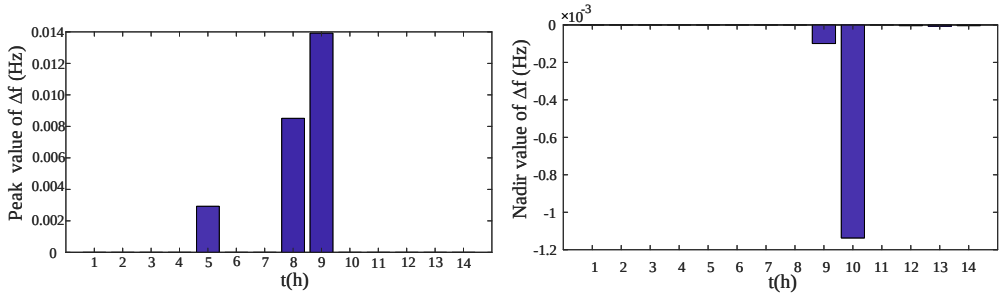

(a) (b)

Figure 6.5: Peak and nadir value of Δf in case I-b).

system state with component status generated over $\mathcal{T}$ by Monte Carlo simulation, while in this chapter the load shedding at each time slot t is optimized over the six hours from t with the component status at time slot t. It can also explain that the start time slot of load curtailment in Chapter 4 is from $t = 7$ while in this chapter it is from $t = 8$.

Under the simulated hurricane, the power system in case I-a) suffers $TENS_e$ as 61.3857 MWh, which is also slightly higher than 59.2848 MWh in Chapter 4 due to different settings. In comparison with case I-a), the power system in case I-b) suffers $TENS_e$ as 61.6553 MWh, increasing by 0.4372%. The results indicate that the frequency control process does have impacts on the power system resilience by introducing indirect energy not supplied during the duration of primary and secondary control. The indirect energy not supplied due to frequency deviation is not significant in case I-b) because generator failures are not considered and the probability of insufficient generation caused by line failures is relatively not very high due to the redundancy of the system networks.

The peak and nadir value of frequency deviation in case I-b) are shown in Fig.6.5. It can be seen from Fig.6.5a that the positive frequency deviation appears at $t = 5$, $t = 8$ and $t = 9$ which means that with some system states the generation output is larger than the system load which results in the increase of system

frequency. This is consistent with the time-varying line failure probabilities described in Chapter 4. For example, at $t = 5$, the hourly UC is determined at $t = 4$ with the system state at $t = 4$ and the assumption that the system state does not change from $t = 4$ to $t = 9$. According to the result of hourly UC, the generators at bus 7 are off and load at bus 8 are supplied through line 8-9 and 8-10. However, line 4-9, 5-10, 8-9 and 8-10 has much higher failure probability at $t = 5$ than at $t = 4$. As a result, it is possible that all components are up at $t = 4$ but line 8-9 and 8-10 fail at $t = 5$, which leads to the isolation of bus 7 and 8 as well as generators and load at bus 7 and 8. The left part of the system experience a sudden loss of load and the system frequency begins to increase. The reason for the positive frequency deviation at $t = 8$ and $t = 9$ is also the isolation of loads or constraints of line capacity due to line failures.

The negative frequency deviation appears at $t = 9, 10, 12, 13, 14$ but the absolute value is much lower than the expected peak value, which means the probability or the extent of negative power imbalance is not as high as the probability or the extent of positive power imbalance. In contrast to the reasons that cause positive frequency deviation, one reason that causes the negative frequency deviation is the isolation of generators due to the line failures. For example, at $t = 10$, line 17-22 and 21-22 have much higher failure probabilities than at $t = 9$. If line 17-22 and 21-22 are normal at $t = 9$ but fail at $t = 10$, bus 12 as well as the generators at bus 12 would be isolated. However, according to the hourly UC at $t = 10$ determined at $t = 9$, some generators at bus 12 are on. Sudden loss of generation leads to a decrease in system frequency.

The number of abnormal frequency deviations in case I-b) is shown in Fig.6.6. The expected number that the frequency exceeds the upper limit at $t = 9$ is higher than at $t = 8$ and $t = 5$, which means the system is of a high risk of losing load at $t = 9$. In comparison with the positive frequency deviation, the expected number

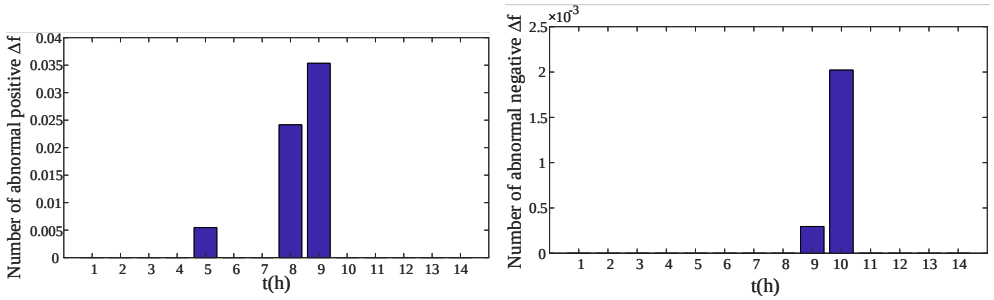

(a) (b)

Figure 6.6: Number of abnormal frequency deviation in case I-b).

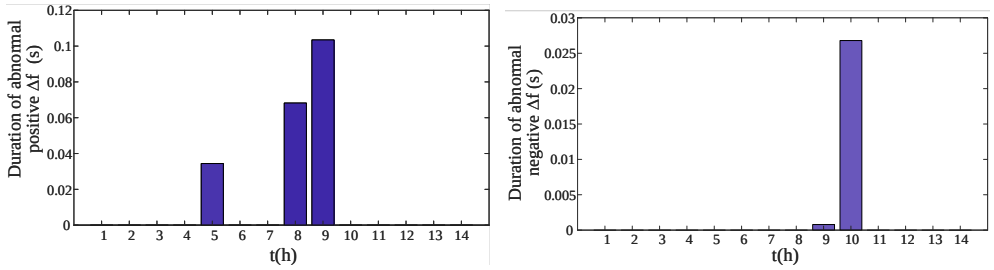

(a) (b)

Figure 6.7: Duration of abnormal frequency deviation in case I-b).

of frequency that out of the low bound is much lower, which means under the hurricane, the main issue is not the loss of generation but the loss of load at some time slots.

The duration of abnormal frequency deviation in case I-b) is shown in Fig.6.7. Both the expected duration of positive or negative frequency deviation that out of the allowed range is no more than 0.15s. However, these are expected values which mean that with some system states, the duration of abnormal frequency deviation may be much higher than the expected values and should be paid with special attention.

6.5 Summary

This chapter proposes a method to include the frequency control process in the performance assessment of power systems under hurricanes. The frequency indices are used to quantify the system frequency behaviors under hurricane impacts. Simulation results show there is a risk that the system would experience frequency deviation out of the allowed range at $t = 5, 8, 9, 10$ caused by the isolation of loads or generator units due to line failures under hurricanes. The method developed could be used as guidance of UC and regulation reserve under EWEs.

Chapter 7

Conclusions and Future Works

This chapter concludes the major contributions made by this thesis. It begins with reviewing of impacts of EWEs, interdependence, and resilience. Methods are proposed in the following chapters to evaluate the power system performance considering impacts of the fuel system, EWEs, and their combined impacts, respectively, with infrastructure, operational and frequency indices. The future work about improving power system resilience assessment under EWEs is also represented in this chapter.

7.1 Conclusion

In this thesis, the contributions are in four aspects: the long-term power system reliability assessment considering the fuel impacts, the spatial-temporal impacts of hurricanes on the power system's short-term reliability, the resilience assessment of integrated energy system under hurricanes, power system reliability considering the frequency control process under hurricanes. It should be emphasized that the works are logically related and they are explained as follows.

The utilization of NG as a primary fuel for electricity generation has been increasing in the past decades and is still a preferable choice for new generation capacity to overtake and replace the units relying on coal, leading to the rising dependence of the power system on the NG system. The reliance on NG for generating capacity imposes risks to power systems, such as failure propagation trigged by NG network contingencies, and affects the power system reliability. In this context, Chapter 3 develops an effective method to assess the impact of the associated NG fuel supply system on the long-term reliability of the transmission power system. It integrates the steady-state NG system model, optimal power flow model and the multi-state GFG model for quantitative measurement purposes, and proposes an integral simulation frame using non-sequential Monte Carlo simulation. The effectiveness of the method is verified by simulation and the results reveal impacts of fuel are significant.

In addition to increasing reliance on NG for generation, power systems also face challenges from EWEs, such as hurricanes. Hurricanes can damage power transmission network structure components, e.g., towers and conductors, and threat the power system reliability. A spatial-temporal reliability and damage assessment method is proposed in Chapter 4 to evaluate the effect of hurricanes. The hurricane can be a simulated, historical or forecasting one for different application

purposes, where the full track hurricane simulation model, historical records and forecasting information are used for the event construction, respectively. In the component failure analysis, the time-varying failure probability of transmission towers and conductors are modeled as functions of the time-varying hurricane intensity. In the reliability and damage assessment, the Monte Carlo simulation is adopted. The Energy Not Supplied and power outage costs caused by the hurricane event are used as operational indices, and the asset damage cost is proposed to quantify the damage of transmission networks. Simulation results show the method can quantify the hurricane impacts, identify the weak network parts, and provide information for pre-event preparedness for forecasting events.

Based on the work of Chapter 3 and Chapter 4, Chapter 5 touches the combined impacts of EWEs and interdependence. Although the impacts of interdependence and EWEs are explored individually, the combined effects should be carefully studied considering the inherent properties of each system and characteristics of interdependence coordinately. A comprehensive method is proposed in Chapter 5 to reflect the spatial-temporal hurricane impacts on interdependent power and NG systems. Mechanism analysis based and data based component failure models are based on the models developed in Chapter 4. The transit NG system model is used in Chapter 5 instead steady-state NG system model developed in Chapter 3. The integrated energy flow is developed to determine minimum joint load shedding. Operational metrics and infrastructure metrics are employed to quantify the service adequacy and network resistance of the interdependent energy systems, respectively. Simulation results show the method can identify weak parts and quantify the performance of interdependent power and natural gas systems under hurricanes to provide information for effective and coordinative preparedness.

Under EWEs, e.g., hurricanes, failures of transmission lines can cause serious power imbalance and result in significant frequency deviation. As a continuation

of Chapter 4 and Chapter 5, Chapter 6 proposes an assessment method is proposed to reflect the negative hurricane impacts on the frequency performance of transmission networks. The day ahead UC is obtained using the two-stage RO model developed in Chapter 5. For each system state with component failures generated by Monte Carlo simulation, at each time slot, the frequency regulation process is modeled including the primary, secondary and tertiary frequency control considering the physical constraints. The amount of load shedding in tertiary control at each time slot is determined based on the day ahead UC using the model developed in Chapter 4. In addition to the infrastructure and operational indices proposed in Chapter 4, frequency indices are used to reflect the system frequency performance. Simulation results show the hurricanes could cause frequency nadir or peak out of the required range and neglect of the frequency regulation process would lead to underestimation of the hurricane impacts. The method developed could be used as guidance of UC and regulation reserve under EWEs.

7.2 Recommendations for Further Research

In addition to the works in this thesis, there are some other promising research topics that worth meticulous investigations in the near future. These topics are detailed as follows.

A: Impacts of Flood due to Hurricanes on Integrated Energy Systems

Chapter 4 to Chapter 6 have shown how to assess the performance of power systems and integrated energy systems under hurricanes. However, they only consider the effects of strong wind and intense rainfall. In fact, hurricanes are a principal cause of flooding due to the volume of rain and storm surge. Unprecedented floods pose a range of challenges to electrical infrastructures.

For example, thy can damage towers, substations, and seriously threaten power plants. Besides, they can make access difficult for repair crews by destroying the transportation system. Although the site selection of electrical facilities is based on design and building criteria, as climate changes, the criteria may become inadequate. Some reviews and reports highlighted the need to protect the CIs from flooding in flood-prone areas in the literature. In this sense, a possible future work is to explore the development of models and methods for assessing flood risks to electrical assets.

B: Restoration Strategies

The work in this thesis mainly focuses on the assessment of system performance under EWEs. However, in addition to the ability of resistance to EWEs, the ability to restore is also a key feature of system resilience. The restoration of a system includes many aspects, such as resource allocation, network reconfiguration, and resources dispatching. The restoration process is also constrained by the physical status of transmission systems which are interdependent with power systems. As such, for future works, the restoration strategies of energy systems under and after EWEs considering constraints of other CIs should be carefully studied. Furthermore, optimization models should also be developed for the determination of cost-effective strategies so that the cost and benefits can be well balanced.

C: Resilience Improvement Strategies

The assessment methods and the indices proposed in this thesis enable the awareness of potential problems while improvement strategies have to be developed to promote system resilience. Chapter 4 to Chapter 6 have provided some suggestions from both short-term and long-term perspective, such as the deployment of the energy storage and the portable power generation, resilient generation

management considering failures of transmission systems to reduce the risk of load curtailment in the short-term, as well as upgrade of the weak transmission lines with much strict design criteria and optimization of generation capacity and relocation in the long-term. However, other potential strategies can contribute to building a more resilient energy system, such as the employment of electrical vehicles and microgrids. However, the cost and benefits of these strategies should be carefully evaluated and integrated into the resilience assessment process.

Appendix

Two-stage Robust Unit Commitment Model for Integrated Energy Systems

Considering uncertain transmission line failures under hurricanes, a two-stage robust UC model is proposed for the independent energy systems. First, this UC is conducted to generate the commitment status and reserve of power generators; then the results are input to the resilience assessment in Section 5.3, Chapter 5.

A.1 Objective Function

The objective is to minimize the start-up, shut-down, fuel and reserve cost of generators, together with the worst case load shedding cost considering the failures and operation status of transmission lines, as follows:

$$\min_{\mathbf{x}\in\mathbf{X}} f(\mathbf{x}) + \max_{\boldsymbol{\xi}\in\mathcal{U}} \left[\mathcal{Q}(\mathbf{x}, \boldsymbol{\xi})\right] \tag{A1}$$

$$f(\mathbf{x}) = \mathbf{c}^{\mathrm{T}}\mathbf{x}$$

$$= \sum_{t\in\mathcal{T}}\sum_{g\in\mathcal{G}} \left\{c_{\mathrm{start},g}\alpha_g^t + c_{\mathrm{shut},g}\beta_g^t + b_g u_g^t + \left[a_g p_{\mathrm{eg},g}^t + c_{\mathrm{r},g} R_g^t\right]\Delta t\right\} \tag{A2}$$

$$\mathcal{Q}(\mathbf{x}, \boldsymbol{\xi}) = \min_{\mathbf{y}\in\mathbf{Y}} \mathbf{d}^{\mathrm{T}}\mathbf{y} = VOLL \sum_{t\in\mathcal{T}} \sum_{j\in\mathcal{N}_{\mathrm{ed}}} P_{\mathrm{lc},j}^t \Delta t$$

$$\text{s.t.} \qquad \mathbf{E}\mathbf{y} \geq \mathbf{h} - \mathbf{G}\mathbf{x} - \mathbf{M}\boldsymbol{\xi} \tag{A3}$$

where $\boldsymbol{\xi}$ is the uncertainty variable vector. $\mathcal{T}$ is the set of scheduling time periods which is divided into equal time intervals with a length of Δt = 1h, and $T = |\mathcal{T}|$. $c_{\mathrm{start},g}$ (\$), $c_{\mathrm{shut},g}$ (\$), and $c_{\mathrm{r},g}$ (\$·MWh^{-1}) are the start-up, shut-down, and reserve

cost of generator g, respectively. a_g, b_g ($\cdot$MWh^{-1}) are fuel cost of generator g. $\mathbf{x} = \{\alpha_g^t, \beta_g^t, u_g^t, p_{\mathrm{eg},g}^t, R_g^t, p_{\mathrm{br},k}^t, \gamma_{\mathrm{br},k}^{+,t}, \gamma_{\mathrm{br},k}^{-,t}, q_{\mathrm{gs},s}^t, \mathbb{P}_{\mathrm{gp},k}^{+,t}, \mathbb{P}_{\mathrm{gp},k}^{-,t}, q_{\mathrm{gp},k}^{+,t}, q_{\mathrm{gp},k}^{-,t}, \mathbb{P}_{\mathrm{gc},c}^{+,t}, \mathbb{P}_{\mathrm{gc},c}^{-,t}, Hp_{\mathrm{gc},c}^t, q_{\mathrm{gfg},g}^t, p_{\mathrm{egc},c}^t\}$ is the first stage decision variables. α_g^t and β_g^t are the start-up and shut-down command of generator g, respectively. u_g^t is binary variables, 1 if generator g is on-line, 0 otherwise. $p_{\mathrm{eg},g}^t$ (MW) is the output of generator g. R_g^t (MW) is the reserve capacity of generator g. $p_{\mathrm{br},k}^t$ is the power transfer on line k. $\gamma_{\mathrm{br},k}^{+,t}$, $\gamma_{\mathrm{br},k}^{-,t}$ are the angle at from and to bus of line k, respectively. $q_{\mathrm{gs},s}^t$ (MMSCF$\cdot$h^{-1}) is the gas supply of source s. $\mathbb{P}_{\mathrm{gp},k}^{+,t}$ (psia), $\mathbb{P}_{\mathrm{gp},k}^{-,t}$ (psia) are the pressure at from and to node of pipeline k, respectively. $q_{\mathrm{gp},k}^{+,t}$ (MMSCF$\cdot$h^{-1}), $q_{\mathrm{gp},k}^{-,t}$ (MMSCF$\cdot$h^{-1}) are gas injection to and extraction from pipeline k, respectively. $\mathbb{P}_{\mathrm{gc},c}^{+,t}$, $\mathbb{P}_{\mathrm{gc},c}^{-,t}$ (psia) are pressure at outlet and inlet node of compressor c, respectively. $Hp_{\mathrm{gc},c}^t$ (hp) is the horsepower of compressor c. $q_{\mathrm{gfg},g}^t$ (MMSCF$\cdot$h^{-1}) is the gas consumption of GFG g. $p_{\mathrm{egc},c}^t$ (MW) is the electricity consumption of compressor c. *VOLL* ($\cdot$MWh^{-1}) is the value of load loss. $\mathbf{y} = \{P_{\mathrm{eg},g}^t, P_{\mathrm{br},k}^t, \theta_{\mathrm{br},k}^{+,t}, \theta_{\mathrm{br},k}^{-,t}, P_{\mathrm{lc},j}^t\}$ is the second stage decision variables. $\mathcal{N}_{\mathrm{ed}}$ is the set of power buses with loads. $P_{\mathrm{eg},g}^t$(MW) is the active power output of generator g. $P_{\mathrm{br},k}^t$ (MW) is the power transfer on line k. $\theta_{\mathrm{br},k}^{+,t}$, $\theta_{\mathrm{br},k}^{-,t}$ are the angle at from and to bus of line k, respectively. $P_{\mathrm{lc},j}^t$ (MW) is the power load shedding at bus j. $\mathbf{X}$ is the constraint set for the day-ahead scheduling, including both electrical systems and gas systems, depicted in A.2. $\mathbf{Y}$ is the constraint set for real-time operation of electrical systems after the realization of transmission lines, depicted in A.3. The constraint set for uncertainty variables, i.e., $\mathcal{U}$ is illustrated in A.4.

A.2 First-stage Constraint Set

The first-stage constraint set, i.e., **X**, includes the constraints for 1) power system and 2) NG system.

A.2.1 Power System

The technical constraints of power generators, transmission lines, power balance and reserve requirements are formulated as follows:

$$\alpha_g^t - \beta_g^t = u_g^t - u_g^{t-1},\ \forall t \in \mathcal{T}, g \in \mathcal{G} \tag{A4}$$

$$\sum_{h=t-\mathrm{UT}_g+1}^{t} \alpha_g^h \le u_g^t,\ \forall t \in \{\mathrm{UT}_g, ..., T\}, g \in \mathcal{G} \tag{A5}$$

$$\sum_{h=t-\mathrm{DT}_g+1}^{t} \beta_g^h \le 1 - u_g^t,\ \forall t \in \{\mathrm{DT}_g, ..., T\}, g \in \mathcal{G} \tag{A6}$$

$$u_g^t = u_g^0,\ \forall t \in \{\Delta t, ..., \mathrm{UT_r} + \mathrm{DT_r}\}, g \in \mathcal{G} \tag{A7}$$

$$u_g^t P_{\mathrm{eg},g}^{\min} \le p_{\mathrm{eg},g}^t - R_g^t,\ \forall t \in \mathcal{T}, g \in \mathcal{G} \tag{A8}$$

$$p_{\mathrm{eg},g}^t + R_g^t \le P_{\mathrm{eg},g}^{\max} u_g^t \Delta t,\ \forall t \in \mathcal{T}, g \in \mathcal{G} \tag{A9}$$

$$0 \le R_g^t \le \mathrm{R}_g^{10+} u_g^t,\ \forall t \in \mathcal{T}, g \in \mathcal{G} \tag{A10}$$

$$p_{\mathrm{eg},g}^t - p_{\mathrm{eg},g}^{t-1} \le \mathrm{R}_g^{60+} u_g^{t-1} \Delta t + \alpha_g^t \mathrm{SU}_g,\ \forall t \in \mathcal{T}, g \in \mathcal{G} \tag{A11}$$

$$p_{\mathrm{eg},g}^{t-1} - p_{\mathrm{eg},g}^t \le \mathrm{R}_g^{60-} u_g^t \Delta t + \beta_g^t \mathrm{SD}_g,\ \forall t \in \mathcal{T}, g \in \mathcal{G} \tag{A12}$$

$$\sum_{g \in \mathcal{G}_j} p_{\mathrm{eg},g}^t + \sum_{k \in \mathcal{E}_{\mathrm{br},j}^+} p_{\mathrm{br},k}^t - \sum_{k \in \mathcal{E}_{\mathrm{br},j}^-} p_{\mathrm{br},k}^t$$

$$= P^{t}_{\mathrm{ed},j} + \sum_{c \in \mathcal{E}_{\mathrm{egc},j}} p^{t}_{\mathrm{egc},c},\ \forall t \in \mathcal{T}, j \in \mathcal{N}_{\mathrm{e}} \tag{A13}$$

$$p^{t}_{\mathrm{br},k} - B_{\mathrm{br},k}\left(\gamma^{+,t}_{\mathrm{br},k} - \gamma^{-,t}_{\mathrm{br},k}\right) = 0,\ \forall t \in \mathcal{T}, k \in \mathcal{E}_{\mathrm{br}} \tag{A14}$$

$$P^{\min}_{\mathrm{br},k} \leq p^{t}_{\mathrm{br},k} \leq P^{\max}_{\mathrm{br},k},\ \forall t \in \mathcal{T}, k \in \mathcal{E}_{\mathrm{br}} \tag{A15}$$

$$\sum_{g \in \mathcal{G}} R^{t}_{g} \geq \delta \sum_{j \in \mathcal{N}_{\mathrm{ed}}} P^{t}_{\mathrm{ed},j},\ \forall t \in \mathcal{T} \tag{A16}$$

where UT_g (h) and DT_g (h) are minimum up and down time of generator g, respectively. $\mathrm{UT_r}$ and $\mathrm{DT_r}$ (h) are remaining up and down time of generator g, respectively. $P^{\min}_{\mathrm{e},g}$ (MW) and $P^{\max}_{\mathrm{e},g}$(MW) are the low and up bound of real power output of unit g, respectively. R^{10+}_{g} ($\mathrm{MW{\cdot}h^{-1}}$) is the ramp up limitation within 10 minutes of generator g. R^{60+}_{g} ($\mathrm{MW{\cdot}h^{-1}}$) and R^{60-}_{g} ($\mathrm{MW{\cdot}h^{-1}}$) are the maximum 60-min ramp-up and ramp-down rate of unit g. SU_g (MW) and SD_g (MW) are start-up and shut-down ramp limit of generator g, respectively. $P^{t}_{\mathrm{ed},j}$ (MW) is the power load forecast at bus j. $\mathcal{E}_{\mathrm{egc},j}$ is the set of gas compressors fed by power bus j. $B_{\mathrm{br},k}$ (S) is the susceptance of branch k. $P^{\min}_{\mathrm{br},k}$ (MW) and $P^{\max}_{\mathrm{br},k}$ (MW) are the minimal and maximal power allowed of branch k. δ (%) is the reserve requirement.

(A4) is the status transition of generators. (A5)-(A7) are the minimal up, down time duration, and initial status constraint of generators [163]. (A8)-(A10) are the power capacity limitation with reserves [163], [164]. (A11)-(A12) are the ramp up and down limitation [164]. The power balance of each bus is given in (A13), together with the compressor horse power. The power transmitted on each line is given in (A14), and the power is limited by (A15). Considering the uncertainty of load forecasting, the reserve requirement is given in (A16).

A.2.2 NG System

The constraints of gas sources, pipelines, compressors and gas flow are formulated as follows:

$$Q_{\mathrm{gs},s}^{\min} \leq q_{\mathrm{gs},s}^{t} \leq Q_{\mathrm{gs},s}^{\max},\ \forall t \in \mathcal{T}, s \in \mathcal{S} \tag{A17}$$

$$\begin{aligned} & L_{\mathrm{gp},k}\left(\left(\mathbb{P}_{\mathrm{gp},k}^{+,t}+\mathbb{P}_{\mathrm{gp},\,k}^{-,t}\right)-\left(\mathbb{P}_{\mathrm{gp},k}^{+,t\text{-}1}+\mathbb{P}_{\mathrm{gp},k}^{-,t\text{-}1}\right)\right) \\ &= 2\Delta t C_{\mathrm{gp},k}^{1}\left(q_{\mathrm{gp},k}^{-,t}-q_{\mathrm{gp},k}^{+,t}\right),\ \forall t \in \mathcal{T}, k \in \mathcal{E}_{\mathrm{gp}} \end{aligned} \tag{A18}$$

$$\begin{aligned} & \frac{1}{4} L_{\mathrm{gp},k} C_{\mathrm{gp},k}^{2}\left(q_{\mathrm{gp},k}^{-,t}+q_{\mathrm{gp},k}^{+,t}\right)\left|q_{\mathrm{gp},k}^{-,t}+q_{\mathrm{gp},k}^{+,t}\right| \\ &= \left(\mathbb{P}_{\mathrm{g},k}^{+,t}\right)^{2}-\left(\mathbb{P}_{\mathrm{g},k}^{-,t}\right)^{2},\ \forall t \in \mathcal{T}, k \in \mathcal{E}_{\mathrm{gp}} \end{aligned} \tag{A19}$$

$$-Q_{\mathrm{gp},k}^{\max} \leq q_{\mathrm{gp},k}^{+,t} \leq Q_{\mathrm{gp},k}^{\max},\ \forall t \in \mathcal{T}, k \in \mathcal{E}_{\mathrm{gp}} \tag{A20}$$

$$-Q_{\mathrm{gp},k}^{\max} \leq q_{\mathrm{gp},k}^{-,t} \leq Q_{\mathrm{gp},k}^{\max},\ \forall t \in \mathcal{T}, k \in \mathcal{E}_{\mathrm{gp}} \tag{A21}$$

$$\mathbb{P}_{\mathrm{gc},c}^{+,t} = RC_{\mathrm{gc},c}^{t}\mathbb{P}_{\mathrm{gc},c}^{-,t},\ \forall t \in \mathcal{T}, c \in \mathcal{E}_{\mathrm{gc}} \tag{A22}$$

$$Hp_{\mathrm{gc},c}^{t} = \frac{a_{\mathrm{hp}}\mathcal{P}_{\mathrm{sc}}T q_{\mathrm{gc},c}^{t} c_{\mathrm{k}}}{T_{\mathrm{sc}}\eta_{\mathrm{gc},c}\left(c_{\mathrm{k}}-1\right)}\left(\left(RC_{\mathrm{gc},c}^{t}\right)^{\frac{c_{\mathrm{k}}\text{-}1}{c_{\mathrm{k}}}}-1\right),\ \forall t \in \mathcal{T}, c \in \mathcal{E}_{\mathrm{gc}} \tag{A23}$$

$$0 \leq Hp_{\mathrm{g},c}^{t} \leq HP_{\mathrm{g},c}^{\max},\ \forall t \in \mathcal{T}, c \in \mathcal{E}_{\mathrm{gc}} \tag{A24}$$

$$\mathcal{P}_{j}^{\min} \leq \mathbb{P}_{j}^{t} \leq \mathcal{P}_{j}^{\max},\ \forall t \in \mathcal{T}, j \in \mathcal{N}_{\mathrm{g}} \tag{A25}$$

$$\begin{aligned} & \sum_{s\in\mathcal{S}_{j}} q_{\mathrm{gs},s}^{t}+\sum_{k\in\mathcal{E}_{\mathrm{gp},j}^{+}} q_{\mathrm{gp},k}^{+,t}-\sum_{k\in\mathcal{E}_{\mathrm{gp},j}^{-}} q_{\mathrm{gp},k}^{-,t}+\sum_{c\in\mathcal{E}_{\mathrm{gc},j}^{+}} q_{\mathrm{gc},c}^{t}-\sum_{c\in\mathcal{E}_{\mathrm{gc},j}^{-}} q_{\mathrm{gc},c}^{t} \\ &= Q_{\mathrm{gd},j}^{t}+\sum_{g\in\mathcal{G}_{\mathrm{gfg},j}} q_{\mathrm{gfg},g}^{t},\ \forall t \in \mathcal{T}, j \in \mathcal{N}_{\mathrm{g}} \end{aligned} \tag{A26}$$

$$q^t_{\mathrm{gfg},g} = C_{\mathrm{g2e},g}\eta_{\mathrm{g2e},g}P^t_{\mathrm{e},g},\ \forall t \in \mathcal{T},\ g \in \mathcal{G}_{\mathrm{gfg}} \tag{A27}$$

$$p^t_{\mathrm{egc},c} = \eta_{\mathrm{e2g},c}Hp^t_{\mathrm{gc},c},\ \forall t \in \mathcal{T}, c \in \mathcal{E}_{\mathrm{egc}} \tag{A28}$$

where $\mathcal{S}$ is the set of gas sources. $Q^{\min}_{\mathrm{gs},s}$ (MMSCF·h^{-1}) and $Q^{\max}_{\mathrm{gs},s}$ (MMSCF·h^{-1}) are minimal and maximal output of gas resource s, respectively. $\mathcal{E}_{\mathrm{gp}}$ is the set of gas pipelines. $L_{\mathrm{gp},k}$ (mile) and $Q^{\max}_{\mathrm{gp},k}$ (MMSCF·h^{-1}) are the length and capacity rate of pipeline segment k. $RC^t_{\mathrm{gc},c}$ is the compression ratio of compressor c. $\mathcal{E}_{\mathrm{gc}}$ is the set of gas compressors. $HP^{\max}_{\mathrm{gc},c}$ (hp) is the maximum horsepower of compressor c. a_{hp} is constant. c_{k} is the gas specific heat ratio. $\eta_{\mathrm{gc},c}$ is the compressor efficiency. $\mathcal{N}_{\mathrm{g}}$ is the set of gas nodes. $\mathcal{P}^{\min}_j$ (psia) and $\mathcal{P}^{\max}_j$ (psia) are minimal and maximal allowed pressure at node j, respectively. $Q^t_{\mathrm{gd},j}$ (MMSCF·h^{-1}) is the gas load forecast at node j during time slot t. $\mathcal{N}_{\mathrm{gd}}$ is the set of gas nodes with loads. $\mathcal{S}_j$ is the set of gas sources located at node j. $\mathcal{E}^{+}_{\mathrm{gp},j}$ and $\mathcal{E}^{-}_{\mathrm{gp},j}$ are the set of gas pipelines to and from node j, respectively. $\mathcal{E}^{+}_{\mathrm{gc},j}$ and $\mathcal{E}^{-}_{\mathrm{gc},j}$ are the set of gas compressors to and from node j, respectively. $\mathcal{G}_{\mathrm{gfg},j}$ is the set of GFGs fed by node j. $\mathcal{G}_{\mathrm{gfg}}$ is the set of GFGs. $C_{\mathrm{g2e},g}$ is a constant. $\eta_{\mathrm{g2e},g}$ is the energy conversion efficiency of GFG g.

The capacity bounds of each gas sources are depicted by (A17). The dynamic gas flow in a pipeline k is illustrated in (A18)-(A19). The volume flow rate is limited by (A20)-(A21). For the compressor, the pressure ratio and horsepower are given in (A22) and (A23), respectively. The horsepower of each compressor is constrained by (A24). Within the gas networks, the pressure of each node is to operate within a given range in (A25). Considering the consumption of gas turbines, the gas node balance equation is shown in (A26). The gas consumption of gas turbine and electricity consumption of compressors are given in (A27) and (A28), respectively.

A.3 Second-stage Constraint Set

Without considering the failures within the gas systems, the second stage constraint set, i.e., **Y** includes the real-time scheduling of generators, power flow and load shedding after the realization of transmission line failures, as follows:

$$p^t_{\mathrm{eg},g} - R^t_g \le P^t_{\mathrm{eg},g} \le p^t_{\mathrm{eg},g} + R^t_g,\ \forall t \in \mathcal{T}, g \in \mathcal{G} \tag{A29}$$

$$-\mathrm{R}^{60\text{-}}_g \Delta t \le P^t_{\mathrm{eg},g} - P^{t-1}_{\mathrm{eg},g} \le \mathrm{R}^{60+}_g \Delta t,\ \forall t \in \mathcal{T}, g \in \mathcal{G} \tag{A30}$$

$$\begin{aligned}\left(I_{\mathrm{br},k} - 1\right) M \le P^t_{\mathrm{br},k} - B_{\mathrm{br},k}\left(\theta^{+,t}_{\mathrm{br},k} - \theta^{-,t}_{\mathrm{br},k}\right)\\ \le \left(1 - I_{\mathrm{br},k}\right) M,\ \forall t \in \mathcal{T}, k \in \mathcal{E}_{\mathrm{br}}\end{aligned} \tag{A31}$$

$$-I_{\mathrm{br},k} P^{\max}_{\mathrm{br},k} \le P^t_{\mathrm{br},k} \le I_{\mathrm{br},k} P^{\max}_{\mathrm{br},k},\ ;\forall t \in \mathcal{T}, k \in \mathcal{E}_{\mathrm{br}} \tag{A32}$$

$$P^t_{\mathrm{ed},j} \ge P^t_{\mathrm{lc},j} \ge 0,\ \forall t \in \mathcal{T}, j \in \mathcal{N}_{\mathrm{ed}} \tag{A33}$$

$$\sum_{g \in \mathcal{G}_j} P^t_{\mathrm{eg},g} + \sum_{k \in \mathcal{E}^+_{\mathrm{br},j}} P^t_{\mathrm{br},k} - \sum_{k \in \mathcal{E}^-_{\mathrm{br},j}} P^t_{\mathrm{br},k} = P^t_{\mathrm{ed},j} + \sum_{c \in \mathcal{E}_{\mathrm{gc},j}} P^t_{\mathrm{egc},c} \tag{A34}$$

$$-P^t_{\mathrm{lc},j},\ \forall t \in \mathcal{T}, j \in \mathcal{N}_{\mathrm{e}} \tag{A35}$$

The real-time generator output constraints are given in (A29)-(A30). Considering the operating status of transmission lines, the power transmitted on each line is limited by (A31)-(A32). For a specific bus, the amount of load shedding is given in (A33). The real-time power balancing at each bus is depicted by (A34).

A.4 Uncertainty Set

Considering the impacts of hurricane on transmission lines [165], only the operating status of transmission lines is treated as the uncertainty factors. The

uncertainty set, i.e., $\mathcal{U}$ is depicted as follows

$$\sum_{k \in \mathcal{E}_{\text{br}}} I_{\text{br},k} \geq |\mathcal{E}_{\text{e}}| - K \tag{A36}$$

where $|\mathcal{E}_{\text{br}}|$ is the number of power transmission lines.

A.5 Solution Methods

The formulated problem (A1) is a non-convex mixed-integer min-max-min optimization problem, due to the non-convexity of constraint (A19). There are different methods to convexify this constraint, and the incremental piece-wise linear method [158] is adopted. $\mathbf{X}$ is reformulated to $\bar{\mathbf{X}}$, where constraint (A19) is piece-wise linearized, as follows:

$$\min_{\mathbf{x} \in \bar{\mathbf{X}}} f(\mathbf{x}) + \max_{\boldsymbol{\xi} \in \mathcal{U}} [\mathcal{Q}(\mathbf{x}, \boldsymbol{\xi})] \tag{A37}$$

Problem is a standard two-stage robust optimization problem. In problem (A37), $\max_{\boldsymbol{\xi} \in \mathcal{U}}[\mathcal{Q}(\mathbf{x}, \boldsymbol{\xi})]$ is a max-min problem, and the inner problem is a linear programming problem. The column-and-constraint generation method [166] is adopted to solve this problem. It should be noted that the dual approach is adopted to solve $\max_{\boldsymbol{\xi} \in \mathcal{U}} [\mathcal{Q}(\mathbf{x}, \boldsymbol{\xi})]$, while in [166] it is solved by a primal problem.

The formulated problem (A1) - (A37) is implemented after the close of day-ahead market, e.g., at 10:30 for PJM [31] before the operating day. The updated hurricane information and load forecasting information are input for the day-ahead two-stage robust UC problem. After the of day-ahead results are posted and before the close of rebid, e.g., 13:30 to 14:15 for PJM, the commitment status of generators before the assessment period are determined and input to minimize the load shedding, as shown in (5.21) in Chapter 5. Due to the line failures, some committed generators might be shut down to meet the power balance and security requirements.

List of Publications

Journal Publications

[1] **H. Zhang**, L. Cheng, S. Yao, T. Zhao, and P. Wang, "Spatial-temporal Reliability and Damage Assessment of Transmission Networks under Hurricanes," *IEEE Trans. Smart Grid*, vol. PP, no. c, pp. 1–1, 2019.

[2] S. Yao, P. Wang, X. Liu, **H. Zhang**, and T. Zhao, "Rolling Optimization of Mobile Energy Storage Fleets for Resilient Service Restoration," *IEEE Trans. Smart Grid*, vol. PP, no. c, pp. 1–1, 2019.

[3] **H. Zhang**, P. Wang, S. Yao, X. Liu, and T. Zhao, "Resilience Assessment of Interdependent Energy Systems under Hurricanes," *IEEE Trans. Power Syst.* (Under Review)

[4] T. Zhao, **H. Zhang**, X. Liu, S. Yao, and P. Wang, "Resilient Unit Commitment for Day-ahead Market Considering Probabilistic Impacts of Hurricanes," *IEEE Trans. Power Syst.* (Under Review)

Conference Proceedings

[1] **H. Zhang**, T. Zhao, S. Yao, P. Wang, and L. K. Goel, "Power System Hurricane Resilience Assessment Considering Fuel Supply System," *2018 IEEE Power Energy Soc. Gen. Meet.*, vol. 2018-Augus. IEEE, 2018, pp. 1–5.

[2] **H. Zhang**, T. Zhao, P. Wang, and S. Yao, "Power System Resilience Assessment Considering of Integrated Natural Gas System," *IET Int. Conf. Resil. Transm. Distrib. Networks (RTDN)*, Institution of Engineering and Technology, 2017, pp. 1–7.

[3] S. Yao, T. Zhao, **H. Zhang**, P. Wang, and L. Goel, "Two-stage Stochastic Scheduling of Transportable Energy Storage Systems for Resilient Distribution Systems," *IEEE Int. Conf. Probabilistic Methods Appl. to Power Syst.*, IEEE, 2018, pp. 1–6.

[4] S. Yao, T. Zhao, P. Wang, and **H. Zhang**, "Resilience-oriented Distribution System Reconfiguration for Service Restoration considering Distributed Generations," *Power Energy Soc. Gen. Meet.*, vol. 2018-Janua. IEEE, 2017, pp. 1–5.

Bibliography

[1] International Energy Agency, *Electricity Information 2019*, ser. Electricity Information. Paris: OECD, 2019. [Online]. Available: https://doi.org/10.1787/e0ebb7e9-en

[2] International Energy Agency, *Key World Energy Statistics 2019*, ser. Key World Energy Statistics. Paris: OECD, 2019. [Online]. Available: https://doi.org/10.1787/71b3ce84-en

[3] International Energy Agency, *Natural Gas Information 2019*, ser. Natural Gas Information. Paris: OECD, 2019. [Online]. Available: https://doi.org/10.1787/4d2f3232-en

[4] National Centers for Environmental Information (NCEI), "Billion-Dollar Weather and Climate Disasters: Overview." [Online]. Available: https://www.ncdc.noaa.gov/billions/

[5] Munich Re, "Loss Events Worldwide 2018," 2018. [Online]. Available: https://www.munichre.com/site/corporate/get/params_E646594957_Dattachment/1707978/munichre-natcat-2018_worldmap.pdf

[6] W. Li, *Risk Assessment of Power Systems: Models, Methods, and Applications*. Hoboken, New Jersey: John Wiley & Sons, Inc., 2005.

[7] S. Babin and R. Sterner, "Atlantic Hurricane Track Maps & Images." [Online]. Available: http://fermi.jhuapl.edu/hurr/

[8] Department of Atmospheric Sciences (DAS) at University of Illinois Urbana-Champaign (UIUC), "WW2010 (the weather world 2010 project)." [Online]. Available: http://ww2010.atmos.uiuc.edu/(Gh)/guides/mtr/hurr/stages/cane/pswd.rxml

[9] S. Clegg and P. Mancarella, "Integrated Electrical and Gas Network Flexibility Assessment in Low-Carbon Multi-Energy Systems," *IEEE Trans. Sustain. Energy*, vol. 7, no. 2, pp. 718–731, 2016.

[10] National Electricity of Singapore, "Market Report 2004," Tech. Rep. April, 2004.

[11] C. M. Correa-Posada and P. Sanchez-Martin, "Stochastic Contingency Analysis for the Unit Commitment with Natural Gas Constraints," in *2013 IEEE Grenoble Conf.* IEEE, 2013, pp. 1–6.

[12] NERC, "2011 Special Reliability Assessment: A Primer of the Natural Gas and Electric Power Interdependency in the United States," Tech. Rep., 2011.

[13] Federal Energy Regulatory Commission North American Electric Reliability Corporation, "Report on Outages and Curtailments During the Southwest Cold Weather Event of February 1-5, 2011," Tech. Rep., 2011.

[14] P. J. Hibbard and T. Schatzki, "The Interdependence of Electricity and Natural Gas: Current Factors and Future Prospects," *Electr. J.*, vol. 25, no. 4, pp. 6–17, 2012.

[15] North American Electric Reliability Council, "Gas/Electricity Interdependencies and Recommendations," Tech. Rep., 2004.

[16] S. M. Rinaldi, "Modeling and Simulating Critical Infrastructures and Their Interdependencies," in *Proc. Hawaii Int. Conf. Syst. Sci.*, vol. 37, no. C, 2004, pp. 873–880.

[17] N. Judson, "Interdependence of the Electricity Generation System and the Natural Gas System and Implications for Energy Security," Tech. Rep., 2013.

[18] Energy Information Administration Office of Oil and Gas, "Natural Gas

Processing: The Crucial Link between Natural Gas Production and Its Transportation to Market," Tech. Rep., 2006. [Online]. Available: http://www.eia.doe.gov/oil{_}gas/natural{_}gas/data{_}publications/

[19] Q. Xie and R. Zhu, "Earth, Wind, and Ice," *IEEE Power Energy Mag.*, vol. 9, no. 2, pp. 28–36, 2011.

[20] U.S. Department of Energy, "Tropical Cyclone Michael | Report #17 - Final," Tech. Rep., 2018.

[21] J. Dell, S. Tierney, G. Franco, R. G. Newell, R. Richels, J. Weyant, and T. J. Wilbanks, "Ch. 4: Energy Supply and Use. Climate Change Impacts in the United States: The Third National Climate Assessment," U.S. Global Change Research Program, Washington, DC, Tech. Rep., 2014.

[22] W. Li *et al.*, *Reliability Assessment of Electric Power Systems Using Monte Carlo Methods*. Springer Science & Business Media, 2013.

[23] R. N. Allan *et al.*, *Reliability Evaluation of Power Systems*. Springer Science & Business Media, 2013.

[24] Langlois Sébastien, "Effect of High Intensity Winds on Overhead Transmission Lines." CIGRÉ WG, B,2, 2006, pp. 1–77.

[25] D. A. Reed, M. D. Powell, and J. M. Westerman, "Energy Infrastructure Damage Analysis for Hurricane Rita," *Nat. Hazards Rev.*, vol. 11, no. 3, pp. 102–109, 2010.

[26] U.S. Department of Energy, "Comparing the Impacts of the 2005 and 2008 Hurricanes on U.S. Energy Infrastructure," Tech. Rep., 2005.

[27] Sandy Rebuilding Task Force, "Hurricane Sandy Rebuilding Strategy," Tech. Rep., 2013. [Online]. Available: http://portal.hud.gov/hudportal/documents/huddoc?id=hsrebuildingstrategy.pdf

[28] NERC, "Hurricane Irma Event Analysis Report," Tech. Rep., 2018.

[29] New Mexico Public Regulation Commission Informal Task Force, "Severe Weather Event of February, 2011 and Its Cascading Impacts on NM Utility Service," Tech. Rep., 2011.

[30] H. Hui, "Reliability Unit Commitment In ERCOT Nodal Market," Ph.D. dissertation, The University of Texas at Arlington, 2013.

[31] J. Ciabattoni, "Commitment Process & Uplift Drivers," PJM, Tech. Rep., 2017.

[32] R. Billinton and Y. Kumar, "Transmission Line Reliability Models Including Common Mode and Adverse Weather Effects," *IEEE Trans. Power Appar. Syst.*, vol. PAS-100, no. 8, pp. 3899–3910, 1981.

[33] R. Billinton and G. Singh, "Application of Adverse and Extreme Adverse Weather: Modelling in Transmission and Distribution System Reliability Evaluation," *IEE Proc. - Gener. Transm. Distrib.*, vol. 153, no. 1, p. 115, 2006.

[34] R. Billinton and R. N. Allan, *Reliability Evaluation of Power Systems*. Boston, MA: Springer US, 1996.

[35] R. Billinton and L. Cheng, "Incorporation of Weather Effects in Transmission System Models for Composite System Adequacy Evaluation," in *IEE Proceedings C (Generation, Transmission and Distribution)*, vol. 133, no. 6. IET, 1986, pp. 319–327.

[36] R. Billinton and J. Acharya, "Consideration of Multi-State Weather Models in Reliability Evaluation of Transmission and Distribution Systems," *Can. Conf. Electr. Comput. Eng.*, vol. 2005, pp. 619–622, 2005.

[37] R. Billinton and W. Li, *Reliability Assessment of Electric Power Systems Using Monte Carlo Methods*. Boston, MA: Springer US, 1994.

[38] Yuanzhang Sun, Lin Cheng, Haitao Liu, and Shan He, "Power System

Operational Reliability Evaluation Based on Real-Time Operating State," in *2005 Int. Power Eng. Conf.* IEEE, 2005, pp. 722–727 Vol. 2.

[39] Y. Sun, P. Wang, L. Cheng, and H. Liu, "Operational Reliability Assessment of Power Systems Considering Condition-Dependent Failure Rate," *IET Gener. Transm. Distrib.*, vol. 4, no. 1, pp. 60–72, 2009.

[40] Y. Zhou, A. Pahwa, and S.-S. Yang, "Modeling Weather-Related Failures of Overhead Distribution Lines," *IEEE Trans. Power Syst.*, vol. 21, no. 4, pp. 1683–1690, 2006.

[41] G. Li, P. Zhang, P. B. Luh, W. Li, Z. Bie, C. Serna, and Z. Zhao, "Risk Analysis for Distribution Systems in the Northeast U.S. Under Wind Storms," *IEEE Trans. Power Syst.*, vol. 29, no. 2, pp. 889–898, 2014.

[42] J. Ainscough, I. Forrest *et al.*, "Predicting medium-voltage underground-distribution cable failures," in *Proc. IEEE PES-ICC Fall Meeting*, 2009, pp. 1–11.

[43] Y. Gill, "Development of an electrical cable replacement simulation model to aid with the management of aging underground electric cables," *IEEE Electrical Insulation Magazine*, vol. 27, no. 1, pp. 31–37, 2011.

[44] A. Carvalho, M. Cormenzana, H. Furuta, W. Grieshaber, A. Hyrczak, D. Kopejtkova, J. Krone, M. Kudoke, D. Makareinis, J. Martins *et al.*, "Final report of the 2004–2007 international enquiry on reliability of high voltage equipment," *Electra*, vol. 264, pp. 49–53, 2012.

[45] J. L. Aznarte and N. Siebert, "Dynamic Line Rating Using Numerical Weather Predictions and Machine Learning: a Case Study," *IEEE Trans. Power Deliv.*, vol. 32, no. 1, pp. 335–343, 2017.

[46] D. Srinivasan, A. C. Liew, and C. S. Chang, "Applications of Fuzzy Systems in Power Systems," *Electr. Power Syst. Res.*, vol. 35, no. 1, pp. 39–43, 1995.

[47] A. Hamada and A. El Damatty, "Failure Analysis of Guyed Transmission Lines During F2 Tornado Event," *Eng. Struct.*, vol. 85, pp. 11–25, 2015.

[48] X. Fu and H.-N. Li, "Uncertainty Analysis of the Strength Capacity and Failure Path for a Transmission Tower under a Wind Load," *J. Wind Eng. Ind. Aerodyn.*, vol. 173, pp. 147–155, 2018.

[49] H. Hangan, E. Savory, A. E. Damatty, J. Galsworthy, and C. Miller, "Modeling and Prediction of Failure of Transmission Lines Due to High Intensity Winds," *Proc. 2008 Struct. Congr. - Struct. Congr. 2008 Crossing Borders*, vol. 314, 2008.

[50] K. Alvehag and L. Soder, "A Reliability Model for Distribution Systems Incorporating Seasonal Variations in Severe Weather," *IEEE Trans. Power Deliv.*, vol. 26, no. 2, pp. 910–919, 2011.

[51] X. Fu, H.-N. Li, and G. Li, "Fragility Analysis and Estimation of Collapse Status for Transmission Tower Subjected to Wind and Rain Loads," *Struct. Saf.*, vol. 58, pp. 1–10, 2016.

[52] A. Shafieezadeh, U. P. Onyewuchi, M. M. Begovic, and R. Desroches, "Age-Dependent Fragility Models of Utility Wood Poles in Power Distribution Networks Against Extreme Wind Hazards," *IEEE Trans. Power Deliv.*, vol. 29, no. 1, pp. 131–139, 2014.

[53] M. Benini, S. Canevese, D. Cirio, and A. Gatti, "Battery energy storage systems for the provision of primary and secondary frequency regulation in Italy," *EEEIC 2016 - Int. Conf. Environ. Electr. Eng.*, pp. 1–6, 2016.

[54] F. Zhang, Z. Hu, X. Xie, J. Zhang, and Y. Song, "Assessment of the Effectiveness of Energy Storage Resources in the Frequency Regulation of a Single-Area Power System," *IEEE Trans. Power Syst.*, vol. 32, no. 5, pp. 3373–3380, 2017.

[55] M. Aunedi, P.-A. Kountouriotis, J. E. O. Calderon, D. Angeli, and G. Strbac, "Economic and Environmental Benefits of Dynamic Demand in Providing Frequency Regulation," *IEEE Trans. Smart Grid*, vol. 4, no. 4, pp. 2036–2048, 2013.

[56] B. Delfino, S. Massucco, A. Morini, P. Scalera, and F. Silvestro, "Implementation and comparison of different under frequency load-shedding schemes," *2001 Power Eng. Soc. Summer Meet. Conf. Proc. (Cat. No.01CH37262)*, vol. 1, pp. 307–312 vol.1, 2002.

[57] N. Nguyen and J. Mitra, "An analysis of the effects and dependency of wind power penetration on system frequency regulation," *IEEE Trans. Sustain. Energy*, vol. 7, no. 1, pp. 354–363, 2016.

[58] C. Liang, P. Wang, X. Han, W. Qin, R. Billinton, and W. Li, "Operational Reliability and Economics of Power Systems with Considering Frequency Control Processes," *IEEE Trans. Power Syst.*, vol. 32, no. 4, pp. 2570–2580, 2017.

[59] D. Ganger, J. Zhang, and V. Vittal, "Forecast-based anticipatory frequency control in power systems," *IEEE Trans. Power Syst.*, vol. 33, no. 1, pp. 1004–1012, 2018.

[60] N. Nguyen and J. Mitra, "Reliability of power system with high wind penetration under frequency stability constraint," *IEEE Trans. Power Syst.*, vol. 33, no. 1, pp. 985–994, 2018.

[61] M. Panteli and P. Mancarella, "Modeling and Evaluating the Resilience of Critical Electrical Power Infrastructure to Extreme Weather Events," *IEEE Syst. J.*, vol. 11, no. 3, pp. 1733–1742, 2017.

[62] M. Panteli, P. Mancarella, D. N. Trakas, E. Kyriakides, and N. D. Hatziargyriou, "Metrics and Quantification of Operational and Infrastructure

Resilience in Power Systems," *IEEE Trans. Power Syst.*, vol. 32, no. 6, pp. 4732–4742, 2017.

[63] S. Chanda and A. K. Srivastava, "Defining and Enabling Resiliency of Electric Distribution Systems with Multiple Microgrids," *IEEE Trans. Smart Grid*, vol. 7, no. 6, pp. 2859–2868, 2016.

[64] M. Bessani, J. A. Massignan, R. Z. Fanucchi, M. H. Camillo, J. B. London, A. C. Delbem, and C. D. Maciel, "Probabilistic Assessment of Power Distribution Systems Resilience under Extreme Weather," *IEEE Syst. J.*, vol. 13, no. 2, pp. 1747–1756, 2019.

[65] F. Teymouri, T. Amraee, H. Saberi, and F. Capitanescu, "Toward controlled islanding for enhancing power grid resilience considering frequency stability constraints," *IEEE Trans. Smart Grid*, vol. 10, no. 2, pp. 1735–1746, 2019.

[66] P. J. Hibbard and T. Schatzki, "The Interdependence of Electricity and Natural Gas: Current Factors and Future Prospects," *Electr. J.*, vol. 25, no. 4, pp. 6–17, 2012.

[67] X. Liu, P. Mancarella, and J. Wu, "A Tool for Integrated Analysis of Multi-Vector District Energy Networks," in *2015 IEEE Eindhoven PowerTech*, vol. 6, no. 4. IEEE, 2015, pp. 1–6.

[68] X. Zhang, L. Che, M. Shahidehpour, A. S. Alabdulwahab, and A. Abusorrah, "Reliability-Based Optimal Planning of Electricity and Natural Gas Interconnections for Multiple Energy Hubs," *IEEE Trans. Smart Grid*, vol. 8, no. 4, pp. 1658–1667, 2017.

[69] C. He, L. Wu, T. Liu, and Z. Bie, "Robust Co-Optimization Planning of Interdependent Electricity and Natural Gas Systems with a Joint N-1 and Probabilistic Reliability Criterion," *IEEE Trans. Power Syst.*, vol. 33, no. 2,

pp. 2140–2154, 2018.

[70] Seungwon An, Qing Li, and T. Gedra, "Natural Gas and Electricity Optimal Power Flow," in *2003 IEEE PES Transm. Distrib. Conf. Expo. (IEEE Cat. No.03CH37495)*, vol. 1, no. 1. IEEE, 2003, pp. 138–143.

[71] A. Martinez-Mares and C. R. Fuerte-Esquivel, "A Unified Gas and Power Flow Analysis in Natural Gas and Electricity Coupled Networks," *IEEE Trans. Power Syst.*, vol. 27, no. 4, pp. 2156–2166, 2012.

[72] C. M. Correa-Posada and P. Sanchez-Martin, "Security-Constrained Optimal Power and Natural-Gas Flow," *IEEE Trans. Power Syst.*, vol. 29, no. 4, pp. 1780–1787, 2014.

[73] J. Fang, Q. Zeng, X. Ai, Z. Chen, and J. Wen, "Dynamic Optimal Energy Flow in the Integrated Natural Gas and Electrical Power Systems," *IEEE Trans. Sustain. Energy*, vol. 9, no. 1, pp. 188–198, 2018.

[74] M. Shahidehpour, Yong Fu, and T. Wiedman, "Impact of Natural Gas Infrastructure on Electric Power Systems," *Proc. IEEE*, vol. 93, no. 5, pp. 1042–1056, 2005.

[75] T. Li, M. Eremia, and M. Shahidehpour, "Interdependency of Natural Gas Network and Power System Security," *IEEE Trans. Power Syst.*, vol. 23, no. 4, pp. 1817–1824, 2008.

[76] M. Urbina and Z. Li, "Modeling and Analyzing the Impact of Interdependency between Natural Gas and Electricity Infrastructures," in *2008 IEEE Power Energy Soc. Gen. Meet. - Convers. Deliv. Electr. Energy 21st Century*. IEEE, 2008, pp. 1–6.

[77] I. Goroohi Sardou, M. E. Khodayar, and M. Ameli, "Coordinated Operation of Natural Gas and Electricity Networks with Microgrid Aggregators," *IEEE Trans. Smart Grid*, vol. 9, no. 1, pp. 199–210, 2018.

[78] J. Yang, N. Zhang, C. Kang, and Q. Xia, "Effect of Natural Gas Flow Dynamics in Robust Generation Scheduling under Wind Uncertainty," *IEEE Trans. Power Syst.*, vol. 33, no. 2, pp. 2087–2097, 2018.

[79] C. Wang, R. Gao, W. Wei, M. Shafie-Khah, T. Bi, and J. P. Catalão, "Risk-based Distributionally Robust Optimal Gas-Power Flow with Wasserstein distance," *IEEE Trans. Power Syst.*, vol. 34, no. 3, pp. 2190–2204, 2019.

[80] S. Badakhshan, M. Kazemi, and M. Ehsan, "Security Constrained Unit Commitment with Flexibility in Natural Gas Transmission Delivery," *J. Nat. Gas Sci. Eng.*, vol. 27, pp. 632–640, 2015.

[81] J. Munoz, N. Jimenez-Redondo, J. Perez-Ruiz, and J. Barquin, "Natural Gas Network Modeling for Power Systems Reliability Studies," in *2003 IEEE Bol. Power Tech Conf. Proceedings,*, vol. 4. IEEE, 2003, pp. 20–27.

[82] E. Dialynas, T. Diagoupis, L. Daoutis, E. Dialynas, and L. Daoutis, "Reliability Assessment of Natural Gas Transmission Systems and Their Impact on the Operational Performance of Electric Power Systems," in *8th Mediterr. Conf. Power Gener. Transm. Distrib. Energy Convers. (MEDPOWER 2012)*. Institution of Engineering and Technology, 2012, pp. 48–48.

[83] M. Chaudry, J. Wu, and N. Jenkins, "A Sequential Monte Carlo Model of the Combined GB Gas and Electricity Network," *Energy Policy*, vol. 62, pp. 473–483, 2013.

[84] T. C. Ly, J. N. Moura, and G. Velummylum, "Assessing the Bulk Power System's Resource Resilience to Future Extreme Winter Weather Events," in *2015 IEEE Power Energy Soc. Gen. Meet.*, vol. 2015-Septe. IEEE, 2015, pp. 1–4.

[85] C. Shao, M. Shahidehpour, X. Wang, X. Wang, and B. Wang, "Integrated

Planning of Electricity and Natural Gas Transportation Systems for Enhancing the Power Grid Resilience," *IEEE Trans. Power Syst.*, vol. 32, no. 6, 2017.

[86] M. Shahidehpour, F. Wen, Y. Li, and Z. Li, "Minimax-Regret Robust Co-optimization for Enhancing the Resilience of Integrated Power Distribution and Natural Gas System," *IEEE Trans. Sustain. Energy*, vol. PP, no. c, pp. 1–1, 2018.

[87] M. H. Amirioun, F. Aminifar, and M. Shahidehpour, "Resilience-Promoting Proactive Scheduling Against Hurricanes in Multiple Energy Carrier Microgrids," *IEEE Trans. Power Syst.*, vol. 34, no. 3, pp. 2160–2168, 2019.

[88] M. Panteli and P. Mancarella, "The Grid: Stronger, Bigger, Smarter?: Presenting a Conceptual Framework of Power System Resilience," *IEEE Power Energy Mag.*, vol. 13, no. 3, pp. 58–66, 2015.

[89] C. S. Holling, "Resilience and Stability of Ecological Systems," *Annu. Rev. Ecol. Syst.*, vol. 4, no. 1973, pp. 1–23, 1973.

[90] Y. Y. Haimes, "On the Definition of Resilience in Systems," *Risk Anal.*, vol. 29, no. 4, pp. 498–501, 2009.

[91] H. R. Heinimann, "A Generic Framework for Resilience Assessment," in *IRGC Resour. Guid. Resil.*, v29-07-201 ed. Lausanne: EPFL International Risk Governance Center, 2016, pp. 1–6.

[92] A. Sharifi and Y. Yamagata, "Principles and Criteria for Assessing Urban Energy Resilience: A Literature Review," *Renew. Sustain. Energy Rev.*, vol. 60, pp. 1654–1677, 2016.

[93] The White House, "Presidential Policy Directive 21 - Critical Infrastructure Security and Resilience," 2013. [Online]. Avail-

able: https://obamawhitehouse.archives.gov/the-press-office/2013/02/12/presidential-policy-directive-critical-infrastructure-security-and-resil

[94] M. Chaudry, P. Ekins, K. Ramachandran, A. Shakoor, G. Strbac, X. Wang, and J. Whitaker, "Building a Resilient UK Energy System Research Report," UK ENERGY RESEARCH CENTRE, Tech. Rep., 2011.

[95] Cabinet Office, "Keeping the Country Running: Natural Hazards and Infrastructure," Tech. Rep., 2011.

[96] G. P. Cimellaro, A. M. Reinhorn, and M. Bruneau, "Framework for analytical quantification of disaster resilience," *Eng. Struct.*, vol. 32, no. 11, pp. 3639–3649, 2010.

[97] C. S. Renschler, a. E. Frazier, L. a. Arendt, G. P. Cimellaro, a. M. Reinhorn, and M. Bruneau, "A Framework for Defining and Measuring Resilience at the Community Scale: The PEOPLES Resilience Framework," U.S. Department of Commerce; National Institute of Standards and Technology, Tech. Rep., 2010.

[98] P. Mancarella, I. Cotton, C. Pickering, S. Wilkinson, M. Panteli, K. Anderson, R. Wood, X. Hu, D. Calverley, and R. Dawson, "Impact of Climate Change on the Resilience of the UK Power System," in *IET Int. Conf. Resil. Transm. Distrib. Networks 2015*. Institution of Engineering and Technology, 2015, pp. 8 (6 .)–8 (6 .).

[99] H. H. Willis and K. Loa, "Measuring the Resilience of Energy Distribution Systems," Tech. Rep., 2015.

[100] P. J. Maliszewski and C. Perrings, "Factors in the Resilience of Electrical Power Distribution Infrastructures," *Appl. Geogr.*, vol. 32, no. 2, pp. 668–679, 2012.

[101] D. Henry and J. Emmanuel Ramirez-Marquez, "Generic Metrics and

Quantitative Approaches for System Resilience as a Function of Time," *Reliab. Eng. Syst. Saf.*, vol. 99, pp. 114–122, 2012.

[102] D. Gama Dessavre, J. E. Ramirez-Marquez, and K. Barker, "Multidimensional Approach to Complex System Resilience Analysis," *Reliab. Eng. Syst. Saf.*, vol. 149, pp. 34–43, 2016.

[103] Y. Wang, C. Chen, J. Wang, and R. Baldick, "Research on Resilience of Power Systems under Natural Disasters—A Review," *IEEE Trans. Power Syst.*, vol. 31, no. 2, pp. 1604–1613, 2016.

[104] M. Ouyang and L. Dueñas-Osorio, "Time-Dependent Resilience Assessment and Improvement of Urban Infrastructure Systems," *Chaos An Interdiscip. J. Nonlinear Sci.*, vol. 22, no. 3, p. 033122, 2012.

[105] M. Ouyang, L. Dueñas-Osorio, and X. Min, "A Three-Stage Resilience Analysis Framework for Urban Infrastructure Systems," *Struct. Saf.*, vol. 36-37, pp. 23–31, 2012.

[106] K. Barker, J. E. Ramirez-Marquez, and C. M. Rocco, "Resilience-based Network Component Importance Measures," *Reliab. Eng. Syst. Saf.*, vol. 117, pp. 89–97, 2013.

[107] R. Francis and B. Bekera, "A Metric and Frameworks for Resilience Analysis of Engineered and Infrastructure Systems," *Reliab. Eng. Syst. Saf.*, vol. 121, pp. 90–103, 2014.

[108] M. Ouyang and L. Dueñas-Osorio, "Multi-Dimensional Hurricane Resilience Assessment of Electric Power Systems," *Struct. Saf.*, vol. 48, pp. 15–24, 2014.

[109] M. Panteli, P. Mancarella, S. Wilkinson, R. Dawson, and C. Pickering, "Assessment of the Resilience of Transmission Networks to Extreme Wind Events," in *2015 IEEE Eindhoven PowerTech*. IEEE, 2015, pp. 1–6.

[110] M. Panteli and P. Mancarella, "Operational Resilience Assessment of Power Systems under Extreme Weather and Loading Conditions," in *2015 IEEE Power Energy Soc. Gen. Meet.*, vol. September. IEEE, 2015, pp. 1–5.

[111] J.-P. Watson, R. Guttromson, C. Silva-Monroy, R. Jeffers, K. Jones, J. Ellison, C. Rath, J. Gearhart, D. Jones, T. Corbet, C. Hanley, and L. T. Walker, "Conceptual Framework for Developing Resilience Metrics for the Electricity, Oil, and Gas Sectors in the United States," Sandia National Laboratories, Tech. Rep., 2015.

[112] M. N. Albasrawi, N. Jarus, K. A. Joshi, and S. S. Sarvestani, "Analysis of Reliability and Resilience for Smart Grids," in *2014 IEEE 38th Annu. Comput. Softw. Appl. Conf.* IEEE, 2014, pp. 529–534.

[113] S. Chiaradonna, F. D. Giandomenico, and N. Murru, "On a Modeling Approach to Analyze Resilience of a Smart Grid Infrastructure," in *2014 Tenth Eur. Dependable Comput. Conf.* IEEE, 2014, pp. 166–177.

[114] S. R. Gupta, F. S. Kazi, S. R. Wagh, and N. M. Singh, "Probabilistic Framework for Evaluation of Smart Grid Resilience of Cascade Failure," in *2014 IEEE Innov. Smart Grid Technol. - Asia (ISGT ASIA)*. IEEE, 2014, pp. 255–260.

[115] D. A. Ghanem, S. Mander, and C. Gough, ""I Think We Need to Get a Better Generator": Household Resilience to Disruption to Power Supply during Storm Events," *Energy Policy*, vol. 92, no. February 2014, pp. 171–180, 2016.

[116] The National Electrical Manufacturers Association, "Storm Reconstruction: Rebuild Smart Reduce Outages, Save Lives, Protect Property," Tech. Rep., 2013.

[117] Y. Xu, C.-C. Liu, K. P. Schneider, and D. T. Ton, "Toward a Resilient

Distribution System," in *2015 IEEE Power Energy Soc. Gen. Meet.*, vol. 2015-Septe. IEEE, 2015, pp. 1–5.

[118] S&C Electric Company, "Distributed Intelligence Provides Resilience in Storms," Tech. Rep., 2014.

[119] M. Amin, "Challenges in Reliability, Security, Efficiency, and Resilience of Energy Infrastructure: toward Smart Self-Healing Electric Power Grid," in *2008 IEEE Power Energy Soc. Gen. Meet. - Convers. Deliv. Electr. Energy 21st Century*. IEEE, 2008, pp. 1–5.

[120] Electric Power Research Insititute, "Enhancing Distribution Resiliency-Opportunities for Applying Innovative Technologies," Tech. Rep., 2013.

[121] S. Maharjan, Y. Zhang, S. Gjessing, O. Ulleberg, and F. Eliassen, "Providing Microgrid Resilience during Emergencies Using Distributed Energy Resources," in *2015 IEEE Globecom Work.* IEEE, 2015, pp. 1–6.

[122] M. S. Saleh, A. Althaibani, Y. Esa, Y. Mhandi, and A. A. Mohamed, "Impact of Clustering Microgrids on Their Stability and Resilience during Blackouts," in *2015 Int. Conf. Smart Grid Clean Energy Technol.* IEEE, 2015, pp. 195–200.

[123] M. Panteli, D. N. Trakas, P. Mancarella, and N. D. Hatziargyriou, "Boosting the Power Grid Resilience to Extreme Weather Events Using Defensive Islanding," *IEEE Trans. Smart Grid*, vol. 7, no. 6, pp. 2913–2922, 2016.

[124] Osiadacz, Andrzej J and Control systems centre (Manchester, GB), "Simulation and analysis of gas networks," 1987.

[125] T. Weymouth, "Problems in Natural Gas Engineering," *Trans. Am. Soc. Mech. Eng.*, vol. 34, pp. 185–231, 1912.

[126] T. Achterberg, T. Berthold, T. Koch, and K. Wolter, "Constraint Integer Programming: a New Approach to Integrate CP and MIP," Tech. Rep.,

2008.

[127] A. Martinez-Mares, C. R. Fuerte-Esquivel, and I. de Ingenieria, "Integrated Energy Flow Analysis in Natural Gas and Electricity Coupled Systems," in *2011 North Am. Power Symp.* IEEE, 2011, pp. 1–7.

[128] D. De Wolf and Y. Smeers, "The Gas Transmission Problem Solved by an Extension of the Simplex Algorithm," *Manage. Sci.*, vol. 46, no. 11, pp. 1454–1465, 2000.

[129] Probability Subcommittee, "IEEE Reliability Test System," *IEEE Trans. Power Appar. Syst.*, vol. PAS-98, no. 6, pp. 2047–2054, 1979.

[130] A. Helseth and A. T. Holen, "Reliability Modeling of Gas and Electric Power Distribution Systems; Similarities and Differences," in *2006 Int. Conf. Probabilistic Methods Appl. to Power Syst.* IEEE, 2006, pp. 1–5.

[131] C. Unsihuay, J. W. M. Lima, and A. Z. de Souza, "Modeling the Integrated Natural Gas and Electricity Optimal Power Flow," in *2007 IEEE Power Eng. Soc. Gen. Meet.* IEEE, 2007, pp. 1–7.

[132] M. Bollen, "Effects of Adverse Weather and Aging on Power System Reliability," *IEEE Trans. Ind. Appl.*, vol. 37, no. 2, pp. 452–457, 2001.

[133] "Hurricanes: Science and Society: Hurricane Life Cycle." [Online]. Available: http://www.hurricanescience.org/science/science/hurricanelifecycle/

[134] A. M. Salman, Y. Li, and M. G. Stewart, "Evaluating System Reliability and Targeted Hardening Strategies of Power Distribution Systems Subjected to Hurricanes," *Reliab. Eng. Syst. Saf.*, vol. 144, pp. 319–333, 2015.

[135] A. Rei and M. Schilling, "Reliability Assessment of the Brazilian Power System Using Enumeration and Monte Carlo," *IEEE Trans. Power Syst.*, vol. 23, no. 3, pp. 1480–1487, 2008.

[136] K. Zou, A. P. Agalgaonkar, K. M. Muttaqi, and S. Perera, "An Analytical Approach for Reliability Evaluation of Distribution Systems Containing Dispatchable and Nondispatchable Renewable DG Units," *IEEE Trans. Smart Grid*, vol. 5, no. 6, pp. 2657–2665, 2014.

[137] E. Savory, G. A. Parke, M. Zeinoddini, N. Toy, and P. Disney, "Modelling of Tornado and Microburst-Induced Wind Loading and Failure of a Lattice Transmission Tower," *Eng. Struct.*, vol. 23, no. 4, pp. 365–375, 2001.

[138] M. Powell, G. Soukup, S. Cocke, S. Gulati, N. Morisseau-Leroy, S. Hamid, N. Dorst, and L. Axe, "State of Florida Hurricane Loss Projection Model: Atmospheric Science Component," *J. Wind Eng. Ind. Aerodyn.*, vol. 93, no. 8, pp. 651–674, 2005.

[139] P. J. Vickery, P. F. Skerlj, and L. A. Twisdale, "Simulation of Hurricane Risk in the U.S. Using Empirical Track Model," *J. Struct. Eng.*, vol. 126, no. 10, pp. 1222–1237, 2000.

[140] R. W. R. Darling, "Estimating Probabilities of Hurricane Wind Speeds Using a Large-Scale Empirical Model," *J. Clim.*, vol. 4, no. 10, pp. 1035–1046, 1991.

[141] P. J. Vickery, "Simple Empirical Models for Estimating the Increase in the Central Pressure of Tropical Cyclones after Landfall along the Coastline of the United States," *J. Appl. Meteorol.*, vol. 44, no. 12, pp. 1807–1826, 2005.

[142] G. J. Holland, "An Analytic Model of the Wind and Pressure Profiles in Hurricanes," *Mon. Weather Rev.*, vol. 108, no. 8, pp. 1212–1218, 1980.

[143] P. J. Vickery, D. Wadhera, L. a. Twisdale, and F. M. Lavelle, "U.S. Hurricane Wind Speed Risk and Uncertainty," *J. Struct. Eng.*, vol. 135, no. 3, pp. 301–320, 2009.

[144] A. G. Davenport, "Rationale for Determining Design Dind Velocities," *ASCE J. Struct. Div.*, vol. 86, no. 5, pp. 39–68, 1960.

[145] P. J. Vickery, J. Lin, P. F. Skerlj, L. A. Twisdale, and K. Huang, "HAZUS-MH Hurricane Model Methodology. I: Hurricane Hazard, Terrain, and Wind Load Modeling," *Nat. Hazards Rev.*, vol. 7, no. 2, pp. 82–93, 2006.

[146] American Society of Civil Engineers (ASCE), *ASCE/SEI 7-05 Minimum Design Loads for Buildings and Other Structures*. Reston, Virginia: Amer Society of Civil Engineers, 2006.

[147] F. Xiao, J. D. McCalley, Y. Ou, J. Adams, and S. Myers, "Contingency Probability Estimation Using Weather and Geographical Data for On-Line Security Assessment," in *2006 Int. Conf. Probabilistic Methods Appl. to Power Syst.* IEEE, 2006, pp. 1–7.

[148] Y. Liu and C. Singh, "A Methodology for Evaluation of Hurricane Impact on Composite Power System Reliability," *IEEE Trans. Power Syst.*, vol. 26, no. 1, pp. 145–152, 2011.

[149] G. Morales-Espana, J. M. Latorre, and A. Ramos, "Tight and Compact MILP Formulation of Start-Up and Shut-Down Ramping in Unit Commitment," *IEEE Trans. Power Syst.*, vol. 28, no. 2, pp. 1288–1296, 2013.

[150] N. Li, C. Uckun, E. M. Constantinescu, J. R. Birge, K. W. Hedman, and A. Botterud, "Flexible Operation of Batteries in Power System Scheduling with Renewable Energy," *IEEE Trans. Sustain. Energy*, vol. 7, no. 2, pp. 685–696, 2016.

[151] P. J. Vickery and L. A. Twisdale, "Wind-Field and Filling Models for Hurricane Wind-Speed Predictions," *J. Struct. Eng.*, vol. 121, no. 11, pp. 1700–1709, 1995.

[152] B. Harper, J. Kepert, and J. Ginger, "Guidelines for Converting Between Various Wind Averaging Periods in Tropical Cyclone Conditions," World Meteorological Organization, Tech. Rep., 2010.

[153] C. Grigg, P. Wong, P. Albrecht, R. Allan, M. Bhavaraju, R. Billinton, Q. Chen, C. Fong, S. Haddad, S. Kuruganty, W. Li, R. Mukerji, D. Patton, N. Rau, D. Reppen, A. Schneider, M. Shahidehpour, and C. Singh, "The IEEE Reliability Test System-1996. A Report Prepared by the Reliability Test System Task Force of the Application of Probability Methods Subcommittee," *IEEE Trans. Power Syst.*, vol. 14, no. 3, pp. 1010–1020, 1999.

[154] J. Tang and H. R. Heinimann, "Quantitative Evaluation of Consecutive Resilience Cycles in Stock Market Performance: A Systems-oriented Approach," *arXiv preprint arXiv:1903.03201*, 2019.

[155] S. Ma, B. Chen, and Z. Wang, "Resilience Enhancement Strategy for Distribution Systems under Extreme Weather Events," *IEEE Trans. Smart Grid*, vol. 9, no. 2, pp. 1442–1451, 2016.

[156] G. Huang, J. Wang, C. Chen, J. Qi, and C. Guo, "Integration of Preventive and Emergency Responses for Power Grid Resilience Enhancement," *IEEE Trans. Power Syst.*, vol. 32, no. 6, pp. 4451–4463, 2017.

[157] M. H. Amirioun, F. Aminifar, S. Member, and M. Shahidehpour, "Resilience-Promoting Proactive Scheduling against Hurricanes in Multiple Energy Carrier Microgrids," *IEEE Trans. Power Syst.*, vol. 34, no. 3, pp. 2160 – 2168, 2019.

[158] C. M. Correa-posada and P. Sánchez-martín, "Gas Network Optimization: A comparison of Piecewise Linear Models," *Optim. online*, pp. 133–159, 2014.

[159] "Gurobi Optimization-The State-of-the-Art Mathematical Programming Solver." [Online]. Available: http://www.gurobi.com/index

[160] K. Pambour, B. Cakir Erdener, R. Bolado-Lavin, and G. Dijkema, "Development of a Simulation Framework for Analyzing Security of Supply in Integrated Gas and Electric Power Systems," *Appl. Sci.*, vol. 7, no. 1, p. 47, 2017.

[161] Energy Emergencies Executive Committee, "GB Power System Disruption – 9 August 2019," Department for Business, Energy & Industrial Strategy, Tech. Rep., 2019.

[162] P. Kundur, N. J. Balu, and M. G. Lauby, *Power system stability and control*. McGraw-hill New York, 1994, vol. 7.

[163] G. Morales-España, J. M. Latorre, and A. Ramos, "Tight and Compact MILP Formulation of Start-Up and Shut-Down Ramping in Unit Commitment," *IEEE Trans. Power Syst.*, vol. 28, no. 2, pp. 1288–1296, 2012.

[164] N. Li, C. Uckun, E. M. Constantinescu, J. R. Birge, K. W. Hedman, and A. Botterud, "Flexible Operation of Batteries in Power System Scheduling with Renewable Energy," *IEEE Trans. Sustain. Energy*, vol. 7, no. 2, pp. 685–696, 2015.

[165] H. Zhang, L. Cheng, S. Yao, T. Zhao, and P. Wang, "Spatial-temporal reliability and damage assessment of transmission networks under hurricanes," *IEEE Trans. Smart Grid*, 2019.

[166] B. Zeng and L. Zhao, "Solving two-stage robust optimization problems using a column-and-constraint generation method," *Operations Research Letters*, vol. 41, no. 5, pp. 457–461, 2013.